THREE-PHASE THREE-LIMB TRANSFORMER MODELS IN THE HARMONIC DOMAIN

Maria Luiza Viana Lisboa, BE, Msc.

A thesis presented for the degree of
Doctor of Philosophy
in
Electrical and Electronic Engineering
at the
University of Canterbury,
Christchurch, New Zealand.

30 October 1996

ABSTRACT

This thesis describes a new three-limb three-phase electromagnetic transformer model in the Harmonic Domain. It is a composite model, with the linear circuit represented by the short-circuit impedances, and the non-linear magnetic circuit represented in a linearised form by means of Norton equivalents.

The proposed Norton equivalents accurately represent the magnetic circuit, as they are derived from the linearisation (in the Harmonic Domain) of individual magnetising characteristics for the magnetic branches and the magnetic circuit laws. A Newton-Raphson iterative procedure is also developed to accurately determine the non-linear distribution of the magnetic fluxes.

The influence of the magnetising characteristic approximation upon the harmonic solution is investigated. The adequacy of several approximations, including cubic splines, are assessed and Singular Value Decomposition have been explored to determine the equation parameters.

The widely accepted assumption of equally distributing the magnetising currents between the primary and secondary terminals is also investigated. For single-phase transformer models this assumption is shown to be inaccurate, at harmonic frequencies, and inadequate, for star-connected three-phase transformer models and improved harmonic distribution factors for the magnetising currents are proposed.

Three-phase three-limb electromagnetic transformer models for the most commonly used winding electrical configurations are derived, and the simulations results analysed by means of sensitivity analysis and comparisons with the practical and theoretical knowledge reported in the literature.

ACKNOWLEDGEMENTS

There are a number of people that I would like to acknowledge for their direct or indirect contribution to this thesis. First and foremost, my sincere thanks to my supervisor Professor Jos Arrillaga for his guidance, friendship and patience throughout the course of this work.

Many thanks are also due to Dr. Alan Wood. His patience and interest for countless discussions, advice, support and friendship have been invaluable. God bless you, Al.

I also wish to express my gratitude to Dr. M. Zavahir for his valuable suggestions at the early stage of this research and to Dr. Bruce Smith for many useful discussions, unconditional support and encouragement.

Special recognition is due to the Conselho Nacional de Ensino e Pesquisa-CNPq for the financial support of my Doctoral studies. Particular thanks to Drs. Oscar M. Astorga, J.C. de Oliveira, J. Campos-Barros, E. Watanabe and M. Szechtman for having encouraged me to pursue this further step in my career path.

Thanks also to the computing staff Mike Shurety and Dave Van Leeuwen and my postgraduate colleagues Simon Todd, Chen Zheng-Hong, Thomas Keppler, Dr. Chen Shiun, Dinh Nhut-Quang, Suo Li, Graeme Bathurst, Donna-Maree Ward, Matthew Hebley and Andrew Bain-Bridge Smith for their help and words of encouragement.

At the last stage of this thesis, the moral support provided by my friends Dr. Roger Brough, Dr. Melanie North, Tracey Watson, Jacqueline Ryan, Judith and Lou Macdonald saved me, for which I am very grateful. Angels do exist.

I would also like to express my deepest appreciation of my partner Stu's love and patience throughout the course of my study.

Finally, I wish to acknowledge the strong support and encouragement of my family during these years and throughout my life, particularly my father, Sebastiao Lisboa, to whom I humbly dedicate this work.

CONTENTS

LIST OF FIGURES

LIST OF TABLES

Chapter 1

INTRODUCTION

1.1 GENERAL

In ideal electric systems, loads would be supplied with a perfectly sinusoidal voltage of constant amplitude and frequency. In practice, however, the nonlinearity of power system components and loads causes waveform distortion, generally expressed in terms of harmonics, which can propagate throughout the power system. Inductive interference with telecommunication systems, overvoltages and excessive currents on the system resulting from parallel or series resonance at harmonic frequencies, degradation of protective relay performance and misoperation of electronic equipments are among the many problems associated with power system harmonics.

Studies of voltage and current waveform distortion in power systems date back to the beginning of this century, when transformers were the major sources of harmonics. With the increasing use of power electronics devices the harmonic problems are on increase. The change in equipment design philosophy also contributes to the problem: in order to be competitive, power plant equipments are more critically designed nowadays. In the case of iron core devices, they are designed to operate closer to the nonlinear regions, which can result in a sharp rise in harmonics [IEEE working group on power system harmonics 1983]. Harmonic distortion control is therefore a more complex problem now than in the past.

To try and maintain high standard of power quality, many utilities are establishing harmonic distortion limits at customer connections [Duffey and Stratford 1989] [Bradley *et al.* 1985]. Extensive research has been carried out to improve harmonic measuring techniques and instrumentation [Arrillaga 1981]. But, the interconnected nature and rapid expansion of power systems have increased the difficulties and cost of adequate harmonic monitoring systems.

Preventive actions are generally cheaper than corrective ones and hence, research has also been directed towards the development of analysis tools to be used at the planning stage of a power system. For economical and practical reasons, simulation based on digital computers helped by advances in numerical techniques, has become

a more convenient alternative to analyse the electric network behaviour than physical scale-down simulations.

System imbalance play an important part in the harmonic distortion, and therefore accurate harmonic prediction can only be achieved by modelling power systems in the phases [Arrillaga and Arnold 1990] or sequence components [Mahamoud and Schultz 1982] frames of reference.

Time domain simulation based on the trapezoidal integration technique [Dommel 1969] is widely used in power system transient analysis and can upon reaching the steady-state provide information of the harmonic distortion. However, a linearisation technique associated with a new frame of reference, called the Harmonic Domain, has been shown to be a more accurate and efficient tool for steady state harmonic analysis [Acha *et al.* 1989]. In the Harmonic Domain, busbars, phases, harmonics and cross-coupling between harmonics are explicitly represented. Linear and linearised, non-linear components are represented by harmonic transfer admittances and Norton equivalents, respectively, and a solution is achieved through an iterative procedure based on the Newton-Raphson method. Several network components have already been modeled in the Harmonic Domain, including the power converter [Smith 1995].

1.2 NEED FOR ACCURATE TRANSFORMER MODELS

Transformer is one of the contributors to the harmonic current production and is certainly affected by its consequences. Standard ANSI/IEEE C57.12.00-1987 [C57 distribution, power and regulating transformers standards 1990] states that power transformer should not be expected to carry harmonic load currents exceeding 5 percent of rating. However, this standard is rarely followed in practice, nonlinear loads being routinely connected to the power system with little regard to their harmonic currents[Bishop *et al.* 1996].

The presence of harmonic overvoltages can cause a complete transformer failure as a result of insulation breakdown. Although a complete failure is more likely to occur in transient conditions, cases have been reported where they occurred during quiescent system conditions [Lee and Schneider 1989].

In the northern hemisphere, geomagnetically induced currents (GIC) due to magnetic storms can enter a power system by way of grounded wye transformers causing half-cycle saturation and therefore extremely large harmonic content in the exciting currents. Transformer dc saturation caused by GIC although is extremely unusual, it can persist for extended periods of minutes or hours [IEEE transmission and distribution committee 1993]

The failure of a large power transformer is a costly event both in terms of equipment and undelivered energy prior to its replacement. A large number of transformer failures

has been reported in recent years causing concern among power utilities and manufacturers [CIGRE Working group 05 of study commitee 12 1983]. A re-evaluation of the adequacy of simulation techniques and current level of understanding of transformer-system interaction has become a subject of major importance [Morched *et al.* 1996].

The evaluation of transformer-system harmonic interaction at the planning stage is extremely valuable for both power utilities and manufacturers: transformer design modifications could then be made ahead of the transformer construction and the risk of field failure minimised. For this analysis to be effective, both system and transformer models must be accurate. Although the transformer is one of the most familiar power system components, it is also one of the most difficult to model accurately. Difficulties in its modelling stem from the fact that some of the transformer parameters are both nonlinear and frequency dependent. For transient analysis, accurate representation of the iron core losses due to saturation as well hysteresis and eddy currents must be taken into account; however, for steady state analysis, hysteresis and eddy currents can be neglected considering the level of voltages and narrow hysteresis loops of modern power transformers.

Various transformer models with different levels of accuracy are currently used for analysis and design of transformers. These models are based either on physical layout and construction details of the transformer or on input-output behaviour. For power system analysis, the former approach suffers from unavailability of some data parameters, which are considered proprietary by transformer manufacturers. The use of external characteristics is restricted by the difficulty in measuring some of the parameters and often have to rely on practical experience.

1.3 THESIS OUTLINE

The main objective of this work is to derive an electromagnetic transformer model which accurately takes into consideration the core geometry and also the different winding electrical configurations.

Chapter 2 introduces the fundamental concepts of the three-phase transformer harmonic behaviour. The influence of the windings electrical configuration, iron core geometry and external system impedance upon the transformer harmonic response is analysed in detail.

Chapter 3 presents the general formulation of the Harmonic Domain and its application.

In Chapter 4, the influence of the magnetising characteristic representation upon the harmonic solution is thoroughly investigated. Simulations using the Harmonic Domain algorithm are carried out using the most commonly used magnetising characteristic representations and their adequacy assessed. Singular Value Decomposition is

used to determine the rational-fraction and hyperbola coefficients. Representation of the magnetising characteristic by cubic splines is also explored.

Chapter 5 proposes a new three-phase three-limb transformer model. The magnetic circuit is described by harmonic Norton equivalents, derived from the Harmonic Domain linearisation of the iron core magnetic non-linearities, with the core geometry adequately taken into account. The electric circuit is represented by leakage admittances, and a composite electromagnetic transformer model is developed. An iterative procedure based on the Newton-Raphson's method is used to determine an accurate distribution of the fluxes among the various magnetic branches. Several cases are analysed and the solutions verified against time domain simulations.

The widely accepted assumption of equally distributing the magnetising branches between the transformer terminals to derive a π-equivalent transformer model is discussed in Chapter 6. The inadequacy of this assumption is assessed with respect to single-phase and three-phase transformer connections. Improved harmonic distribution factors are proposed to derive more accuratet π-equivalent harmonic transformer models.

Chapter 7 develops three-phase transformer models for the most commonly used winding electrical configurations. Particular attention is paid to the modelling of zero-sequence voltages in star-connected transformers with ungrounded neutral.

Finally Chapter 8 summarises the work presented in this thesis, and offers suggestions for further research.

Chapter 2

FUNDAMENTAL CONCEPTS

2.1 INTRODUCTION

In three-phase power systems the main effect of the transformer connection and core configurations relates to the presence of zero sequence voltage and current components. These are thoroughly discussed in the literature for the fundamental frequency and third harmonic (i.e. for symmetrical three-phase systems), though mainly with empirical models.

The increasing presence of power electronic devices is producing a multitude of characteristic and uncharacteristic harmonics of different sequences. In the case of single-phase loads, triplen harmonics are still the main zero sequence components. The three-phase converters do not produce zero sequence harmonics, although they can generate positive sequence triplens under asymmetrical conditions[Arrillaga *et al.* 1985]. Moreover, due to transmission system asymmetry, the converter positive and negative sequence currents also give rise to zero sequence content along the line (not just at triplen but all existing harmonic frequencies) [Wood, A.R. 1993]. It is thus important to consider the accuracy of existing and proposed transformer models to represent zero sequence behaviour.

As an introduction to the rest of the work, and to provide a better understanding of the results, this chapter emphasizes the fundamental concepts that influence the zero sequence behaviour of three-phase transformers.

2.2 OVERVIEW OF THE TRANSFORMER ZERO SEQUENCE HARMONIC RESPONSE

In three-phase electric systems, the zero sequence harmonic transformer response will be largely dependent on the method of connection and core configuration. Transformer windings are generally connected either in star or delta arrangements. The former imposes that the sum of the currents flowing to and from the neutral is zero, while the latter imposes that the sum of the voltages round the delta closed path is zero. If

the three-phase electric system is symmetrical, these restrictions affect only the triplen harmonic voltages and currents as they are all in phase with one another; however in asymmetrical systems, all zero sequence frequencies are affected.

Multilimb iron-cores have interlinked magnetic circuits, which are subjected to similar laws as an electric circuit. Thus, for similar reasons, the core configuration can affect only the zero sequence harmonic variables. In three-limb transformers, the magnetic path for the zero sequence harmonic fluxes involves the air, while for five-limb core type or three-phase bank of single-phase transformers, these harmonic fluxes remain inside the iron core. The difference between the air path and iron core magnetic branch reluctance is large, and consequently the iron core configuration should affect the transformer harmonic response. Thus the development of an accurate three-phase three-limb transformer model is mainly justified for the solution of zero sequence harmonic problems.

As a consequence of the varying permeability of the iron core, the magnetising current required to produce a sinusoidal voltage at the transformer terminals cannot be purely sinusoidal, but includes odd harmonics. If any of these harmonic components of the magnetising current are suppressed, the voltage waveform must become distorted. This effect is illustrated in Figure 2.1, and is the key factor in the zero sequence harmonic response of three-phase transformers. For a better understanding, the analysis is restricted at this stage to the third harmonic, caused by transformer saturation in symmetrical three-phase systems. For simplicity, the zero sequence third harmonic will be referred to in this work as the third harmonic.

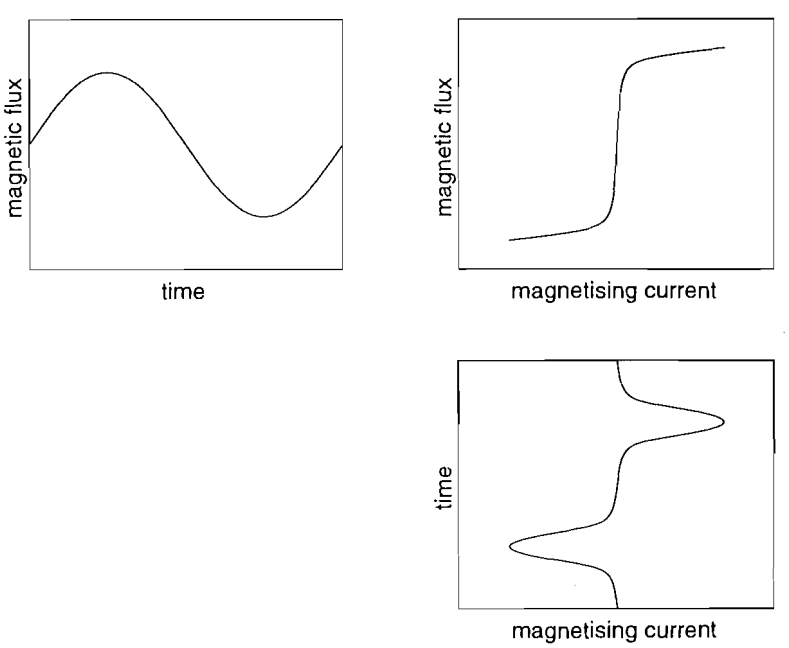

Figure 2.1 Magnetic flux and magnetising current relationship

2.2.1 Basic transformer connections

The two basic connections of a three-phase winding set are star and delta. In star-connected transformers, schematically illustrated in Figure 2.2, no third harmonic currents can flow, and the magnetising currents can no longer induce a truly sinusoidal magnetic flux in each phase, but rather one containing third harmonics (i.e flat-topped waveform [Stigant *et al.* 1941]). Therefore, the corresponding e.m.f. will also be distorted, and the potential of the neutral point will oscillate around the zero point at third frequency. However, line-to-line voltages are free from third harmonics as third harmonic voltage induced across each winding are all in phase, and therefore cancel out between lines. If a path for the third harmonic currents is provided, e.g. by connecting the transformer neutral to the generator neutral, the voltage distortion may be eliminated, but at the expense of third harmonic current flow.

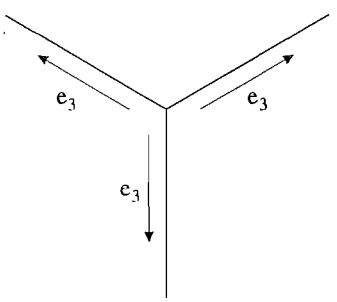

Figure 2.2 Star connection

In delta-connected transformers, illustrated in Figure 2.3, third harmonic voltage can not exist, but third harmonic currents can circulate round the delta.

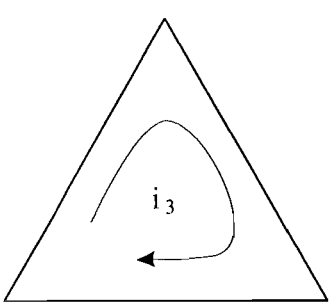

Figure 2.3 Delta connection

Star connection with a tertiary delta connected winding and star-delta connections are used to take advantage of each of these connections as regards costs, flexibility and harmonic response. Some of these schemes are described next.

2.2.1.1 Star-Star

Figure 2.4 shows a star-star connected transformer with ungrounded neutrals. In this case, no third harmonic currents flow. As described earlier, the suppression of this harmonic component from the magnetising currents causes voltage harmonic distortion in the transformer windings, its magnitude being entirely defined by the applied voltage at the transformer terminals, and the magnetising characteristic.

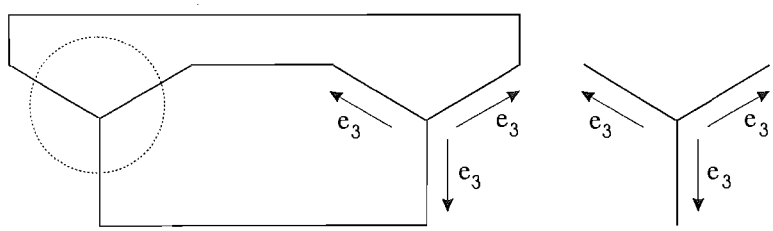

Figure 2.4 Star- Star connected transformer

The induced third harmonic voltage inherent in the star connected transformer, may be eliminated by providing a path for the third harmonic currents, e.g. earthing the secondary neutral, as shown in Figure 2.5. A third harmonic circuit can be completed on the secondary side, through shunt capacitance, if the secondary windings are connected to a transmission line, or through the load neutral. The currents will then flow from the transformer through the neutrals, transmission line and/or load impedance, and back to the transformer. These currents when flowing through the secondary windings will produce third harmonic fluxes on their own which will interact with those originally produced on the primary side. This interaction can result in a total or partial elimination of the original third harmonic flux, or can greatly increase it, depending on the currents' phase relationship[Stigant *et al.* 1941].

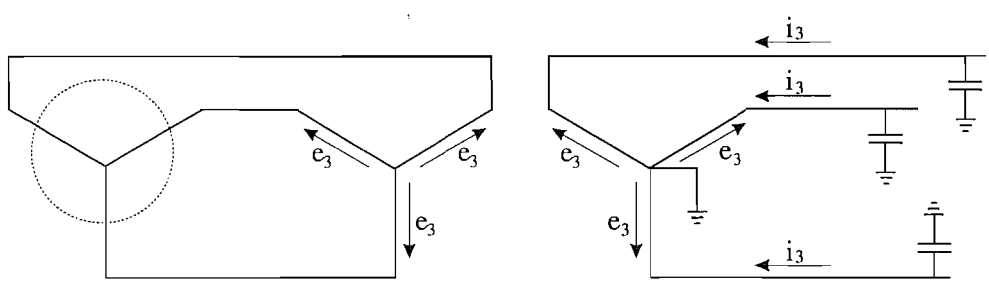

Figure 2.5 Star- Star-G connected transformer

The phase is determined by the total third harmonic impedance on the secondary side, which can be inductive, capacitive or resistive. The influence of the external system impedance upon the the original third harmonic flux is next described with the help of phasor diagrams.

Consider the case of a star/star-grounded connected three-phase transformer as illustrated in Figure 2.6, with only the third harmonic variables involved.

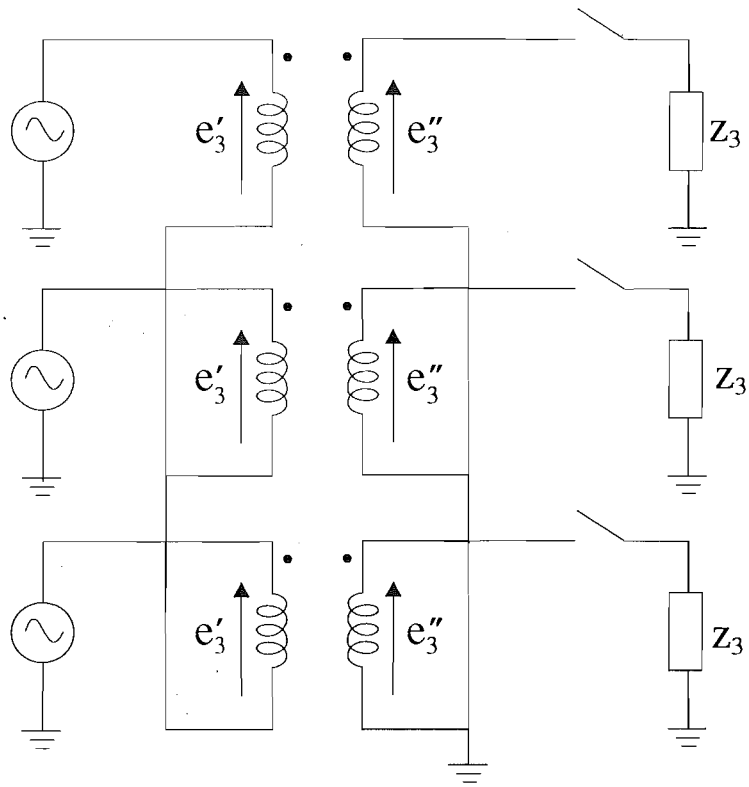

Figure 2.6 Star- Star/grounded connected transformer

A third harmonic e.m.f. (e'_3) appears across each primary winding, as third harmonic current cannot flow on this side, its magnitude being entirely defined by the generator applied voltage and the iron core magnetising characteristic. The third harmonic flux associated with this e.m.f. induces a corresponding third harmonic e.m.f. (e''_3) on the secondary windings, which has the same magnitude of e'_3 if the transformer is open-circuited. However, if a load is connected on the secondary side, third harmonic currents will flow, and they will produce third harmonic fluxes on their own which will interact with those originally defined on the primary side, and consequently will change both the primary and secondary winding e.m.f.'s.

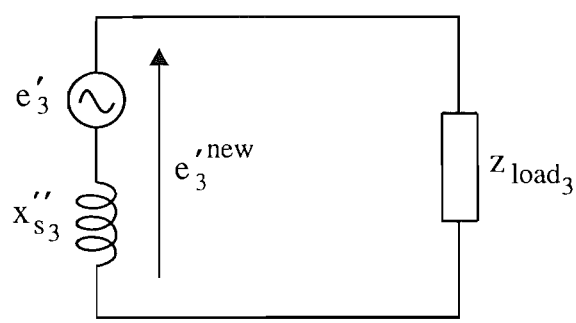

Figure 2.7 Transformer secondary side equivalent circuit

Considering the original third harmonic e.m.f. e'_3 as a constant third harmonic

voltage source applied on the secondary side, the interaction between primary and secondary sides can be described by the circuit illustrated in Figure 2.7.

From the above circuit, the following equations can be written:

$$e'_3{}^{new} = e'_3 - jx''_{s_3}.i''_3 \tag{2.1}$$

$$i''_3 = \frac{e'_3}{z''_{load_3} + jx''_{s_3}} \tag{2.2}$$

where

e'^{new}_3 : Resultant third harmonic e.m.f,
i''_3 : Secondary third harmonic current,
z''_{load_3} : Secondary third harmonic load impedance
(it includes the transformer secondary leakage reactance x''_l),
x''_{s_3} : third harmonic reactance of transformer secondary self inductance.

Eliminating i''_3 between (2.1) and (2.2),

$$e'_3{}^{new} = \frac{z''_{load_3}}{z''_{load_3} + jx''_{s_3}} e'_3, \tag{2.3}$$

or

$$e'_3{}^{new} = \frac{1}{1 + (jx''_{s_3}/z''_{load_3})} e'_3. \tag{2.4}$$

These equations yield the following phasor diagrams.

- Inductive load

  Assuming a purely inductive circuit and using the vector e'_3 as a reference, the current lags the induced voltage by 90 degrees (equation (2.2)) and the e.m.f. produced by the third harmonic current, i.e. $-jx''_s i''_3$ in equation (2.1), will be in opposite direction of e'_3, thus reducing it. The reduction is proportional to the load current, i.e. the smaller the load impedance the larger is the reduction. Thus, a complete elimination of e'_3 only occurs if z''_{load_3} is equal to zero. Considering that z''_{load_3} includes the inductive load and the secondary leakage reactance, in practice, its value is never equal to zero (the minimum value being equal to x''_l when load impedance is equal to zero) and therefore, there is always a residual third harmonic in both transformer terminals. Note that when the load impedance is equal to zero, this condition correspond to a delta-connected secondary windings . The phasor diagram is illustrated in Figure 2.8, and equation (2.4) becomes

$$e'_3{}^{new} = \frac{1}{1 + (x''_{s_3}/x_{load})} e'_3 \tag{2.5}$$

$$x_{load} \to 0, \text{ then } e'_3{}^{new} \to 0$$
$$x_{load} \to \infty, \text{ then } e'_3{}^{new} \to e'_3$$

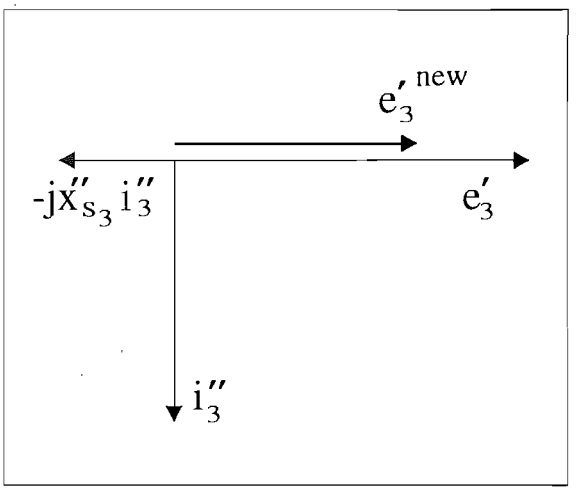

Figure 2.8 Inductive secondary circuit

- Capacitive load

A capacitive load may amplify considerably the original third harmonic e.m.f., leading the transformer deeper into saturation. In this case equation 2.4 becomes

$$e'_3{}^{new} = \frac{1}{1 - (x''_{s_3}/x_{load_3})} e'_3 \tag{2.6}$$

Two cases need to be considered:

i) load reactance larger than the reactance of the self inductance

This case is illustrated by the phasor diagram of Figure 2.9. and from equation (2.6)

$$|x_{load_3}| \to |x''_{s_3}|, \text{ then } e'^{new}_3 \to \infty$$
$$|x_{load_3}| \to \infty, \text{ then } e'^{new}_3 \to e'_3$$

ii) load reactance smaller than the reactance of the self inductance

In this case, amplification may also occur, however the resulting third harmonic voltage will be in anti-phase to the original e'_3 as illustrated by phasor diagram

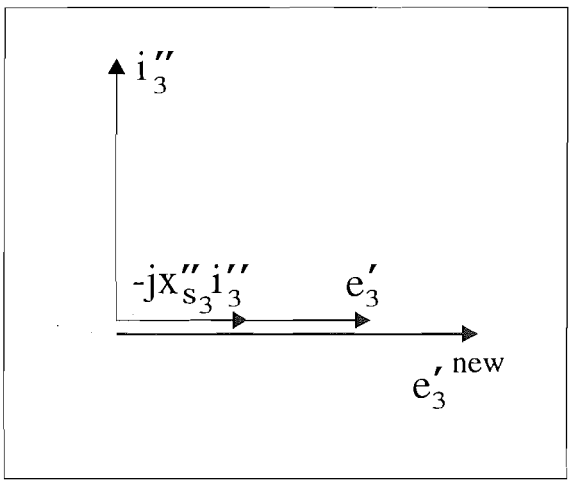

Figure 2.9 Capacitive secondary circuit - case i)

of Figure 2.10. This change of phase has not been reported so far in the literature.

$$|x_{load}| \to 0, \text{ then } e_3'^{new} \to 0$$
$$|x_{load}| \to |x_s''|, \text{ then } e_3'^{new} \to -\infty$$

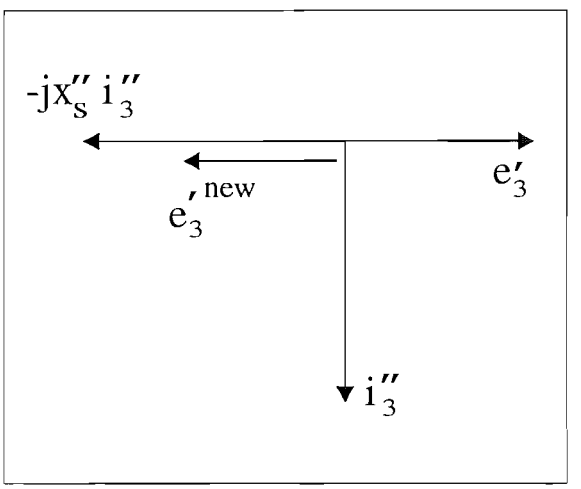

Figure 2.10 Capacitive secondary circuit - case ii)

In both cases, the amplification of the third harmonic voltage occurs when the load capacitance is close to the transformer self inductance, i.e. close to the resonant point.

- Resistive load

$$e'_3{}^{new} = \frac{1}{1 + (jx''_{s_3}/R_{load})} e'_3 \tag{2.7}$$

Similar to the previous analysis, equation (2.7) leads to the phasor diagram of

Figure 2.11.

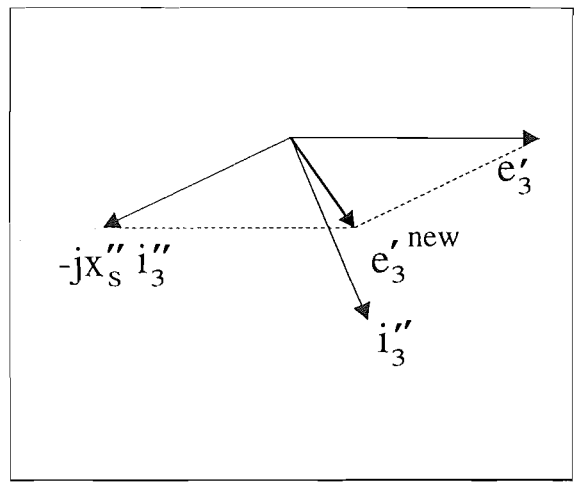

Figure 2.11 Resistive secondary circuit

2.2.1.2 Star-Delta connection

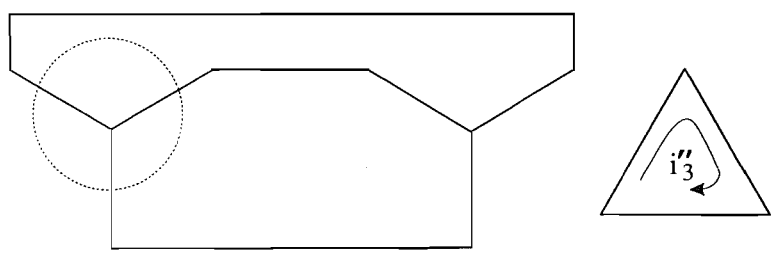

Figure 2.12 Star- Delta connected transformer

As described previously, the star-connection introduces third harmonic flux which circulates round the core and as a consequence, third harmonic voltages will be induced on both primary and secondary sides. As the latter is delta-connected, the induced third harmonic voltages will be short-circuited through the corresponding leakage reactances and hence third harmonic currents will flow. These currents have a demagnetising effect upon the original third harmonic flux and as a result, the induced third harmonic voltages may be reduced to negligible values, depending on the secondary leakage reactances. A schematic diagram of this connection is illustrated in Figure 2.12.

If the primary neutral is grounded, a third harmonic closed path will exist also on this side, and in this case the third harmonic magnetising currents will divide between both circuits in inverse proportion to their third harmonic impedances. A larger proportion of the third harmonic currents usually will flow inside the delta, as the primary impedance includes the generator, transmission lines and neutral impedances.

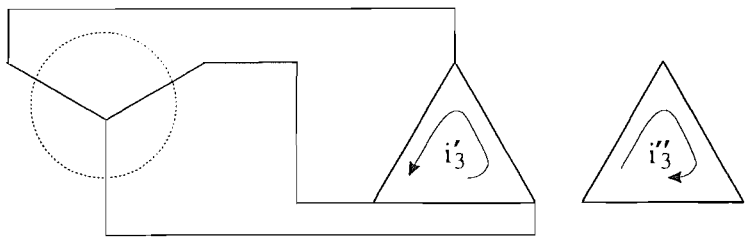

Figure 2.13 Delta-Delta connected transformer

2.2.1.3 Delta-Delta connection

The third harmonic magnetising currents will split between primary and secondary closed delta circuits in inverse proportion to their corresponding leakage impedances. Both sides will be free from third harmonic fluxes and induced voltages. Delta-delta connection has the disadvantage of not offering a neutral point, so that it can not be used to supply phase-to-ground loads.

2.2.2 Core configuration

Figure 2.14 illustrates the three types of iron core configuration most commonly used for three-phase transformers, with the dotted lines indicating the zero sequence flux path. As the magnetic circuit is subjected to similar laws as the electric circuit (Kirchoff's laws), the magnetic flux distribution for three-limb transformers will be quite different from that of single or five-limb core type transformers.

Gauss's law implies that the sum of all harmonic fluxes flowing into or from a node must be equal to zero. As the zero sequence harmonic fluxes are all in phase in each of the three phases, in a three-limb transformer their sum will not be zero at any node if the magnetic circuit is exclusively restricted to the iron core branches, i.e. the zero sequence harmonic fluxes have to complete their paths through the 'air' (i.e. tank and oil). The 'air' reluctance is much larger than the iron core magnetic paths, and hence the resulting zero sequence harmonic fluxes and corresponding induced voltages may be significantly different from those of other core configurations.

If the transformer is *star-connected with grounded neutral*, the transformer zero sequence harmonic response will be defined not only by the zero sequence magnetic path reluctance, but also by the external system impedance and origin of the third harmonic currents (i.e. if they come from the transformer saturation or generated by other external nonlinear devices). These two aspects are analysed next.

2.2.2.1 Third harmonics coming from transformer saturation

To analyse the influence of the core configuration and external system impedance upon a star-connected transformer zero sequence harmonic response, consider an open circuited

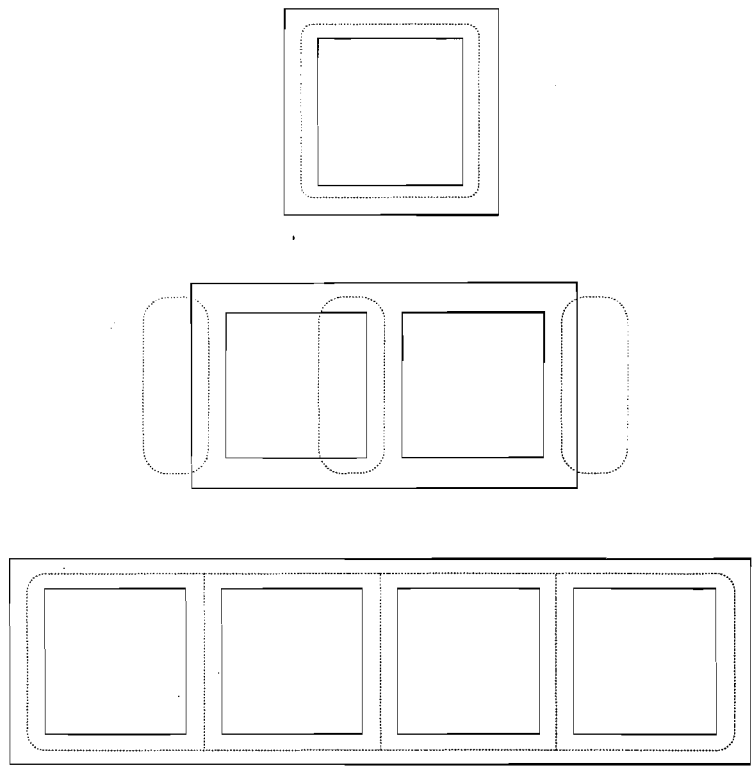

Figure 2.14 Three transformer core configurations

transformer being supplied by a voltage source through an impedance, as illustrated in Figure 2.15.

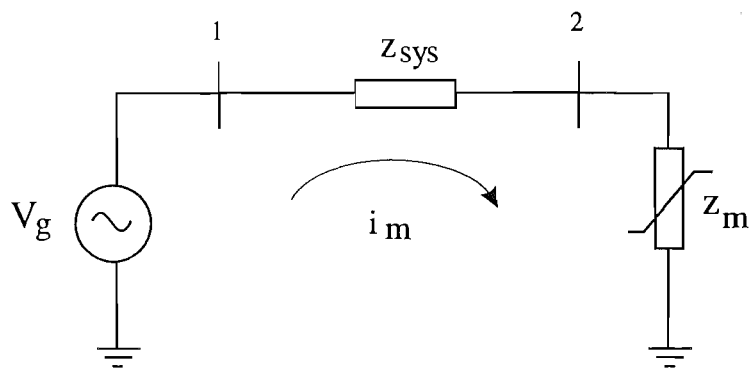

Figure 2.15 Third harmonic circuit (i)

Assume that the harmonic distortion due to transformer saturation takes place in two successive stages. First, consider an ideal voltage source directly applied to the primary terminals of a transformer with no leakages, so that the harmonic currents are entirely defined by the magnetising characteristic. In this case, the transformer primary voltages are purely sinusoidal and the magnetising currents consisting of fundamental and odd harmonics. Then, inserting the generator and transformer impedances, the magnetising currents will flow through the primary circuit and harmonic voltages will appear on the transformer terminals. The magnitude of the third harmonic voltages

will depend on the total harmonic impedance, i.e external system and transformer impedances. As the external system harmonic impedance can be either capacitive, inductive or resistive, the third harmonic current phase can be lagging, leading or in phase with the original third harmonic magnetising currents ($im_3(\phi_1)$).

From the circuit of Figure 2.15, the third harmonic voltage drop across the external system impedance can be expressed by the following equation

$$V_{1_3} - V_{2_3} = im_3(\phi_1) z_{sys_3} \tag{2.8}$$

or,

$$V_{2_3} = -im_3(\phi_1) z_{sys_3} \tag{2.9}$$

as the third harmonic voltage at the generator busbar is equal to zero (the subscript 3 denotes third harmonic quantities, and ϕ_1 the fundamental frequency flux equivalent to the generator applied voltage).

By Faraday's law, the integration of voltage V_{2_3} gives the third harmonic flux ϕ_3, which produces the following mmf drop

$$im_3(\phi_3) = \mathcal{R}(\phi_3)\phi_3 \tag{2.10}$$

where $\mathcal{R}(\phi_3)$ depends on the core configuration. For three-limb core transformers, $\mathcal{R}(\phi_3)$ is the 'air' reluctance while for a three-phase bank of single-phase transformers, it is the iron core reluctance. Taking into consideration equations (2.9) and (2.10), the influence of the external circuit impedance and core geometry upon the transformer third harmonic response can be analysed as follows.

i)Inductive circuit

If the circuit impedance is purely inductive, the transformer third harmonic voltage V_{2_3} is given by

$$V_{2_3} = -im_3(\phi_1)(jx_{sys_3}) = -j\Big(im_3(\phi_1)x_{sys_3}\Big)$$

Thus, the third harmonic voltage is lagging the current $im_3(\phi_1)$ by ninety degrees. By Faraday's law, integrating this voltage yields a third harmonic flux (ϕ_3) which lags the voltage by 90 degrees, thus lagging the current $im_3(\phi_1)$ by 180 degrees. This flux flowing through the magnetic circuit, produces a mmf drop $im_3(\phi_3)$ which is proportional to $\mathcal{R}(\phi_3)$ (equation (2.10)), and with the same phase.

Taking the magnetising current $im_3(\phi_1)$ as reference, the following phasor diagram can be derived.

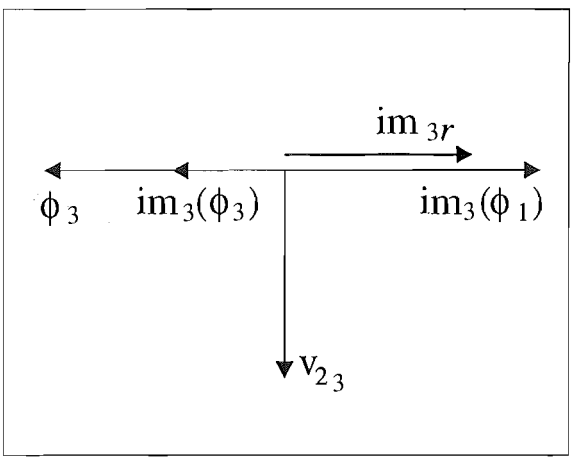

Figure 2.16 Inductive external circuit phasor diagram

The resulting third harmonic current im_{r_3}, illustrated in the phasor diagram of Figure 2.16, is given by

$$im_{3_r} = im_3(\phi_1) + im_3(\phi_3)$$

As the current $im_3(\phi_3)$ is proportional to the branch magnetic reluctance, the resulting third harmonic current tends to be smaller for three-limb transformers.

ii)Capacitive circuit

If the circuit impedance is purely capacitive

$$V_{2_3} = -im_3(\phi_1)(-jx_{sys_3}) = j\left(im_{3h}(\phi_1)x_{sys_3}\right)$$

In this case, the third harmonic voltage is leading the magnetising current $im_3(\phi_1)$ by ninety degrees. Integrating voltage V_{23}, a third harmonic flux ϕ_3 is produced which leads the voltage by 90 degrees, thus leading the current $im_3(\phi_1)$ by 180 degrees. The corresponding phasor diagram is illustrated in Figure 2.17, which clearly indicates that resulting third harmonic current for three-limb transformer must be larger than for a three-phase bank of transformers. This condition has not been reported in the literature.

c)Resistive circuit

Similarly to the other two previous cases, for resistive circuits the voltage V_{2_3} is given by

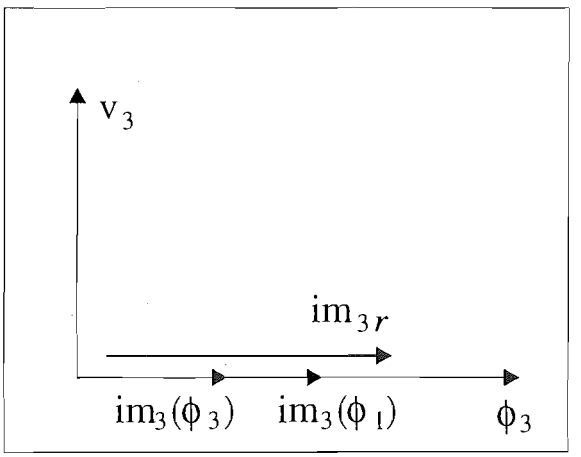

Figure 2.17 Capacitive external circuit

$$V_{2_3} = -im_3(\phi_1)R_{sys} = j\left(im_3(\phi_1)R_{sys}\right)$$

and the corresponding phasor diagram is shown in Figure 2.18. In this case, the difference between a three-limb transformer and a three-phase bank of single-phase transformers will not be significant.

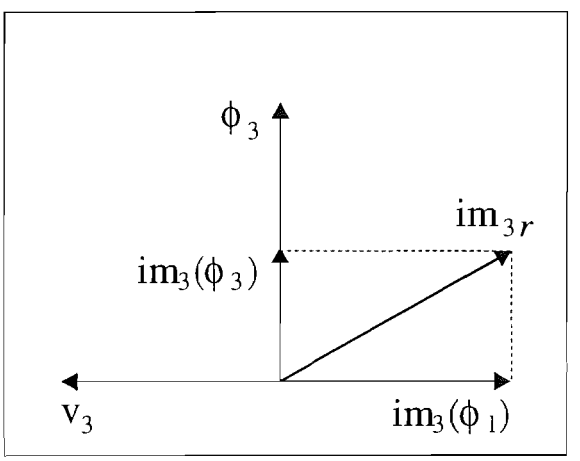

Figure 2.18 Resistive external circuit phasor diagram

2.2.2.2 Third harmonic currents being injected into the transformer

Nonlinear devices other than transformers can also generate zero sequence harmonic currents, which will flow throughout the system if a closed path for them to flow is provided. The transformer connection will represent an open or closed switch for these currents, i.e. if they are injected to a transformer side which is delta or star connected with no neutral, there will be no closed path for them to flow (the transformer

connection represents an infinite zero sequence impedance for the external system). On the other hand, if these currents are injected to a transformer side which is star-connected with neutral, a closed path through the neutral point is provided . In this case, the transformer harmonic zero sequence response will depend on the core configuration, external system impedance as well as the magnetising characteristics.

Considering the external system nonlinear device represented by a voltage source, the zero sequence circuit can be described as that of Figure 2.19.

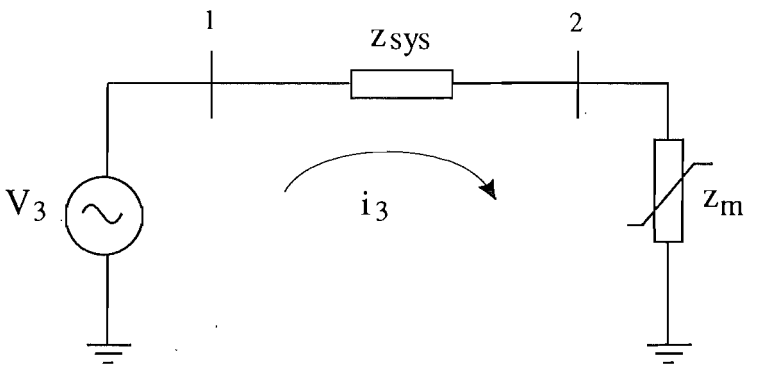

Figure 2.19 Third harmonic circuit (ii)

Under unsaturated conditions, the third harmonic reactance x_{m_3} is much smaller for a three-limb core transformer than for of a three-phase bank of single-phase units ($L_m = \frac{N^2}{\mathcal{R}}$, the air path reluctance being much larger than the iron core branch reluctance). Consequently, if the circuit is mainly inductive, the zero sequence current flowing through the circuit will be much larger for a three-limb transformer: the transformer acts if it were a filter, draining the injected zero sequence harmonic currents. The influence of the core configuration upon the transformer harmonic response is quite the opposite to the case where the zero sequence harmonics come from the transformer saturation, analysed in the previous section.

The corresponding harmonic voltages at the transformer terminals will depend on the transformer magnetising branch and external system impedance and can be determined by the following equation.

$$V_{2_3} = \frac{jx_{m_3}}{jx_{m_3} + z_{sys_3}} V_{1_3} \tag{2.11}$$

If the transformer is operating under saturation condition, the harmonic response will be defined by the superposition of the two effects: zero sequence harmonics coming from the external system and the ones coming from the transformer saturation. In this condition, the reactance x_{m_3} (i.e zero sequence flux path reactance) of a three-phase bank of single-phase units will be that of a saturated iron core, which may be larger than that of a three-limb transformer.

2.2.2.3 Reference basis for comparison between three-limb transformer and three-phase bank of single-phase transformers models

To assess the differences between the harmonic solution using three-limb core and three-phase bank of single-phase transformer models, it is of fundamental importance to define an appropriate basis for comparisons. Both models must have equivalent data, so the solution differences that may be found would be exclusively due to the transformer modelling differences. It has been proposed in previous work [Medina and Arrillaga 1992] to use the $\phi - i$ magnetising characteristic for the single iron core of a three-phase bank equal to the main branch of a three-limb transformer. However, this assumption is not adequate as it implies a larger amount of iron for the three-limb transformer, i.e. besides the main branches, additional iron is taken into account in the yoke branches. (Note that the $\phi - i$ characteristic includes the core geometry). Consequently, this assumption leads to larger values of magnetising currents for the three-limb transformer model and hence, an unfair basis for comparison of the harmonic solutions from both models.

Equivalent cores for both models can be achieved by assuming equal $\phi - i$ characteristic for the single core and the main branches of the three-limb core (l_m= 2a+2b in Figure 2.20) *and* also defining the yoke length (l_y) equal to zero, i.e. a linear characteristic with the slope equal to infinity. Similar assumptions have been used earlier [Rajakovic and Semlyen 1989] and the simulation results would only indicate the differences due to the different zero sequence magnetic path in one and another model.

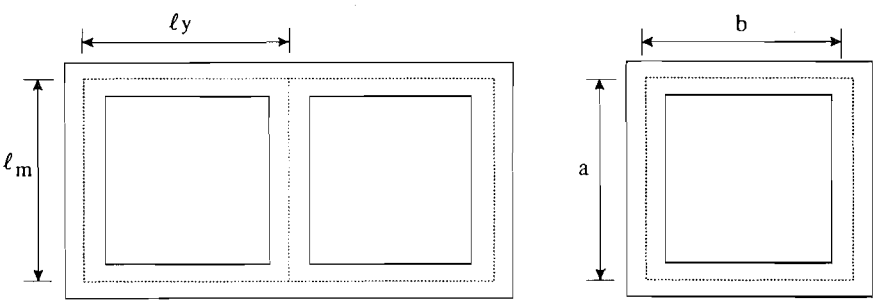

Figure 2.20 Single and three-limb transformers

2.2.3 Numerical examples

Simulations with the Harmonic Domain Analysis (HDA) program have been carried out to assess the harmonic response differences between a three-limb transformer (proposed in Chapter 5) and a three phase bank of single phase transformer models [Acha *et al.* 1989]. The HDA program consists of an iterative procedure based on Newton's method, described in detail in Chapter 3.

The magnetising characteristics have been approximated by hyperbolae (the mathematical formulation is given in Chapter 4) with the parameters described in Appendix B. These parameters correspond to two straight lines based on the slopes of the saturated and unsaturated regions of the experimental magnetising characteristics given in [Dick and Watson 1981].

2.2.3.1 Example 1

The test system consists of a secondary open circuited transformer connected to a generator through a series impedance of 0.1 (p.u.) and a shunt capacitance of 0.6 (p.u.) on the primary side(grounded-star / grounded-star transformer electrical configuration). To assess the influence of the third harmonic external impedance, a variable third harmonic shunt reactance has been added on the primary side. By varying this shunt reactance value, the third harmonic external impedance can be inductive, resonant, and capacitive. A shunt resistance of 1.0 (p.u.) is connected on the primary side to provide some damping for the resonant case and the generator voltage is equal to 1.1 (p.u).

Four sets of fifty simulations have been carried out by varying the third harmonic shunt reactance from -0.5 (p.u.) to 0.33 (p.u) (which is equivalent to vary the system shunt capacitance from -0.143 (p.u.) to -0.5 (p.u.)). A set of simulations has been carried out using the three-phase bank of single-phase transformers connected in grounded-star, grounded-star configuration, and the other three sets have used the three-limb core transformer model with the slope of the linear region (m_1) of the zero sequence flux path magnetising characteristic equal to 6.0 (experimental value given in [Dick and Watson 1981]), 1.0, and 0.1. The simulations included frequencies up to the 7th harmonic, using a tolerance of 0.0001 (p.u.) for the harmonic voltages.

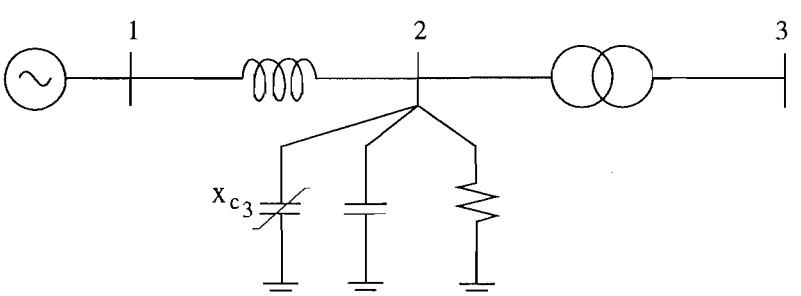

Figure 2.21 Test system

The third harmonic voltages at busbar 2, magnitude and phase angle, are illustrated in Figures 2.22 (a) and (b), respectively. As the three-limb transformer third harmonic impedance is different for different m_1 values, the resonance occurs at different values of third harmonic shunt capacitance. The total third harmonic impedance is

inductive for shunt capacitance values from -0.5 (p.u) until the resonant point, and after that the total third harmonic impedance is capacitive. The three-limb transformer model yields smaller distortion when the circuit is inductive and larger when the circuit is capacitive. However, the difference between the three-limb transformer with m_1 equal to 6.0 and the three-phase bank of single-phase transformers are extremely small. The difference increases if the zero sequence flux path reluctance increases, i.e. for smaller values of m_1.

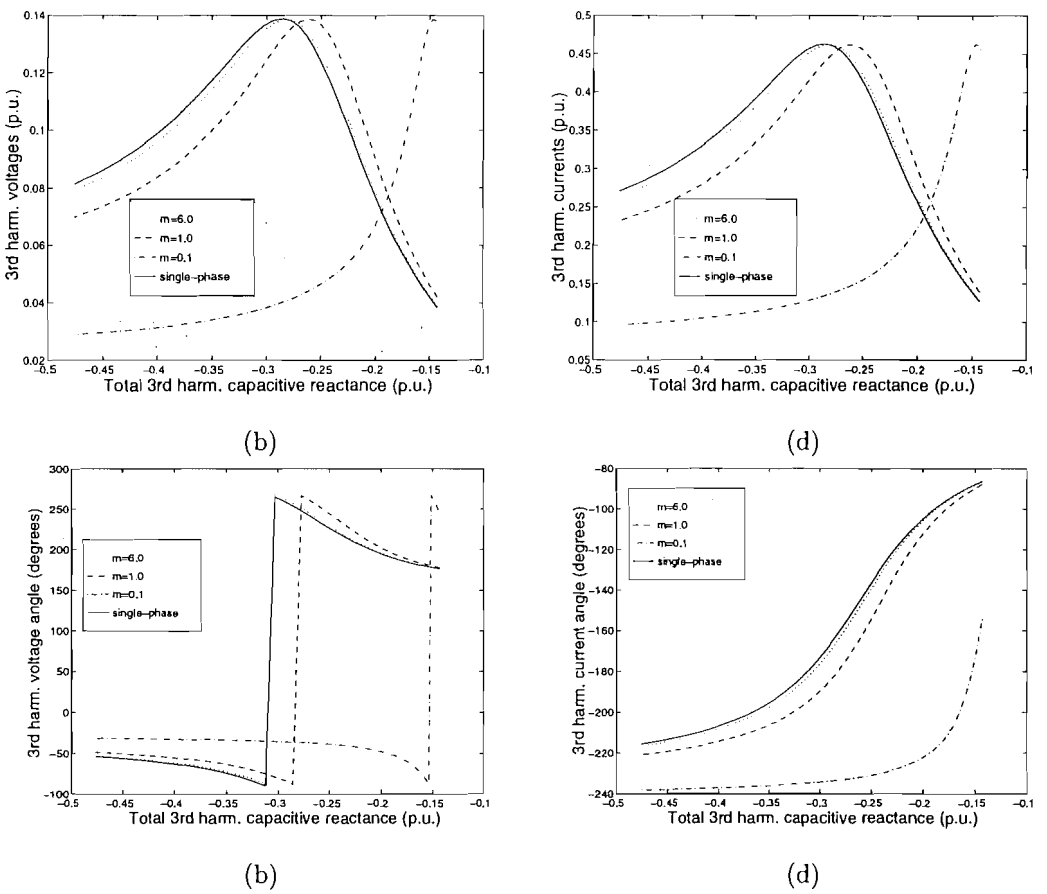

Figure 2.22 Third harmonic currents and voltages, phase A

2.2.3.2 Example 2

Simulations using three-limb core and three-phase bank of single-phase transformer models have been done using the test system shown in Figure 2.23, to assess the transformer harmonic response to an external zero sequence harmonic injection. The generator voltage and reactance are equal to 1.1 and 0.1 (p.u.), respectively. The remaining parameters are those described in the previous example.

Three cases have been analysed:

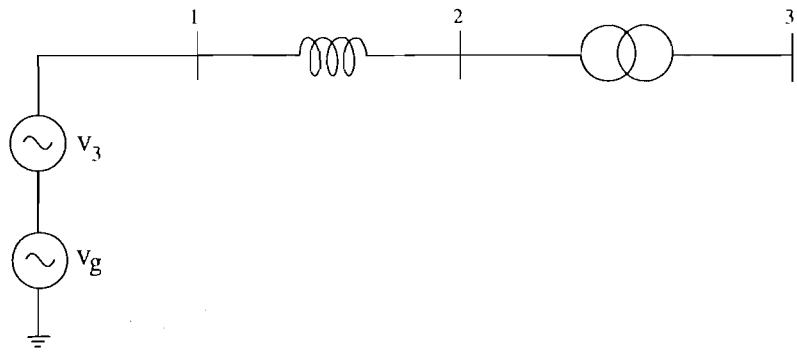

Figure 2.23 Test system 2

i) Unsaturated transformers with external third harmonic applied to 0.05 (p.u) (linear magnetising characteristic),
ii) Saturated transformers without external harmonic injection,
iii) Saturated transformers with external third harmonic applied voltage (0.05 p.u.).

Twelve simulations for each case have been carried out by varying the generator third harmonic reactance from 0.3 to 3.0 (p.u.). The three-limb transformer model has been analysed using two values for the slope of the zero sequence path magnetising characterisitc, i.e. m_1 equal to 1.0 and 6.0.

Figures 2.24 (a) and (b) illustrates the third harmonic phase A voltage and current on the primary side, for case (i). Due to the large third harmonic impedance of the unsaturated three-phase bank transformer, the third harmonic current flowing through the circuit is almost equal to zero. Thus, a negligible third harmonic voltage drop occurs across the generator impedance and consequently, third harmonic voltage at the transformer terminal is nearly equal to the third harmonic voltage source. For the three-limb core transformer, as the third harmonic generator impedance increases, the third harmonic current flowing on the primary side and also the voltage at the transformer terminal decrease. This effect is more noticiable for three-limb transformer with the slope of the zero sequence flux path equal to 1.0.

The third harmonic voltage and current on the primary side for the case (ii), are illustrated in Figures 2.24 (c) and (d), respectively. The explanation for these results are the same as those given in section 2.2.2.1, i.e. in this case, the transformer impedance x_{m_3} has a demagnetising effect, thus, smaller third harmonic voltage and current occurs for transformer with larger zero sequence reluctance (three-limb, m_1 equal to 1.0).

Figures 2.24 (e) and (f) illustrates the third harmonic voltage and current on the primary side for case (iii). With the superposition of both source of harmonics, the three-phase bank transformer present larger values of third harmonic voltage and current.

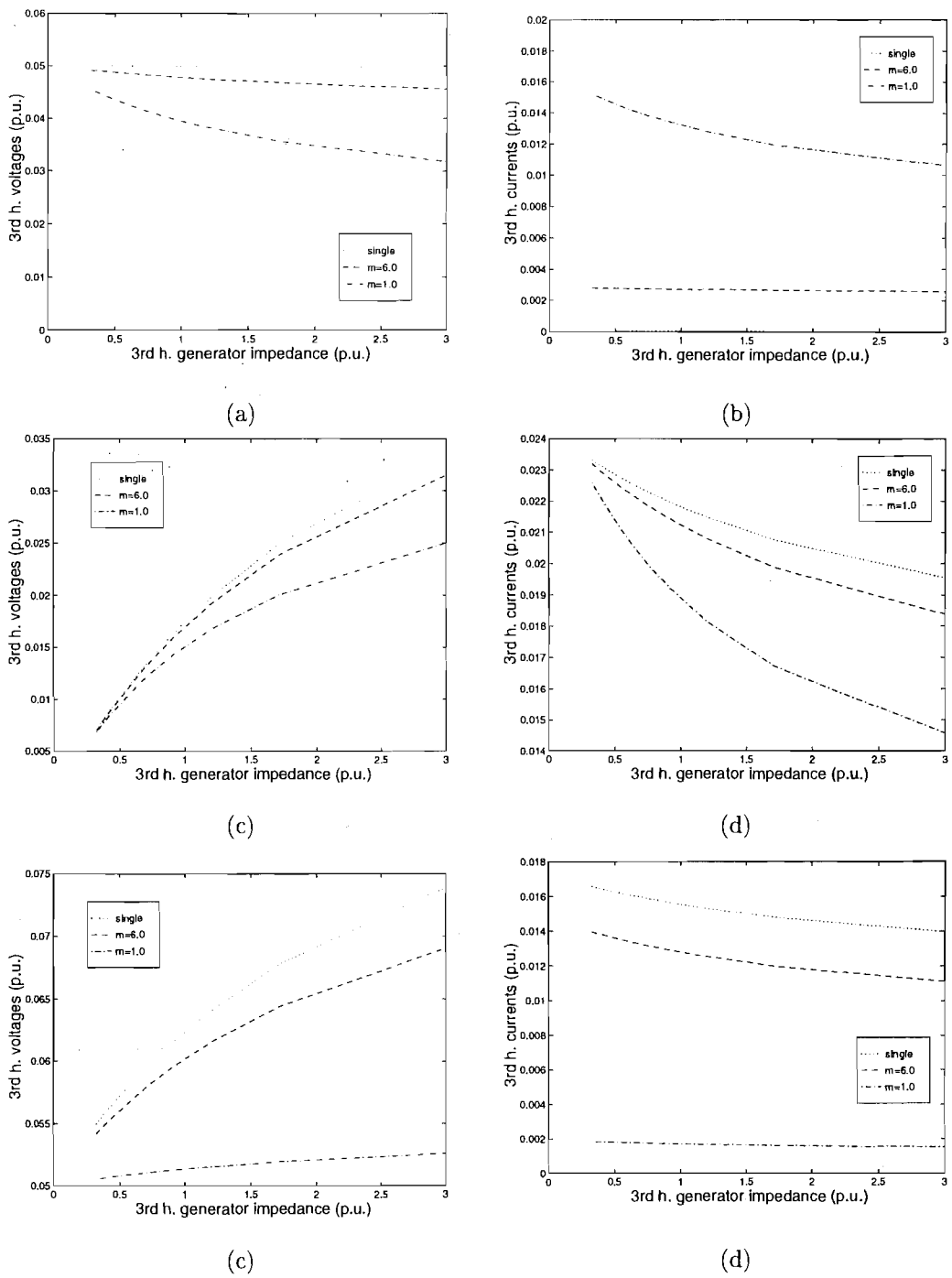

Figure 2.24 Third harmonic currents and voltages, phase A

2.3 CONCLUSIONS

The influence of the external system impedance, electrical and core configuration upon the overall transformer harmonic response has been described by means of phasor diagrams and sensitivity analysis. It has been shown that the core configuration defines the path for the zero sequence fluxes, and therefore its detailed representation is important in some cases, i.e for star-connected transformers. Considering the harmonics coming from the transformer saturation, the main conclusions are:

- If primary and secondary windings are star-connected and both neutrals are ungrounded, the triplen harmonic voltages will be greatly influenced by the core configuration, being smaller for a three-limb transformer.
- If primary and secondary windings are star-connected and one of the neutrals is grounded, the triplen harmonic voltages will be influenced by the core configuration as well by the external impedance connected to the grounded-star connected windings. In this case, the triplen harmonic voltages will be also smaller for a three-limb transformer.
- If one of the windings is star-connected and the other delta connected, the triplen harmonic voltages will basically limited by the delta-connected side leakage reactance. The influence of core configuration will be negligible in this case.

If both windings are grounded-star-connected, the triplen harmonic voltages will be function of the core configuration and the external system impedance at the third harmonic, and also function of the origin of the third harmonic currents. Restricting the analysis to the open-circuited secondary windings condition, it has been shown that if the third harmonic currents come from the transformer saturation and the external impedance at the third harmonic is inductive or resistive, smaller third harmonic voltages will result with a three-limb transformer. However, if the third harmonic external system impedance is capacitive, this type of transformer will lead to larger third harmonic voltages. Finally, if the third harmonic currents come from the external system, the transformer will act as a filter. In this case, three-limb transformers will drain a larger proportion of the third harmonic currents.

Chapter 3

POWER SYSTEM ANALYSIS IN THE HARMONIC DOMAIN

3.1 INTRODUCTION

In conventional power system steady state models the only active power sources are the generators, normally specified as voltages sources of a single frequency at their terminal busbar. Single-phase (symmetrical) studies are considered sufficient to analyse the fundamental frequency behaviour of the system.

The increasing presence of distorting elements in power systems requires accurate prediction of the harmonic content. Such prediction can not be achieved by conventional power system software. Two important considerations in the development of a suitable algorithm, for harmonic modelling, are the frame of reference and the nature of the sources.

Experience with field tests seems to indicate that the harmonic content in power transmission systems is always asymmetrical, and its prediction must therefore be carried out in the three-phase frame of reference.

Regarding the nature of the sources, a distinction needs to be made between the fundamental and harmonic frequencies. For the fundamental frequency the specification of the generators as voltages sources remains valid. At harmonic frequencies, however, the non-linear components (including the salient pole generators) act as current harmonic sources as well harmonic sinks.

A general frame of reference suitable for the harmonic solution of power systems has been derived based on the concept of complex-conjugate harmonic space [Acha *et al.* 1989]. This frame of reference, called the Harmonic Domain (HD), allows the representation of the mutual effects between phases and the cross-coupling between the harmonic frequencies. Besides, voltages and current sources of different frequencies can be simultaneously taken into account. By means of linearisation in the Harmonic Domain, nonlinear components can be described in the form of harmonic Norton equivalents [Semlyen *et al.* 1987a], which allows the harmonic solution for the entire system

to be determined through an iterative procedure based on the Newton's method.

The purpose of this chapter is to describe this frame of reference and its application.

3.2 ANALYSIS IN THE HARMONIC DOMAIN

The three main components in the Harmonic Domain are:

i) the harmonic phasor representation,
ii) the linearisation process,
iii) the unified Newton solution.

Those are described in the following sections.

3.2.1 Harmonic phasor representation

A periodic function $f(t)$ can be expressed by Fourier series,

$$f(t) = \frac{a_0}{2} + \sum_{h=1}^{h=\infty} \left[a_h cos(hwt) + b_h sin(hwt) \right] \tag{3.1}$$

where

$$\begin{aligned} a_0 &= \frac{1}{2\pi} \int_{-\pi}^{\pi} x(wt) d(wt) \\ a_k &= \frac{1}{2\pi} \int_{-\pi}^{\pi} x(wt) cos(hwt) d(wt) \\ b_k &= \frac{1}{2\pi} \int_{-\pi}^{\pi} x(wt) sin(hwt)) d(wt) \end{aligned}$$

w being the fundamental angular frequency and h the harmonic order.

The Fourier expansion can also be expressed either in positive and negative or only positive harmonic phasors as described below.

a)Positive and negative frequency harmonic phasors

The sine and cosine trigonometric functions can be determined by complex exponential terms in the form

$$sin(hwt) = \frac{e^{jhwt} - e^{-jhwt}}{2j} \tag{3.2}$$

$$cos(hwt) = \frac{e^{jhwt} + e^{-jhwt}}{2} \tag{3.3}$$

Back substituting equations (3.2) and (3.3) in (3.1) yields

$$f(t) = \sum_{h=-\infty}^{h=\infty} c_h e^{jhwt} \tag{3.4}$$

where

$$\begin{aligned} c_h &= a_h - jb_h \\ c_{-h} &= {c_h}^* \end{aligned}$$

Fourier series expressed by complex exponential terms (positive and negative harmonic phasors) is very convenient due to its compatibility with Fast Fourier Transform (FFT), a method commomly used to determine the harmonic spectrum of a non-sinusoidal periodic waveform (though convolution can also be used for this purpose alternatively [Rajakovic and Semlyen 1989][Acha and Rico 1994]).

b)Positive frequency harmonic phasors

The Fourier expansion can also be described by a series of phase shifted sine terms by substituting

$$a_h cos(hwt) + b_h sin(hwt) = d_h sin(hwt + \psi_h) \tag{3.5}$$

into equation (3.1), yielding the following expression

$$f(t) = \sum_{h=0}^{h=\infty} Im\{\Psi_h e^{jhwt}\} \tag{3.6}$$

where

$$\begin{aligned} \Psi_h &= d_h e^{j\psi_h} \\ d_h &= \sqrt{{a_h}^2 + {b_h}^2} \\ \psi_h &= tan^{-1}\frac{a_h}{b_h} \end{aligned}$$

Ψ_h being the positive frequency harmonic phasors.

Power electronic devices have their behaviour described by complex variables as well by real valued ones, such as the switching instants. Thus, if an unified harmonic solution for an entire system containing power electronic devices is desired, the solution should be in real components, which implies in positive frequency harmonic phasors [Smith 1995]. Application of FFT is still possible though not directly.

3.2.2 The linearisation process

The periodic steady state behaviour of non-linear power system components can be expressed in a generic form by the relation

$$y = f(x) \tag{3.7}$$

where x and y are periodic variables, expressed by infinite Fourier series in the form

$$x(t) = \sum_{h=-\infty}^{h=\infty} X_h e^{jhwt} \tag{3.8}$$

$$y(t) = \sum_{h=-\infty}^{h=\infty} Y_h e^{jhwt} \tag{3.9}$$

Considering X and Y as vectors of harmonic phasors (X_h and Y_h), equation (3.9) becomes

$$Y = f(X) \tag{3.10}$$

If the non-linear equation (3.7) is differentiable, then for small increments about x_b, y_b, the following relationship is valid

$$\Delta y = f'(x_b)\Delta x \tag{3.11}$$

where

$$\Delta x = \sum_{h=-\infty}^{h=\infty} \Delta X_h e^{jhwt} \tag{3.12}$$

$$\Delta y = \sum_{k=-\infty}^{k=\infty} \Delta Y_k e^{jkwt} \tag{3.13}$$

$$f'(x_b) = \sum_{i=-\infty}^{i=\infty} c_i e^{jiwt} \tag{3.14}$$

Equation (3.11) can be expressed in a general form as follows

$$\Delta\tilde{Y} = [F]\Delta\tilde{X} \tag{3.15}$$

or

$$\begin{bmatrix} \Delta Y_{-n} \\ \cdots \\ \Delta Y_{-1} \\ \Delta Y_0 \\ \Delta Y_1 \\ \cdots \\ \Delta Y_n \end{bmatrix} = \begin{bmatrix} c_0 & \cdots & c_{n-1} & c_n & & & \\ \cdots & \cdots & \cdots & \cdots & \cdots & & \\ c_{-(n-1)} & \cdots & c_0 & \cdots & c_{n-1} & c_n & \\ c_{-n} & c_{-(n-1)} & \cdots & c_0 & \cdots & c_{n-1} & c_n \\ & c_{-n} & c_{-(n-1)} & \cdots & c_0 & \cdots & c_{n-1} \\ & & \cdots & \cdots & \cdots & \cdots & \cdots \\ & & & c_{-n} & c_{-(n-1)} & \cdots & c_0 \end{bmatrix} \begin{bmatrix} \Delta X_{-n} \\ \cdots \\ \Delta X_{-1} \\ \Delta X_0 \\ \Delta X_1 \\ \cdots \\ \Delta X_n \end{bmatrix}$$

Matrix $[F]$ is the Jacobian associated with equation (3.10). It is, in structure, a Toeplitz matrix (mathematical proof is given in [Smith 1995]) which reflects the cross-coupling between frequencies.

Considering that the linearisation process is about an operation point X_b, Y_b, then

$$\Delta\tilde{X} = \tilde{X} - \tilde{X}_b \tag{3.16}$$

$$\Delta\tilde{Y} = \tilde{Y} - \tilde{Y}_b \tag{3.17}$$

Substituting equation (3.16) and (3.17) into equation (3.15) yields

$$\tilde{Y} = [F]\tilde{X} + \tilde{Y_n} \tag{3.18}$$

where

$$\tilde{Y_n} = \tilde{Y_b} - [F]\tilde{X_b} \tag{3.19}$$

$\tilde{Y_n}$ is the vector of Norton harmonic injections.

Equation (3.18) can be interpreted as a harmonic Norton equivalents and represents the linearisation of equation (3.10) in the Harmonic Domain. Similar linearisation can be derived with the periodic variables x and y being expressed by Fourier series based on positive frequency harmonic phasors.

In principle, every non-linear power system component should be amenable to a Norton equivalent representation in the Harmonic Domain. The main non-linear components of the conventional power transmission system have already been modelled in this Domain, these include the salient-pole synchronous generator[Semlyen *et al.* 1987b], the three-phase bank of single-phase transformers[Acha *et al.* 1989], the Static Var Compensator[Xu *et al.* 1991a] and more recently, the power converter [Smith 1995].

The vectors Y and X are the nodal currents and voltages, respectively, and matrix [F] is the total harmonic admittance matrix ($[Y_b]$). Thus, equation (3.18) can be re-written as follows

$$\tilde{I} = [Y_b]\tilde{V} + \tilde{I}_n \tag{3.20}$$

where

$$\tilde{I}_n = \tilde{I}_b - [Y_b]\tilde{V}_b \tag{3.21}$$

3.2.3 The unified Newton solution

The nodal representation of the linear components as transfer admittances is well established [Arrillaga and Arnold 1990]. For use in the Harmonic Domain these admittances are represented by harmonic phasors which, for non-frequency dependent components, are obtained by

$$Y_{self_h} = G_{self} + j\frac{B_{self_f}}{h} \tag{3.22}$$

$$Y_{mutual_h} = G_{mutual} + j\frac{B_{mutual_f}}{h} \tag{3.23}$$

where the subscript f denotes fundamental frequency. However, for linear frequency dependent components, such as the transmission lines, the harmonic admittance is calculated by an appropriate formulation [Enrique Acha Daza 1988]. In both cases, the behaviour of the linear component can be expressed in a generic form as follows

$$\tilde{I} = [Y_l]\tilde{V} \tag{3.24}$$

where $[Y_l]$ is a diagonal harmonic admittance matrix.

The harmonic representation for the complete power system can be achieved following the rules of the nodal analysis, with the linear components represented by the admittance $[Y_l]$, and the non-linear components by the harmonic Norton equivalents, and be expressed in the form

$$\tilde{I} = [Y_j]\tilde{V} \tag{3.25}$$

The nodal admittance matrix $[Y_j]$ of equation (3.25) contains all the network busbars, phases and the selected spectrum of harmonics. The order of each building unit

of the non-singular matrix $[Y_j]$ is equal to the number of phases multiplied by the spectrum of harmonics considered and is, in addition, structurally sparse.

A simple circuit, shown in Figure 3.1, is used to illustrate the structure of the admittance matrix in the Harmonic Domain. It consists of four nodes and three phases and to reduce the display of informations, the admittance matrix only shows the fundamental and frequencies up to the third, as well as a d.c. component. The matrix structure is illustrated in Figure 3.2, and only the transformer nonlinearity (for a three phase bank of single phase transformers) has been considered. Figure 3.3 shows an enlarged view of node 2, which includes the transformer Toeplitz admittance matrix.

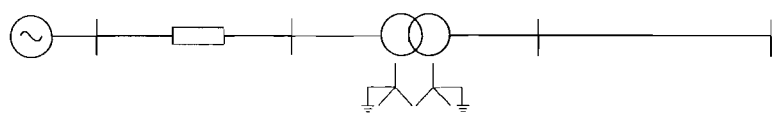

Figure 3.1 Radial system

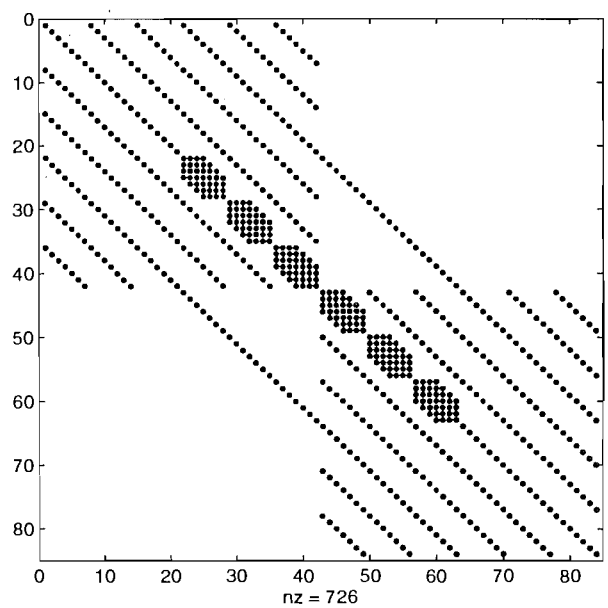

Figure 3.2 Structure of the Jacobian matrix $[Y_j]$

By assembling together all power system components, a unified solution of the complete system can be achieved based on a Newton-type iterative procedure, as illustrated in the block diagram of Figure 3.4, where $[Y_j]$ plays the role of a Jacobian.

The iterative procedure, however, is not a true Newton-Raphson method as only a limited number of harmonics is represented and part of the system is already linear. On the other hand, voltage and current excitations are applied to the network so that a partial inversion of $[Y_j]$ is required. A hybrid algorithm has been developed for this purpose [Medina *et al.* 1990] that exploits efficiently the inverse of matrix $[Y_j]$. The iterative procedure starts from the base case given by the three-phase load-flow solution,

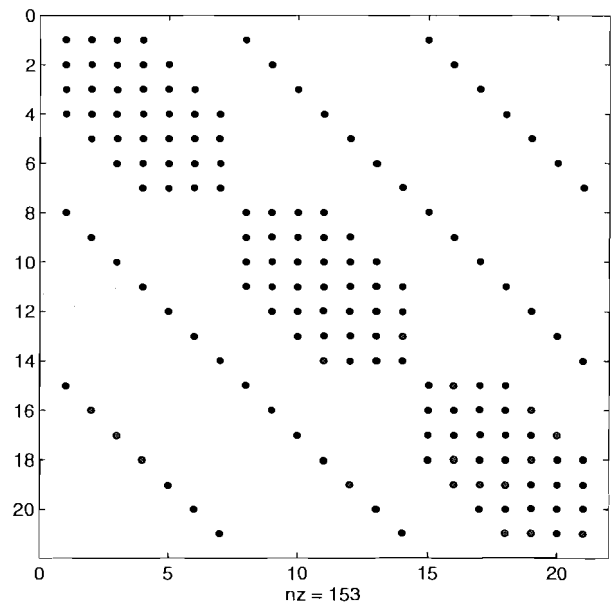

Figure 3.3 Admittance matrix node 2

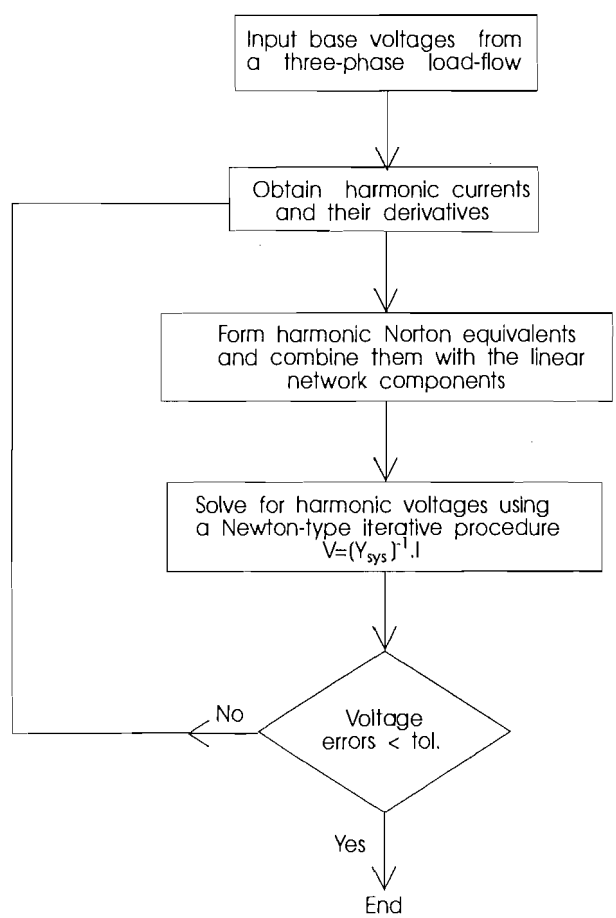

Figure 3.4 HDA basic flow diagram

and it has been found to be more reliable and faster towards convergence when matrix $[Y_j]$ is singly evaluated [Acha *et al.* 1989].

3.2.3.1 Initial Steady State Specification

The steady state operation of a power system is defined by a load-flow program, which provides the fundamental voltage phasors at all specified nodes. However, for a precise definition of the base operating point of the non-linear components, the load flow must be performed in the three-phase frame of reference.

The nodal information derived from the three-phase load-flow needs to be modified for use in the Harmonic Domain as follows:

1. At linear load nodes, the load connected to phase m of a busbar k is calculated in admittance form as

$$Y_{PQ_{self_{km}}} = \frac{P_{km} - jQ_{km}}{|\, V_{km} \,|^2}$$

$$= G_{PQ_{self_{km}}} + jB_{PQ_{self_{km}}}$$

   and at a harmonic of order h

$$Y_{PQ_{self_{kmh}}} = G_{PQ_{self_{km}}} + j\frac{B_{PQ_{self_{km}}}}{h}$$

2. At generator nodes and fundamental frequency the specified terminal voltage and complex power are converted into an internal emf behind synchronous reactance.

3. At each harmonic frequency the generator is normally represented by an appropriate impedance. However, in the presence of saliency and/or saturation, the generator acts as a frequency converter as well as impedance; in this case a more accurate solution requires further modifications and more detailed representation([Semlyen *et al.* 1987b]).

During the iterative process of the Harmonic Domain solution, the internal emf's derived from the initial load-flow remain constant and this aspect is analysed later.

3.2.3.2 Harmonic evaluation of the Norton equivalents

The harmonic Norton admittance and current injections can be determined by means of FFT or discrete convolutions, provided the non-linearity is described by polynomial expressions. The former procedure has been used in this work and can be summarised as follows. At each iteration:

1. Determine the point-by-point voltage waveform by inverse Fourier transforming the harmonic voltages;

2. Determine the current waveform by applying the voltage waveform to the non-linear relationship $i(t) = f(v(t))$;

3. Obtain the current harmonic coefficients (vector I_b in equation (3.21)) by applying FFT to $i(t)$;

4. Repeat step 2 and 3 for the derivative $\frac{di(t)}{dt}$ and with its harmonic coefficients build the harmonic Toeplitz admittance matrix $[Y_b]$;

5. With I_b and $[Y_b]$, determine the harmonic Norton current injections $\tilde{I_n} = \tilde{I_b} - [Y_b]\tilde{V_b}$

Adopting the alternative of keeping the jacobian constant through the iterative procedure, step 4 is just performed at the first iteration.

3.2.4 Case Study

The test system, shown in Figure 3.5, is a small part of the New Zealand South Island 220 KV network which contains a static converter at Tiwai.

Field tests carried out at Tiwai [Densem *et al.* 1984] had already shown the presence of a parallel resonance at a frequency lying somewhat between the fourth and fifth harmonic. This observation is not exclusively to Tiwai but to greater or lesser extent to several of the network busbars.

To investigate this problem and assess the background harmonic noise in this region, the large converter plant at Tiwai has been removed from the model. The generator and load non-linearities have also been ignored, the only harmonic sources being the magnetising currents of the five transformers.

The loads are as specified in the diagram and generators internal emf's are set at 1 (p.u.), with the Manapouri power station acting as the slack bus. Details of the linear and non-linear components and load-flow solution are given in Appendix A. The magnetising characteristic for all transformers is described by a hyperbola, whose parameters are those of curve 1 in Appendix B.

Figures 3.6(a) to (d) illustrate a full period of the voltage waveforms obtained at relevant network busbars (i.e Manapouri, Tiwai, Invercargill and Roxburgh respectively). Figures 3.6(e) to (h) show their respective harmonic content. All the busbars show the presence of considerable fifth harmonic.

Recommended levels for the individual harmonic voltages are the order of 1%. It is clear from Figures 3.6(e) to (h) that this level is exceeded by the third and 5th harmonics at all busbars; this effect is particularly noticiable at the Tiwai bus (Figure

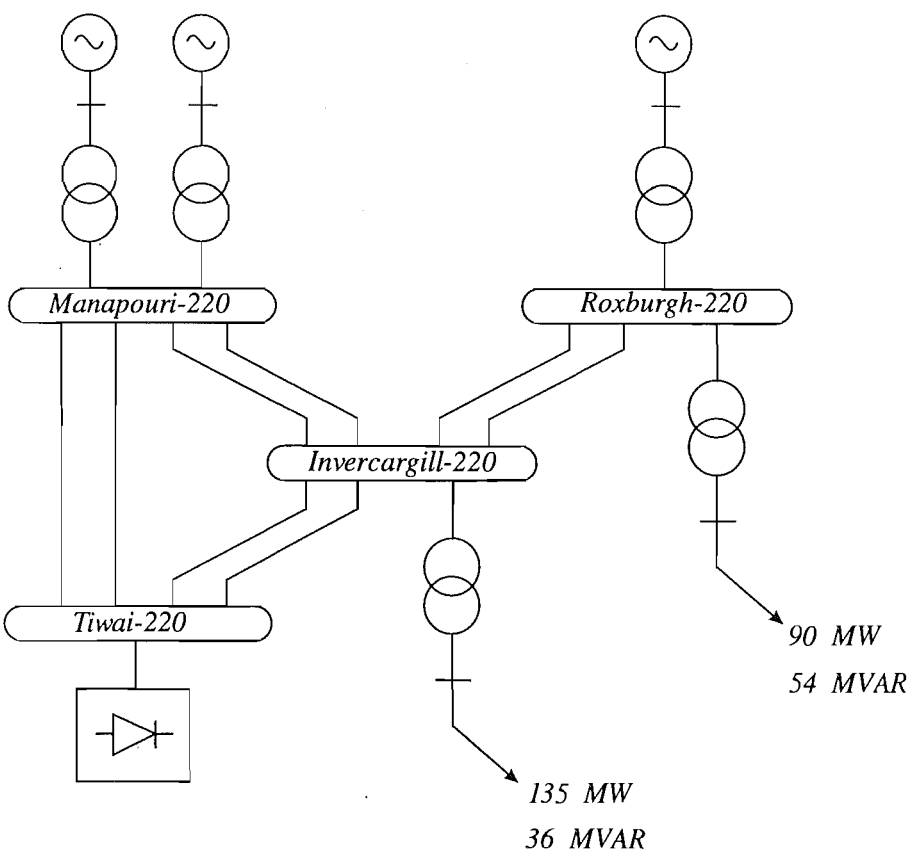

Figure 3.5 South Island test system

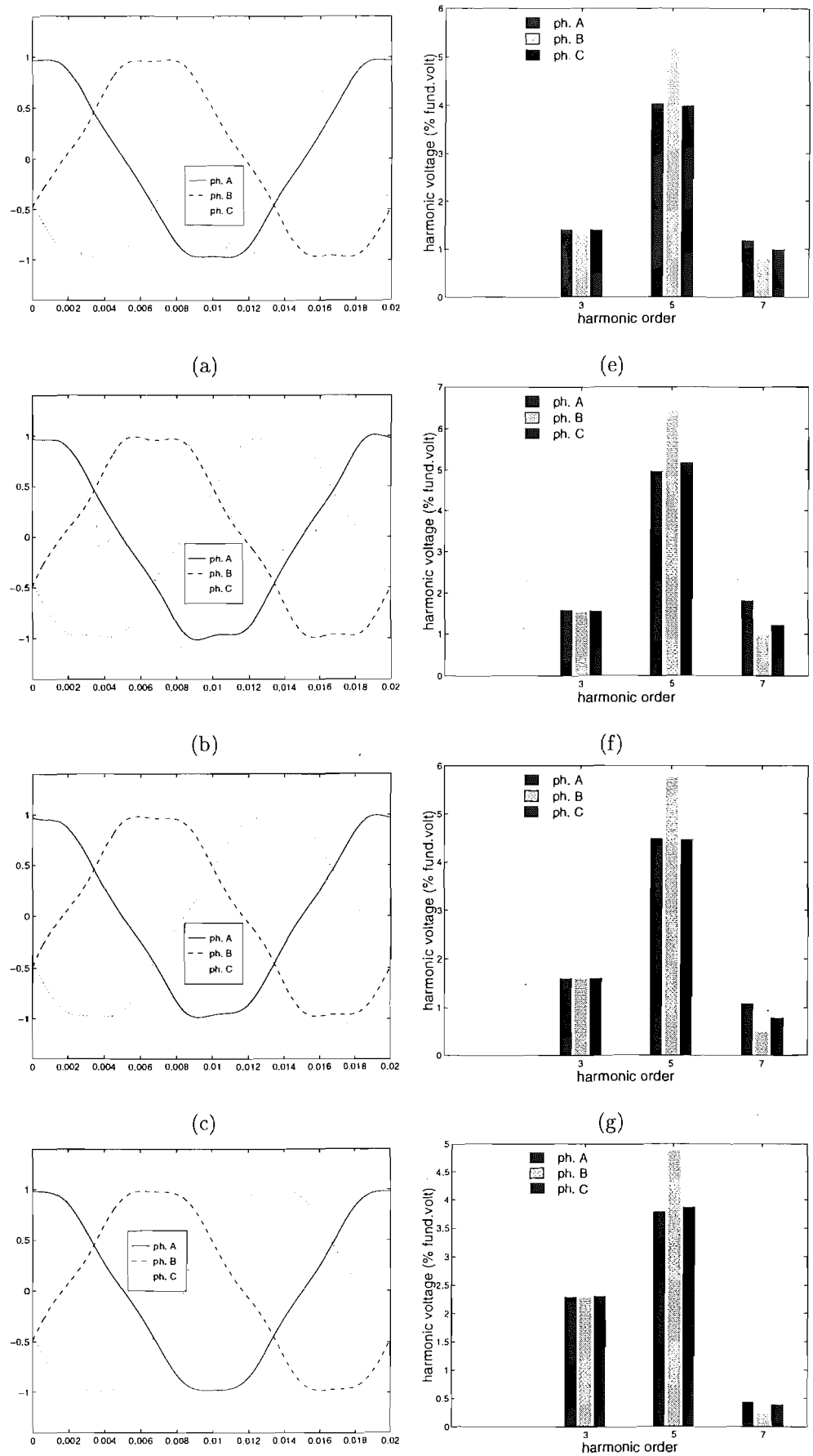

Figure 3.6 voltages waveforms and their harmonic content

3.6) where the 5th harmonic level in one phase exceeds the recommended level by a factor of 7.

While the load flow condition selected may be considered unrealistic, the studies show the importance of representing the conventional system non-linearities in the harmonic domain; without these the test system results would have been perfectly sinusoidal.

3.3 REDUCED NETWORK REPRESENTATION

To alleviate the memory requirements of the Harmonic Domain it is advisable to reduce the size of the problem, retaining only the non-linear nodes. This is justified on the basis that the harmonic balance does not need explicit representation of the linear part of the network, which is passive at harmonic frequencies. A reformulation of the equation is required as follows:

$$\begin{bmatrix} \tilde{I}_1(*) \\ \tilde{I}_2(**) \end{bmatrix} = \begin{bmatrix} Y_{11} & Y_{12} \\ Y_{21} & Y_{22} \end{bmatrix} \begin{bmatrix} \tilde{V}_1 \\ \tilde{V}_2 \end{bmatrix} \tag{3.26}$$

$(*)$: Non-linear components
$(**)$:Linear components

Developing equation (3.26)

$$\tilde{I}_1 = [Y_{11}]\tilde{V}_1 + [Y_{12}]\tilde{V}_2 \tag{3.27}$$

$$\tilde{I}_2 = [Y_{21}]\tilde{V}_1 + [Y_{22}]\tilde{V}_2 \tag{3.28}$$

or solving for $\tilde{V}_2$ in equation (3.28)

$$\tilde{V}_2 = [Y_{22}]^{-1}\left(\tilde{I}_2 - [Y_{21}]\tilde{V}_1\right) \tag{3.29}$$

$$\tilde{I}_1 = \left([Y_{11}] - [Y_{12}][Y_{22}]^{-1}[Y_{21}]\right)\tilde{V}_1 + [Y_{12}][Y_{22}]^{-1}\tilde{I}_2 \tag{3.30}$$

Finally, solving for $\tilde{V}_1$ in equation (3.30)

$$\tilde{V}_1 = [Z_1]\left(\tilde{I}_1 - [K_0]\tilde{I}_2\right) \tag{3.31}$$

where

$$[Z_1] = ([Y_{11}] - [Y_{12}][Y_{22}]^{-1}[Y_{21}])^{-1} \tag{3.32}$$

$$K_0 = [Y_{12}][Y_{22}]^{-1} \tag{3.33}$$

Once obtained the non-linear node voltages from equation (3.31), their substitution in equation (3.29) permits the calculation of the linear node voltages. In the absence of any current injection in the latter nodes (i.e. $I_2 = 0$) the solution of equation (3.29) is very simple.

Finally, the matrix product $[Y_{22}]^{-1}[Y_{21}]$ only needs to be calculated once for use in the equations (3.29), (3.32) and (3.33).

3.4 LOAD FLOW AND HARMONIC ANALYSIS

The Harmonic Domain algorithm provides an accurate solution of the interaction that exists between the fundamental and harmonic frequencies. In the process, however, the solution following convergence requires fundamental voltages slightly different from those specified by the load flow. If the originally specified generator voltages are to be mantained, a new load flow and harmonic solution needs to be carried out.

An algorithm to solve the load flow and harmonic flows simultaneously by the Newton method was described for the case of a static converter connected to a symmetrical power system [Xia and Heydt 1982].

Such algorithm has recently been extended to the three-phase load-flow and applied to derive the harmonic content produced by a Static Var Compensator [Xu *et al.* 1991a] [Xu *et al.* 1991b]. The structure of the simultaneous algorithm is shown in the flow diagram of Figure 3.7. However the generalisation of the simultaneous three-phase load and harmonic flow for use in a system with multiple non-linearities is a problem of great complexity.

Considering the different requirements of the load flow and harmonic studies, it seems more appropriate to solve the two parts sequentially, taking advantage of the simplified harmonic solution described in the previous section. The structure of the resulting sequential algorithm is shown in Figure 3.8.

It involves a double iterative scheme, which starts with the three-phase load flow. Upon convergence of the load flow the nodal information is converted into internal emf's and equivalent nodal admittances, as explained earlier. This is followed by the Harmonic Domain (HD) solution, at the end of which the load flow and harmonic balance tolerances are checked to decide whether another double iterative cycle is required.

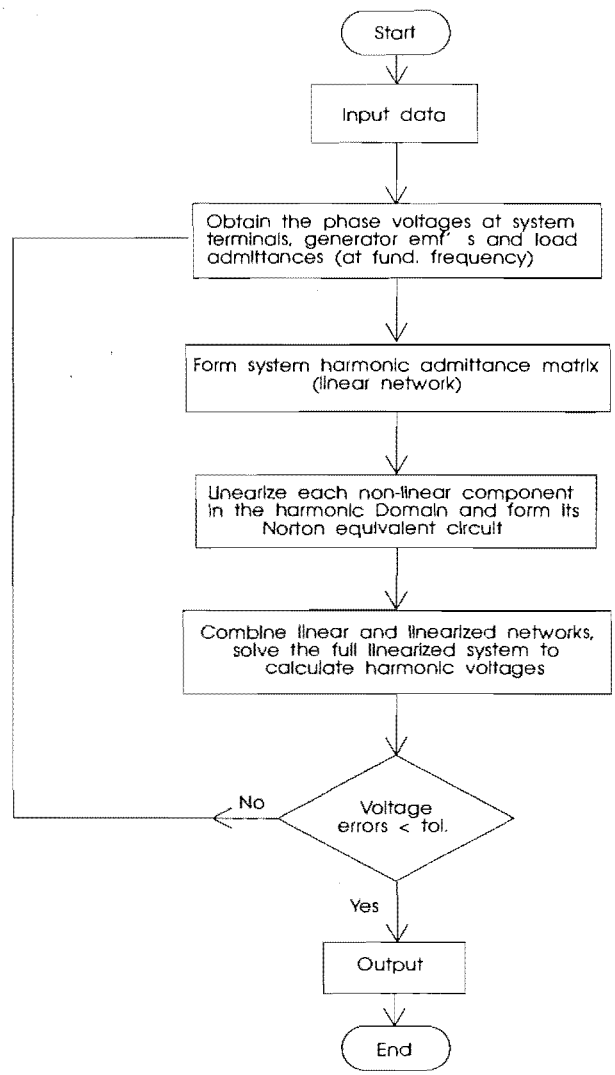

Figure 3.7 Unified HD solution

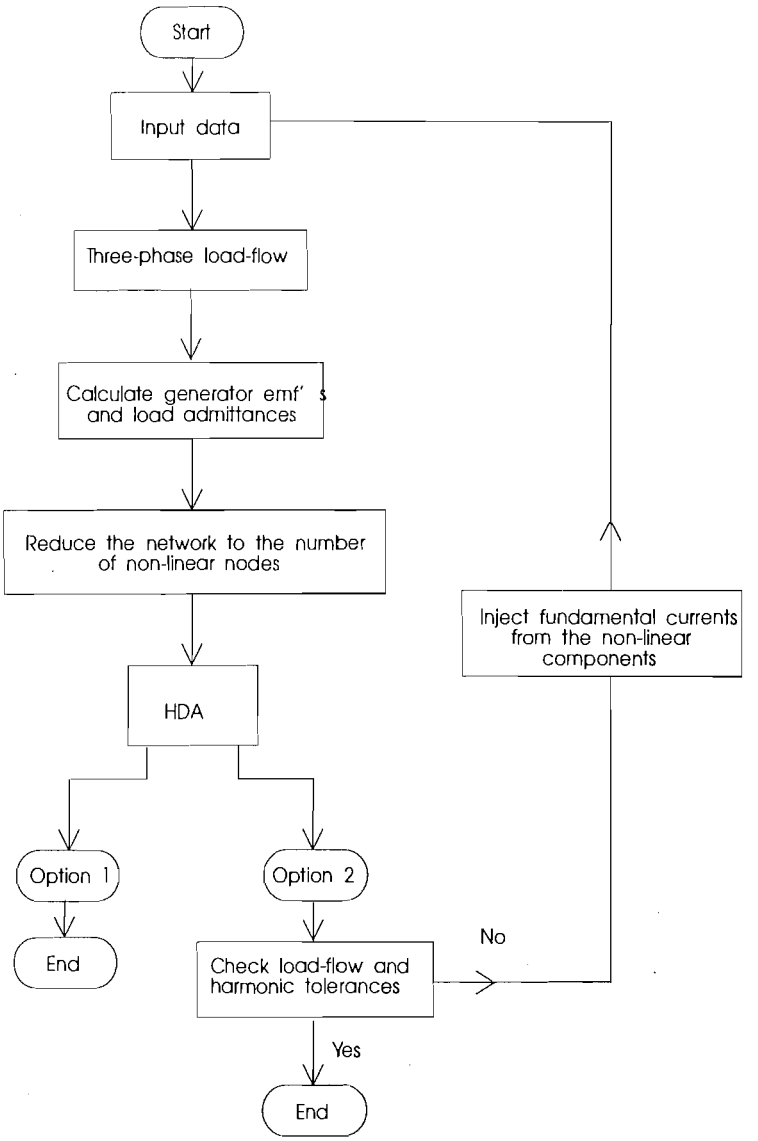

Figure 3.8 Sequential HD solution

The interactions between load and harmonics has been quantified in a recent paper[Arrillaga and Callaghan 1989]. A fictious 6-pulse convertor load rated at 75 MW, plus a PQ load of 250 MW and 60 MVAr. The circuit included filters for the 5th, 7th, 11th and 13th harmonics, under supplied approximately 22 MVAr at fundamental frequency.

The main results, repeated in Table 3.1, show that the non-characteristic harmonics can be greatly affected by the adjusted load flows.

Harmonic order	One load flow	Four load flows
3	0.000434	0.000561 (29%)
9	0.000399	0.000509 (28%)
15	0.000337	0.000417 (29%)
21	0.000260	0.000306 (18%)

Table 3.1 Comparisons of triplen harmonic current injections

3.5 CONCLUSIONS

The structure of the Harmonic Domain, a frame of reference for the harmonic analysis of the power system has been described. In this domain the network busbars and coupling between phases and between harmonics are explicitly represented.

In this frame of reference the harmonic sources are represented as Norton equivalents, whose components vary during the solution. However, the experience gained so far indicates that the Jacobian elements of the Norton admittance matrix vary little from iteration to iteration and it is rarely necessary to recalculate them.

For the calculation of the non-characteristic harmonic injections, it is advisable to use the double iterative scheme, i.e. adjust the load flow following the harmonic Domain iterations.

This general frame of reference has been applied to the harmonic solution of a practical transmission system with detailed representation of the transformers' magnetising non-linearities. The use of the Harmonic Domain at the planning stage should help to assess the best practical value of the transformer magnetising characteristic(s) and thus improve overall economy of a particular system extension.

With the system already in operation, this algorithm will help to assess the influence of the network harmonic distortion of existing nodal voltages and current levels, so that a redistribution of harmonic flows by alternative control actions in real-time could be attempted when required.

Chapter 4

MAGNETISING CHARACTERISTICS

4.1 INTRODUCTION

Saturation and hysteresis are nonlinear effects inherent to the process of magnetisation of ferromagnetic materials. Although these nonlinearities have already been explained in the theory of ferromagnetism, they are not known in an exact analytical form. Nonetheless, the overall nonlinear magnetic behaviour can be quantitatively described by the relationship between the magnetic flux density B and the magnetic field intensity H, i.e. the well-known BH curves. These curves are generally obtained by careful measurements on samples and have the shape shown in Figure 4.1.

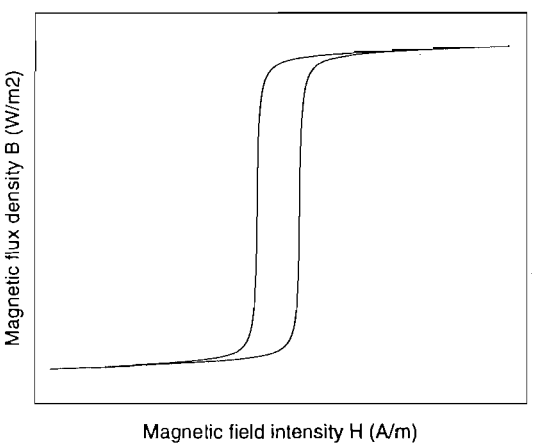

Figure 4.1 BH curve

In rigorous harmonic analysis, an accurate representation of the transformer ferromagnetic core nonlinearities is of fundamental importance. This representation depends on an appropriate reproduction of the experimental magnetising characteristics. For an analysis using computers, it is convenient to approximate them by an analytical expression, ideally, by a single and mathematically simple function able to reproduce the magnetising characteristics over their entire range with a minimum error.

Due to the saturation and hysteresis properties exihibited by these curves the derivation of a mathematical function that is both accurate and simple is a difficult

task. The problem can be simplified by neglecting hysteresis, a reasonable assumption in steady-state analysis and modern cold-rolled steel transformers[Semlyen and Castro 1975a]. In this case, the magnetising characteristic becomes a single valued monotonic function, defined by the average of the hysteresis loop boundaries.

There is a wide range of literature on approximations for magnetising characteristics. Several algebraic and transcendental functions have been compared earlier [Fisher and Moser 1956] and [Trutt *et al.* 1968]. The latter came to the conclusion that a good fit can seldom be obtained by a single function over the entire range of the magnetising characteristic. They suggest, as a satisfactory alternative, subdividing the magnetising characteristic into a large number of sections, each section approximated by linear interpolation.

The possibility of approximation by exponential series has been explored by some researchers. An iterative procedure has been developed by Macfadyen *et al* [1973] to determine the equation coefficients, which became a better alternative than the trial-and-error procedure [El Sherbiny 1973] . Later, an analytical approach has been derived [Hwang and Lord 1976] that approximately calculates the coefficients for the exponential series.

Expansion in power series [Swift 1969] [Prusty and Rao 1980] [Semlyen *et al.* 1987a] has the advantage of being a very simple formulation. However, this kind of approximation fits well only characteristics that rise slowly, and in which the knee portion has a large curvature [Trutt *et al.* 1968].

Very close reproduction of a large range of magnetising characteristics can be obtained by the rational-fraction function [Widger 1969]. However, a very complicated iterative procedure is required to calculate the equation coefficients which has inhibited the use of this formulation. The same level of accuracy can be obtained by a much simpler approach, the hyperbola function suggested by [Mazieres and Forquet 1968] and [Semlyen and Castro 1975a]. A trial-and-error approach is required to calculate the variable associated with the smoothness of the knee region.

More recently, it has been stated in some publications , that two or three piecewise linear segments [Semlyen and Castro 1975b], [Dommel *et al.* 1986] [Hatziantoniu *et al.* 1988](Discussions by R. A. Walling) are sufficient to represent the transformer magnetising characteristics for transient studies. However, an accurate representation of the entire curve might be needed for studies where resonance is an important factor [Talukdar *et al.* 1974]. Moreover, it has been reported in the literature that the 'kinks' caused by the junction of two straight lines have been magnified in the solution of a problem [Widger 1969]. So far, this aspect has not been thoroughly investigated for steady-state harmonic analysis.

While most of the transformer electromagnetic models are based on the flux-current

(ϕi) characteristic, the BH curve representation is more commonly described in the literature. Although the ϕi curve can be obtained by simply rescaling the BH curve by the core dimensions (B=ϕ.A and H=$N.i.l$), the sharpness of the knee region of a ϕi characteristic will depend on the design; this can compromise the adequacy of some mathematical equations describing BH curves to represent ϕi characteristics.

The purpose of this chapter is to analyse the importance of an accurate representation of the magnetising characteristic in harmonic steady-state studies for resonant systems and also analyse the adequacy of piecewise linear, hyperbola and rational-fraction approximations. A procedure based on Singular Value Decomposition (SVD) is investigated as an alternative to determine the rational-fraction and hyperbola coefficients. A more accurate representation for the magnetising characteristic is also proposed based on cubic spline interpolation.

4.2 PIECEWISE LINEAR APPROXIMATIONS

Based on the main branch magnetising characteristic [Dick and Watson 1981] and the 345 KV Jaguara-Taquaril test system [Cunha and Dommel 1973], simulations were carried out with the Harmonic Domain (HDA) program with the three-phase bank of single phase transformers model.

The Jaguara-Taquaril consists of a power plant feeding an unloaded 345 KV transmission line (resonance between the 6th and 7th harmonic frequency) through a step-up transformer, with shunt inductors connected on the secondary side as illustrated in Figure 4.2. The internal generator emf is equal to 0.95 (p.u.), the combined generator-transformer impedance is j0.084 (p.u.), and the shunt reactance j1.79 (p.u.). The magnetising characteristic and transmission line parameters are described in Appendix B.

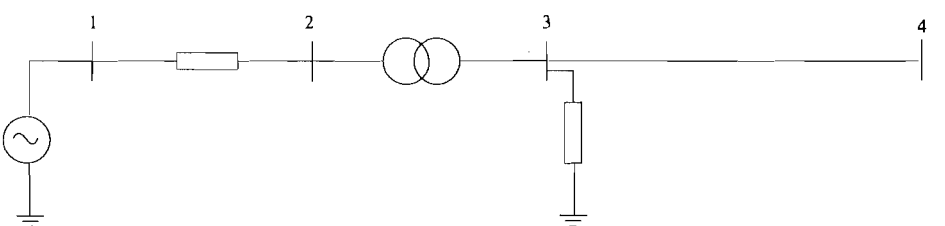

Figure 4.2 Jaguara-Taquaril test system

Fourteen cases have been simulated for each of the magnetising characteristic approximations illustrated in Figure 4.3, i.e. two, three (curve 1) and four piecewise linear approximations. Each case has been obtained by varying the voltage source from 0.94 (pu) to 1.07 (pu). The HDA simulations included frequencies up to the 7th harmonic, and convergence checks have been restricted to voltages using a tolerance of 0.0001 (pu).

Two additional three piecewise linear approximations have been considered, curves 2 and 3 in Figure 4.3, in order to complement the sensitivity analysis.

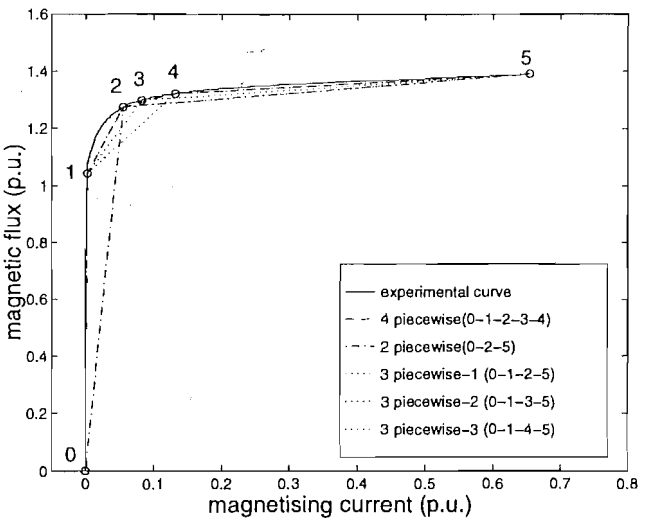

Figure 4.3 Piecewise linear approximations

Only the fundamental and seventh harmonic voltages at busbar 3, phase A, are illustrated in Figures 4.4 (a) to (d), with the legend defined in Figure 4.4(c). The fundamental voltages for all piecewise linear approximations, magnitude and phase angle, are illustrated in Figures 4.4 (a) and (b), and show very close agreement in all cases.

For the seventh harmonic voltage magnitudes, illustrated in Figure 4.4 (c), a reasonable agreement is achieved for applied voltages below 1.04 (p.u.), i.e. when the transformer is not into deep saturation (transformer terminal fundamental voltage below 1.28 (p.u.)). Above this operation point, the seventh harmonic voltages show significant discrepancies. Regarding the phase angle illustrated in Figure 4.4 (d), abrupt variations occur for the two and three piecewise linear approximations, while a more steady value is observed for the four piecewise approximation.

Figure 4.4 (e) illustrates the seventh harmonic voltages as a percentage of the fundamental voltages. For an applied voltage of 1.05 (p.u.), the four and three piecewise (*curve* 2) linear approximations yield similar results, i.e. seventh harmonic voltages about 2%, while the three piecewise linear approximation *curve* 3 yields a seventh harmonic voltage almost equal to zero and the other two approximations about 6%.

Using the four piecewise linear approximation solution as a reference, Figure 4.4 (f) illustrates the percentual difference of the seventh harmonic solution obtained with the two and three piecewise linear approximations . Differences up to about 220% can be observed, which clearly indicates the inadequacy of two and three piecewise linear approximations and the need of further investigations with more accurate mathematical representations for the magnetising characteristic.

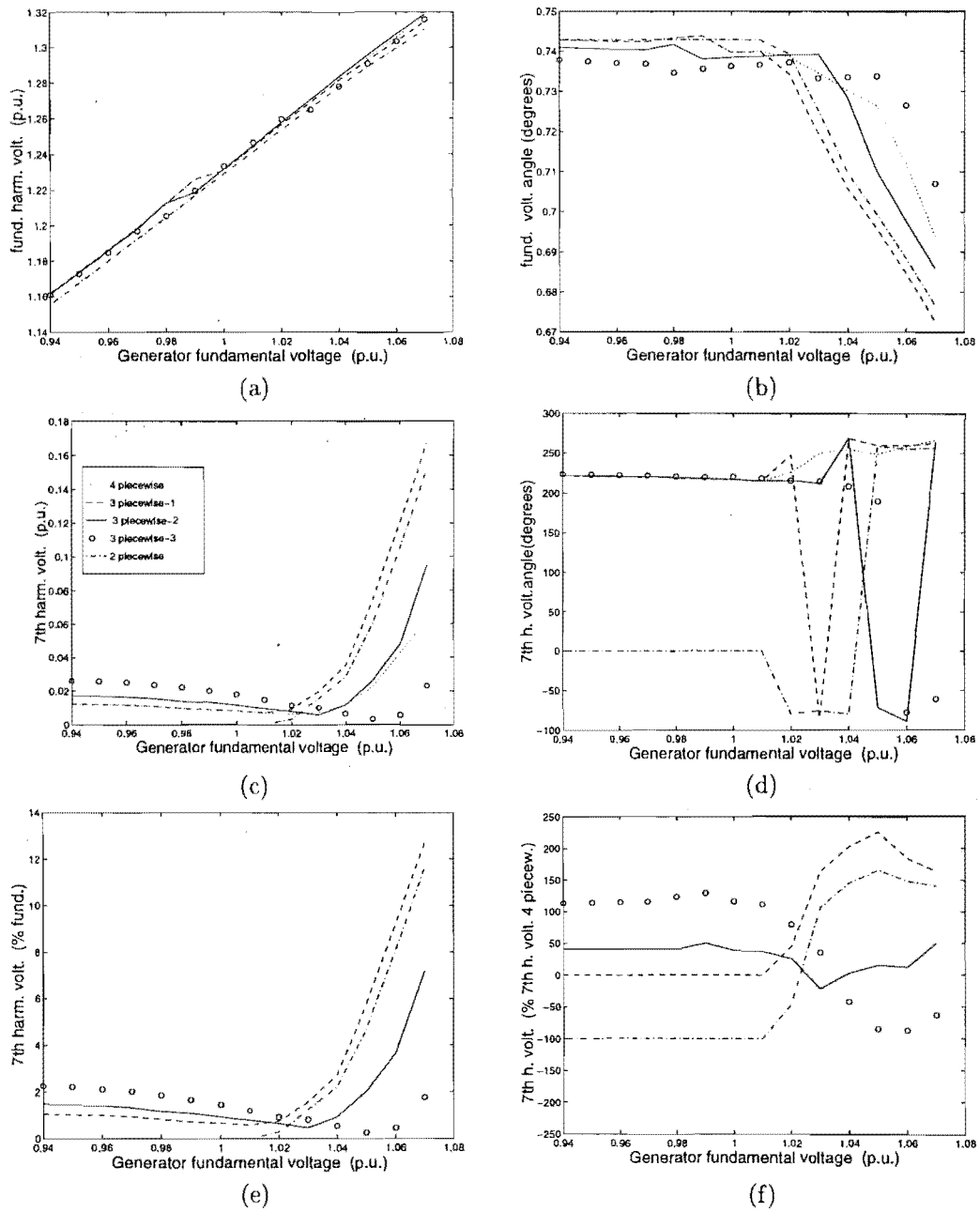

Figure 4.4 Piecewise linear approximations results

4.3 APPROXIMATION BY RATIONAL-FRACTION

The second-order rational-fraction interpolation approach proposed by Widger [1969] is able to reproduce very accurately certain magnetising characteristics. The drawback of this approximation, given by the following equation

$$i_k = \frac{a_0 + a_1\phi_k + a_2{\phi_k}^2}{1 + b_1\phi_k + b_2{\phi_k}^2}(k = 1, ..., n), \tag{4.1}$$

is the difficulty of determining its coefficients. A complicated iterative procedure has been derived to determine them which prevents this approximation from a wide spread acceptance.

A simple mathematical approach has been proposed [Whitefield 1986] and [Braun and Ram 1987] to determine the coefficients of rational-fraction equations for frequency domain curve fitting problems. This approach has been adopted in this work, and its efficiency for magnetising characteristic approximations investigated. It can be summarised as follows.

Re-writing equation (4.1) in the form

$$a_0 + a_1\phi_k + a_2{\phi_k}^2 - i_k(1 + b_1\phi_k + b_2{\phi_k}^2) = 0.$$

and substituting the n tabulated values of ϕ_k and i_k (obtained experimentally), yields

$$\begin{bmatrix} 1 & \phi_1 & {\phi_1}^2 & -i_1\phi_1 & -i_1{\phi_1}^2 \\ \vdots & \vdots & \vdots & \vdots & \vdots \\ 1 & \phi_k & {\phi_k}^2 & -i_k\phi_k & -i_k{\phi_k}^2 \\ \vdots & \vdots & \vdots & \vdots & \vdots \\ 1 & \phi_n & {\phi_n}^2 & -i_n\phi_n & -i_n{\phi_n}^2 \end{bmatrix} \begin{bmatrix} a_0 \\ a_1 \\ a_2 \\ b_1 \\ b_2 \end{bmatrix} = \begin{bmatrix} i_1 \\ \vdots \\ i_k \\ \vdots \\ i_n \end{bmatrix}$$

or

$$[A]\tilde{x} = \tilde{b}$$

where [A] is a rectangular matrix with nx 5 dimension. Thus, the problem of determining the coefficients a_0, a_1, a_2, b_1 and b_2 reduces to solving a set of overdetermined linear equations. A solution that minimizes the least square errors (or Euclidian norm) can be determined based on the concept of the *pseudoinverse*. In others words,

$$\tilde{x} = [A]^+\tilde{b}$$

minimizes the Euclidian norm $\| Ax - b \|^2$, and $[A]^+$ is the pseudoinverse of $[A]$, which is defined by the expression

$$[A]^+ = ([A]^t[A][A]^t)^{-1}$$

Matrix [A] can be ill-conditioned as its elements are determined by polynomial power series [Golub and Loan]. In this case a solution based on Singular Value Decomposition (SVD) is still possible. The solution will not correspond to the smallest Euclidian norm, but it will be the best approximation in the numerical sense [Press *et al.* 1992][Golub and Loan]. SVD consists in decomposing matrix [A] as follows

$$[A] = [U][W][V]^t \tag{4.2}$$

where [W] is a diagonal matrix and [U] and [V] are orthogonal each, which implies that the inverse of [A] can be given by

$$[A]^{-1} = [V][W]^{-1}[U]^t$$

4.3.1 Test results

The experimental magnetising characteristics [Dick and Watson 1981] for the main branch, yoke and zero-sequence path of a five-limb transformer have been used as test cases to assess the performance and accuracy of the rational-fraction approximation.

The coefficients obtained for the main branch magnetising characteristic, yield an interpolating curve that closely matches the experimental curve, as illustrated in Figure 4.5 (a), with an enlarged view of the knee region. Several simulations have been carried out, varying the set of given tabulated points and accuracy is only compromised when a very reduced number of points is given. In none of the cases simulated have problems of ill-conditioned matrix been observed. However, very small values have been determined for the numerator coefficients. To avoid numerical errors, all coefficients, including $b_0 = 1$, can be rescaled by a factor of 10^n and this procedure does not affect the solution. The rational-fraction coefficients for all magnetising characteristics are shown in Table 4.1, with the matrix conditioning listed in the last row.

The coefficients determined for the yoke and zero-sequence path magnetising characteristics could not produce accurate interpolating curves. Several simulations have been carried out varying the number of given points without success. A good agreement is only obtained by increasing the rational-fraction order up to the third. Figure 4.5 (b) illustrates the interpolating curves for the yoke magnetising characteristic obtained by considering a 2nd order rational-fraction and two set of given points (the set with a reduced number of points is indicated by the symbol 'o' and that with a large number of

Curve	Main	Yoke	Zero-Seq.	Hypothetical
a_0	0.000609	-0.013249	0.102550	-0.013190
a_1	-0.000400	0.00422	0.058268	0.003390
a_2	0.000012	0.0	0.0	0.0
a_3	0.0	0.016166	0.0	0.019826
a_4	0.0	-3.086836	0.0	-4.98647
a_5	0.0	-0.00912	0.0	-0.013656
b_1	0.510300	4.5658	-1.88931	6.296000
b_2	-1.42810	-3.37713	0.0	-3.969680
b_3	0.0	1.04272	0.0	1.971490
b_4	0.0	0.00202	0.31906	0.003630
b_5	0.0	-0.140507	0.12828	-0.031100
cond.	1.144e+03	2.399e+07	7.413e+03	5.278e+06

Table 4.1 Rational-fraction coefficients

points by the symbol 'x'). Figure4.5 (c) illustrates the yoke and zero-sequence path interpolating curves considering a 3rd order rational-fraction with twelve and eight given points, respectively. A smaller number of points would be needed to obtain accurate curves if the rational-function order is increased to the 5th. Similar problem with the 2nd and 3rd order has been observed for an hypothetical two straight lines magnetising curve. A good agreement is only achived with a 5th order rational-fraction, shown in Figure 4.5 (f).

4.3.2 Summary

Magnetising characteristics with smooth or sharp knee region can be accurately represented by rational-fraction functions. The SVD technique has proved to be an efficient way to determine the function coeffients, with the convenience of a software package being available. The only restriction is that the order of the numerator and denominator equations must be known.

4.4 APPROXIMATION BY HYPERBOLA

The hyperbola equation [Mazieres and Forquet 1968] is given by

$$\mathcal{E}\phi_k = (m_1 i_k + b_1 - \phi_k)(m_2 i_k + b_2 - \phi_k) - b_1 b_2 \tag{4.3}$$

where

m_1 = slope of unsaturated region

m_2 = slope of saturated region

b_1 = ordinates to the origin of asymptote to m_1

b_2 = ordinates to the origin of asymptote to m_2

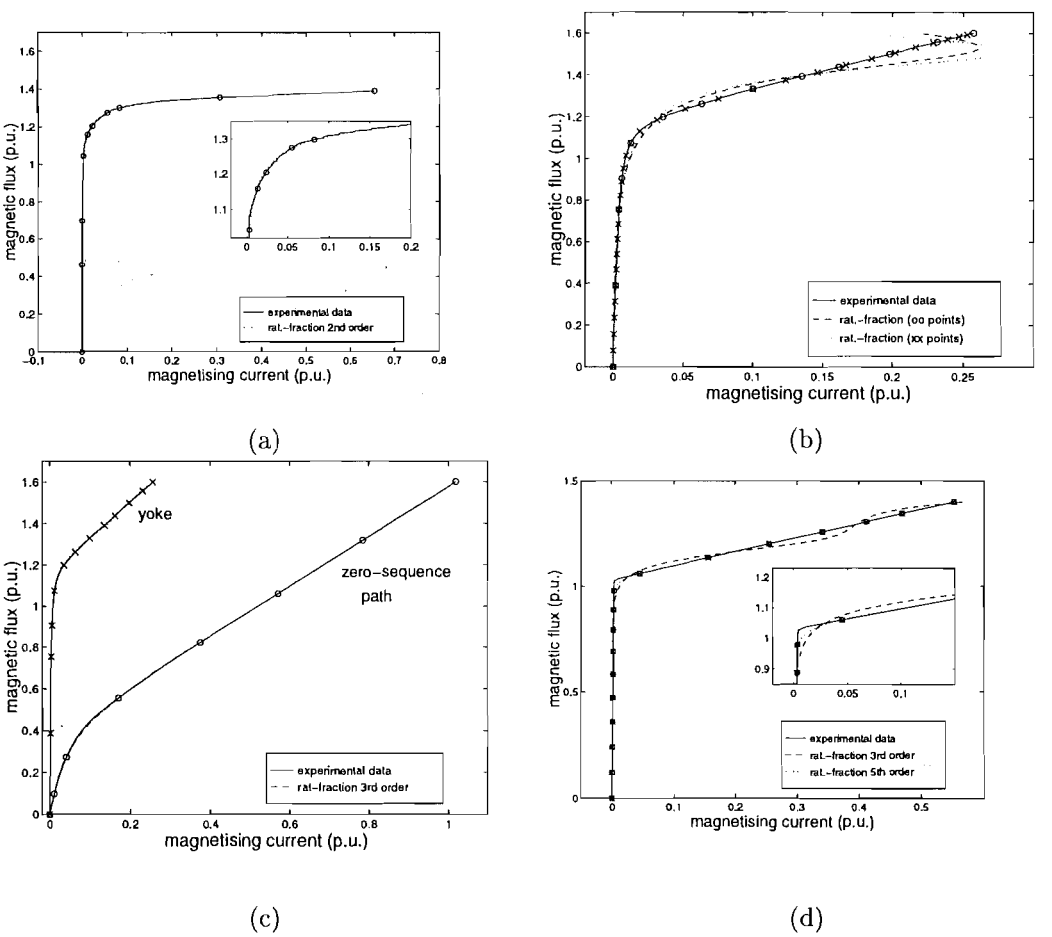

Figure 4.5 Rational-fraction interpolating curves

ϕ_k = magnetic flux at the incremental time t_k
$\mathcal{E}$ = correction term

In principle, all the coefficients can be approximately determined from the experimental curve, except the correction term $\mathcal{E}$ that modulates the sharpness of the knee region of the magnetising characteristics. Nonetheless, an adequate determination of these parameters is not an easy task if an accurate representation of the whole curve is required, particularly those with a smooth knee region. The correction term $\mathcal{E}$ itself is not sufficient to compensate for the approximations made when defining the other coefficients (m_1, m_2, b_1 and b_2) and if so, it still has the inconvenience of being determined by trial-and-error. Based on the method used to the determine the rational-fraction coefficients, a similar method has been derived here to determine the hyperbola coefficients.

Considering that hysteresis is negligible, b_1 is equal to zero. Re-writing equation (4.3) as follows

$$(m_1 {i_k}^2 - i_k\phi_k)m_2 + (m_1 i_k - \phi_k)b_2 - \phi_k\mathcal{E} = m_1 i_k + \phi_k^2$$

and assuming that m_1 is known, the problem of determing the coefficients reduces to the solution of a set of overdetermined linear equations

$$\begin{bmatrix} (m_1 {i_1}^2 - i_1\phi_1) & (m_1 i_1 - \phi_1) & -\phi_1 \\ \vdots & \vdots & \vdots \\ (m_1 {i_k}^2 - i_k\phi_k) & (m_1 i_k - \phi_k) & -\phi_k \\ \vdots & \vdots & \vdots \\ (m_1 {i_n}^2 - i_n\phi_n) & (m_1 i_n - \phi_n) & -\phi_n \end{bmatrix} \begin{bmatrix} m_2 \\ b_2 \\ \mathcal{E} \end{bmatrix} = \begin{bmatrix} m_1 i_1 + \phi_1^2 \\ \vdots \\ m_1 i_k + \phi_k^2 \\ \vdots \\ m_1 i_n + \phi_n^2 \end{bmatrix}$$

The weakness of this approach when applied to the hyperbola problem is the fact that m_1 in fact is not known. Nonetheless, as m_1 represents the slope of the unsaturated region, it can easily be approximated from the experimental data and by solving the equations in the least square sense, the other coefficients can be determined in such way that the inaccuracy in m_1 is compensated for.

4.4.1 Test results

As the approach to determine the hyperbola coefficients is based on the assumption that m_1 is given, and that for the main branch magnetising characteristic is close to

infinity (90 degrees slope), some simulations have been carried out to investigate the influence of this constant on the approach performance.

Three values of m_1 have been considered: 1000, 5000 and 10000, for the main branch magnetising characteristic, and the results are shown in Figure 4.6(a). Contrary to what had been expected, with m_1 equal to 1000 a very poor agreement is obtained, notably on the knee region. A very close match is obtained with m_1 equal to 5000. However, if m_1 is increased above this value the accuracy gain is quite small, as can be seen from the result obtained with m_1 equal to 10000.

Simulation considering $m_1 = 10000$ and 8 points from the tabulated data determined an interpolating curve closely matching the experimental curve, as shown in Figure 4.6(b). However, a small discrepancy is observed on the knee region. Another case has been simulated with a large number of points on that region and the result is illustrated in Figure 4.6(c) with no accuracy gain detected.

The same value of m_1 has been adopted to simulate the yoke, zero-sequence path and hypothetical magnetising characteristics and the results are illustrated in Figure 4.6(d). Excellent agreements between interpolating and experimental curves have been obtained, except a small discrepancy at the knee region for the hypothetical curve. The hyperbola constants for all magnetising charactersitics are described in Table 4.2.

Curve	Main	Yoke	Zero-Seq.	Hypothetical
m_2	0.0957	1.6265	1.1831	0.6629
b_2	1.3326	1.1936	0.4444	1.0357
$\mathcal{E}$	16.7675	16.0918	28.7459	74.1041
cond.	3.797e+03	3.034e+03	7.142e+03	6.367e+04

Table 4.2 Hyperbola coefficients

4.4.2 Summary

The hyperbola is a simple equation that can adequately represent a wide range of magnetising characteristics. For those characterisitcs with sharp knee region, the hyperbola coefficients can be directly approximated from the experimental curve. However, for those with smooth knee region, a mathematical procedure is required to determine the coefficients if an accurate interpolating curve is desired. In principle, it would not be possible to use the SVD technique to determine the coefficients as the set of equations to be solved is non-linear. However, assuming that the slope of the unsaturated region (m_1) is known, the set of equations becomes linear and the SVD technique is applicable. Several simulations have been carried out and the results indicate that by choosing a large m_1 value, the SVD approach can determine coefficients that provide accurate interpolating curves.

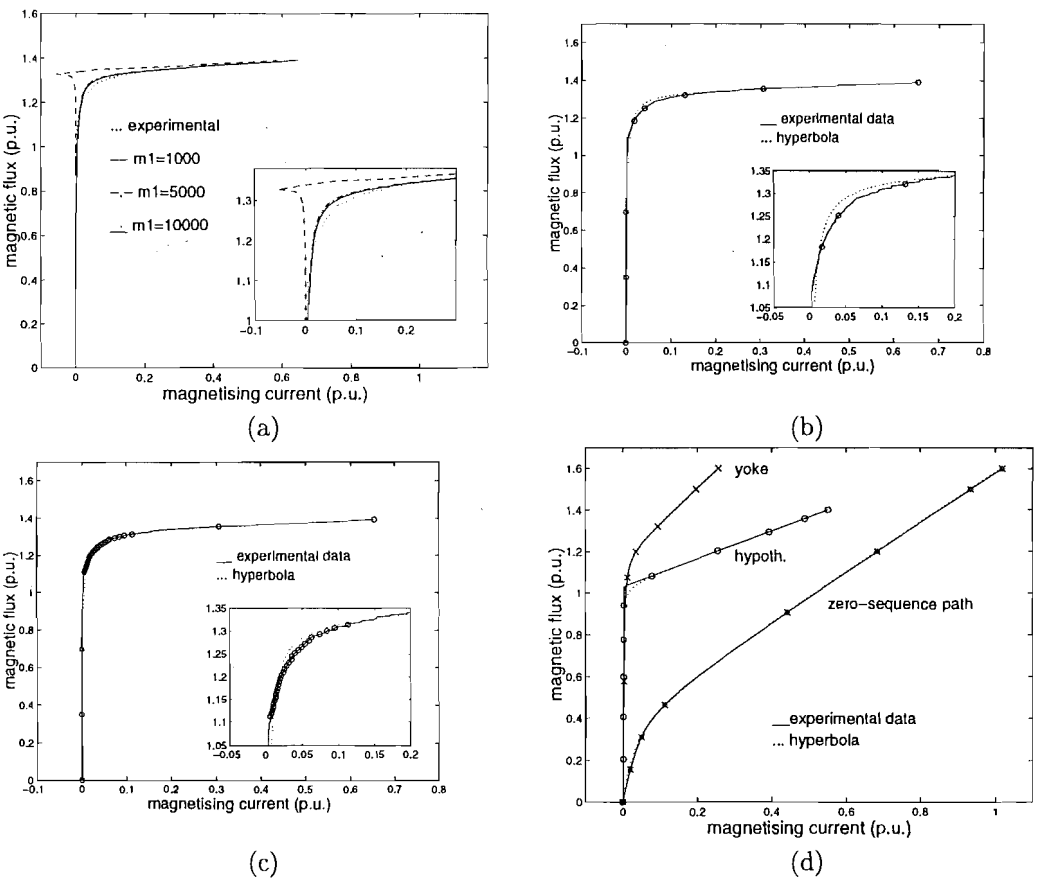

Figure 4.6 Hyperbola approximations

The hyperbola accuracy is slightly inferior than that of a rational-fraction only at the knee region of some magnetising characteristics, e.g main branch and hypothetical magnetising characteristics. It is worth pointing out that this equation can not be used for harmonic domain algorithms based on convolution[Smith 1995].

4.5 CUBIC SPLINES INTERPOLATION

Due to the simplicity of their fundamental properties, flexibility, and the availability of well tested programs for their computation, spline functions are finding applications in an increasing number of numerical methods. They yield smooth interpolating curves which are less susceptible to large oscillations between tabulated points than high degree polynomials. Among them, cubic splines are the most commonly used and their theoretical details are available in an extensive literature. Based on references [Greville 1969], [Stoer and Bulirsch 1993], [Press *et al.* 1992], the basic mathematical aspects are briefly described in this work to form an appropriate introduction for the their application to the magnetising characteristics of the iron cores.

Given a tabulated function $y_i = f(x_i)$, $i = 0, 1, ...n$, with $a = x_0 < x_1 < ... < x_n = b$, a cubic spline function $S(x)$ with the knots $x_0, x_1, ..., x_n$ is a function defined on the interval $[a, b]$ having the following properties:

1. In each subinterval $[x_i, x_{i+1}]$, i=0,1,...,n-1, $S(x)$ is given by a polynomial of degree three.

2. $S(x)$ and its first two derivatives $S'(x)$ and $S''(x)$ are continuous everywhere.

Thus a cubic spline function is a piecewise cubic polynomial function which is twice continuously differentiable, i.e. for any two sucessive subintervals, $[x_{i-1}, x_i], [x_i, x_{i+1}]$, their function values and those of their first two derivatives coincide at their common boundary x_i.

The cubic spline interpolation formula can be expressed in the form

$$S(x_j) = A_j + B_j(x - x_j) + C_j(x - x_j)^2 + D_j(x - x_j)^3 \tag{4.4}$$

for $x \in [x_j, x_{j+1}]$, j=1,...n, where

$$A_j = y_j$$

and the remaining coefficients defined by functions of the second derivatives

$$
\begin{aligned}
B_j &= \frac{y_{j+1}-y_j}{x_{j+1}-x_j} - 2\frac{S''(x_j)-S''(x_{j+1})}{6}(x_{j+1}-x_j) \\
C_j &= \frac{S''(x_j)}{2} \\
D_j &= \frac{S''(x_{j+1})-S(x_j)}{6(x_{j+1}-x_j)}
\end{aligned}
$$

The $(n+1)$ unknown second derivatives $S''(x_j), j = 0, 1, ...n$ can be determined from the $(n-1)$ equations resulting by applying the condition of continuity for the first derivatives, i.e. $S'(x_i)$ in the interval $[x_{i-1}, x_i]$ equal to $S'(x_i)$ in the interval $[x_i, x_{i+1}]$,

$$
\frac{(x_j-x_{j-1})}{6}S''_{j-1} + \frac{(x_{j+1}-x_{j-1})}{3}S''_j + \frac{(x_{j+1}-x_{j-1})}{6}S''_{j+1} = \frac{(y_{j+1}-y_j)}{(x_{j+1}-x_j)} - \frac{(y_j-y_{j-1})}{(x_j-x_{j-1})} \tag{4.5}
$$

and, for a unique solution, two further equations, typically taken from the boundary conditions at x_0 and x_n. The most common ways of specifying these conditions are either

- Case a: Setting one or both S''_0 and S''_n equal to zero (so-called *natural cubic spline*) or,
- Case b: Setting one or both S''_0 and S''_n equal to values calculated from equation (4.5) by specifying any convenient value for the first derivative on either or both boundaries.

The set of equations (4.5), along with those two related to the boundary conditions, is tridiagonal linear and row diagonally dominant. Thus, the solution can be found without any difficulty by Gauss elimination without pivoting.

The magnetising characteristic of ferromagnetic cores can be represented by cubic splines with either way of specifying the boundary conditions. By adopting Case b, an hybrid interpolating formula can be derived with straight lines representing the large slopes and cubic splines representing the smooth parts of the curve, i.e. one or both of saturated and unsaturated regions are represented by straight lines and the knee region represented by cubic splines. In this work, it has been implemented two hybrid approaches have been implemented:

- Hybrid approach 1: The first derivatives S'_0 and S'_n are equal to the slopes of the unsaturated and saturated region, respectively. In doing so, both the saturated and unsaturated regions are represented by straight lines.

- Hybrid approach 2: The first derivative S'_0 is equal to the slope of the unsaturated region and S'_n is equal to zero. In this case, only the unsaturated region is represented by straight lines.

Both natural cubic splines and hybrid interpolation formulas are obtained for the first quadrant, and an appropriate logic can extend it symmetrically to the third quadrant, thus yielding a complete magnetising characteristic.

4.5.1 Test results

4.5.1.1 Natural cubic spline

Initially only four points from the tabulated experimental data have been chosen: the origin, the end and two points at the beginnig and at the end of the knee region (i.e. points 1, 2, 3 and 4 in Figure 4.7(a)). With this reduced number of points (three cubic splines), a poor agreement between experimental and interpolating curves is achieved, particularly in the unsaturated and knee regions. Another simulation is performed with an extra point between the origin and the beginning of the knee region, point 5, and the result is illustrated in Figure 4.7 (b). The discrepancies are still large between the two curves, although reduced if compared with the previous case. A closer match is achieved when an extra point are used, point 6 in Figure 4.7(c). Finally, an excellent agreement is obtained when seven points is given (i.e. six cubic splines) as illustrated in Figure 4.7(d).

The natural cubic spline interpolating curves for the yoke and zero-sequence path magnetising characteristics, illustrated in Figure 4.8 (a), show a very close agreement between experimental and interpolating curves. While the yoke magnetising characterisitic needed eight points to be accurately represented, the zero-sequence path's needed only five points as it has a much smoother knee region.

Finally, another case has been tested considering an hypotetical magnetising characteristic with a sharply defined knee region. Even in this case the match between the two curves has been excellent with nine given points. This result, with an enlarged view of the knee region, is illustrated in Figure 4.8 (b).

4.5.1.2 Hybrid approach 1

The main branch magnetising characteristic with the same number of points which produced a good Natural cubic spline interpolating curve (Figure 4.7(d)) is used to test the Hybrid approach 1 performance. The simulation result, illustrated in Figure 4.9(a), shows a poorer agreement between the two curves than that obtained with Natural cubic splines. Simulations have then been carried out with an increasing number of points until the experimental and hybrid interpolating curves closely match. These results are

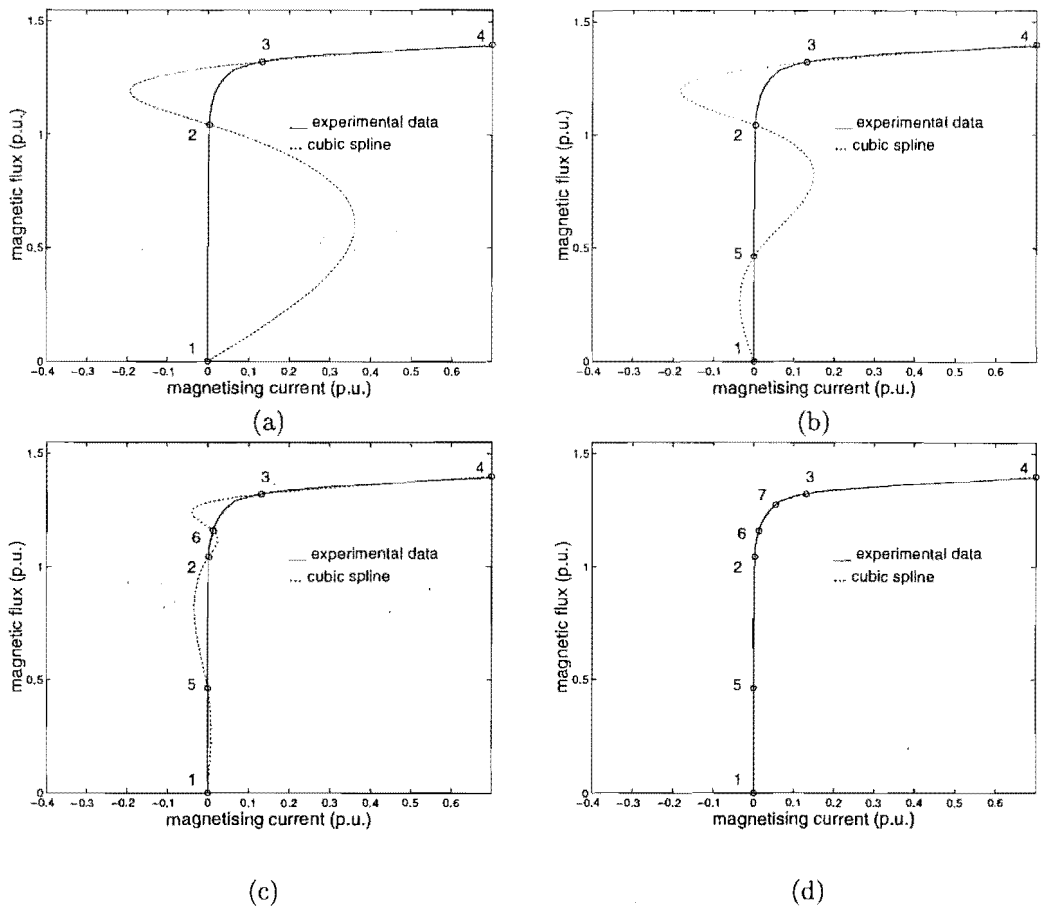

Figure 4.7 Natural cubic spline interpolating curves

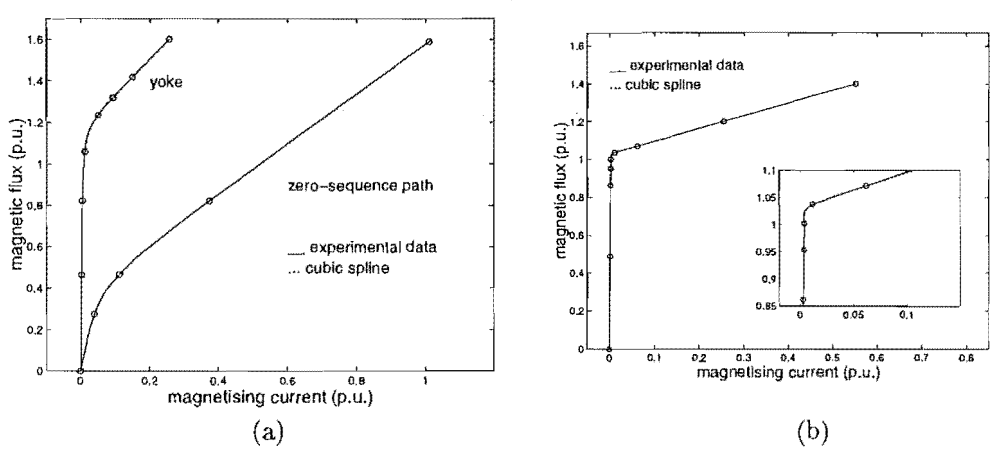

Figure 4.8 Natural cubic spline interpolating curves 2

illustrated in Figures 4.9 (b), (c), and (d), considering 7, 8 and 10 points respectively. As the slopes of the saturated and unsaturated regions are almost perpendicular to each order and joined by a smooth knee region, this has proved a much harder condition for Hybrid approach 1, requiring 10 points to achieve an almost perfect agreement.

The yoke, zero-sequence path and the hypothetical magnetising characteristics have also been simulated with this approach. Less points have been required to obtain the yoke interpolating curve, shown in Figure 4.9 (e), comparing with the number required with the Natural cubic splines: the unsaturated and saturated regions are adequately represented by straight lines and the knee region, by only three cubic splines. For the zero-sequence path, also illustrated in Figure 4.9 (e), the Hybrid approach 1 shows the same performance as the Natural cubic spline. These two magnetising characteristics could be easily represented by this approach as they have smooth knee region and the angle between the two slopes is much greater than 90 degrees.

For the hypothetical magnetising characteristic, just two close points on the knee region are needed for an excellent agreement, as illustrated in Figure 4.9 (f). Therefore, Hybrid 1 approach is perfectly adequate to represent this type of curve.

4.5.1.3 Hybrid approach 2

The same test cases have been repeated to test the Hybrid approach 2. For the main branch magnetising characteristic, a reasonably good agreement is achieved with the same six given points used to simulate the Natural cubic splines, as illustrated in Figure 4.10(a). Thus, the second hybrid approach appears to be more efficient than Hybrid approach 1. For the yoke and zero-sequence paths though, the same number of points is required in both Hybrid approaches. The hypothetical magnetising characteristic result is not illustrated here as a good agreement can not be achieved with less points than in the previous approach.

4.5.2 Summary

Natural cubic splines and hybrid interpolating approaches 1 and 2, have shown different performances for different magnetising characteristics. Nonetheless, all of them can represent any magnetising characteristic with high degree of accuracy if the region to be represented by cubic splines is adequately sampled. As the ideal number of points (i.e splines) cannot be predicted, this problem can easily be overcome by using a large number of tabulated points for the region to be represented by cubic splines. However, this is not needed if one of the cubic spline approaches is adequately chosen to represent a particular magnetising characteristic. From the analysis of the simulations results, it can be concluded:

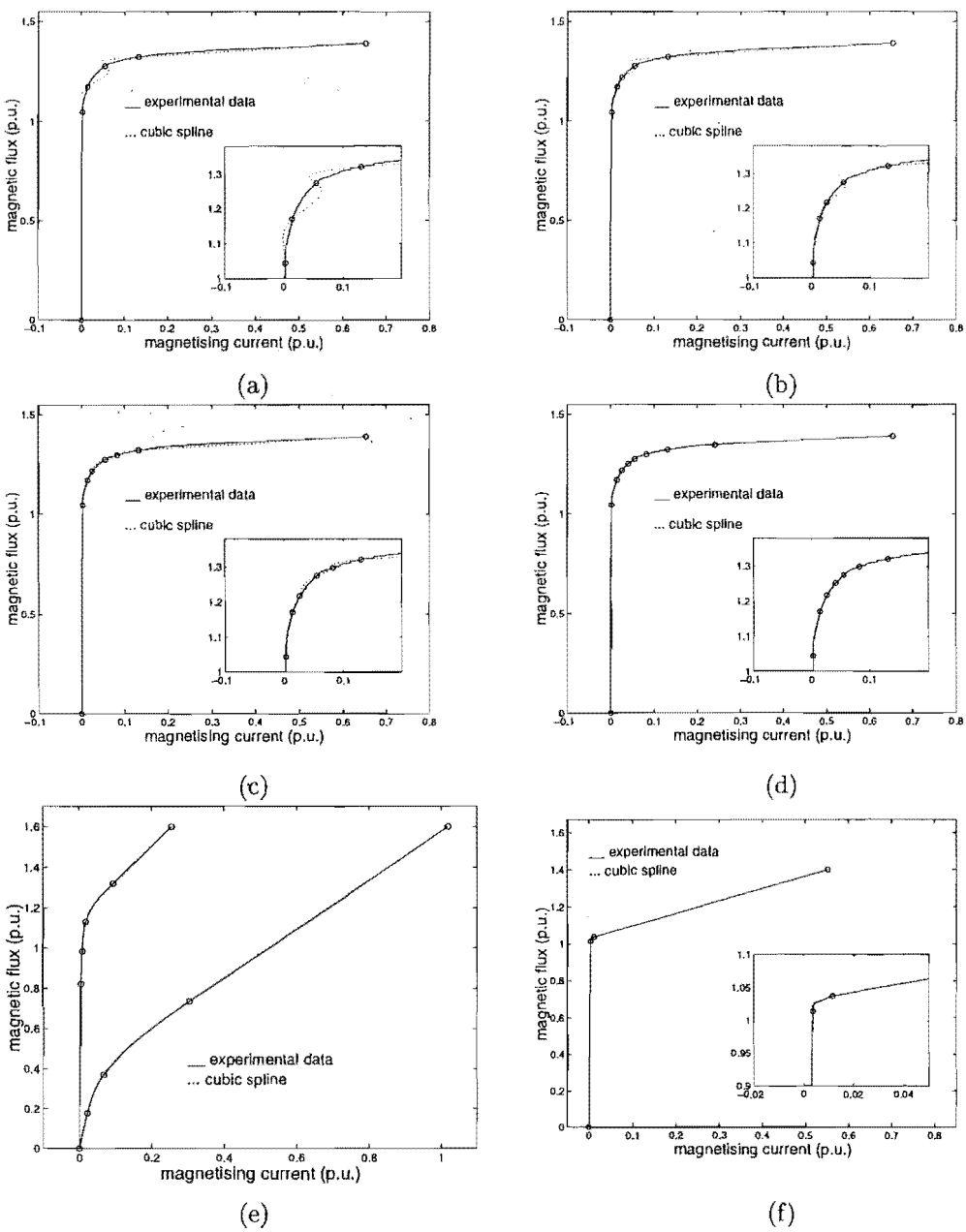

Figure 4.9 Hybrid approach 1

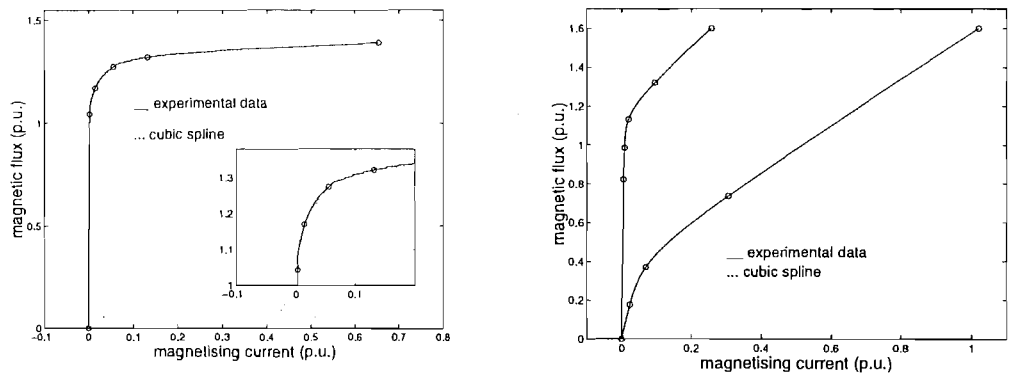

Figure 4.10 Hybrid approach 2

- For magnetising characteristics where the angle between the slopes of saturated and unsaturated regions is close to ninety degrees (main branch type) with smooth knee region, Hybrid Approach 2 is the most appropriate. Experience with this approach shows that no more than 10 points evenly distributed is required to achieve excellent interpolating curves.

- For the magnetising characteristics as defined previously, but with sharply defined knee region (hypothetical type considered in this work), hybrid approach 1 is the most appropriate. It is even better than the usual two piecewise linear approximations as the continuity between the two slopes is ensured without requiring any extra significant computational time or memory.

- For magnetising characteristics such as the yoke and zero-sequence path's type (with the angle formed by unsaturated and saturated regions much bigger than 90 degrees and with smooth knee region), either hybrid approach 1 or 2 can produce excellent interpolating curves with less than 10 given points.

4.6 ADEQUACY OF THE MAGNETISING CHARACTERISTIC APPROXIMATIONS FOR RESONANT SYSTEMS

The same Jagura-Taquaril test system and sensitivity analysis described previously has been repeated here to investigate the adequacy of representing the magnetising characteristics by hyperbola, rational-fraction and four piecewise linear approximations and also to further investigate the cubic spline performance. The interpolating curves for the various magnetic branches obtained with these approaches are illustrated in Figure 4.11. Those related to the main branch are used in the simulations with the three-phase bank of single-phase transformers model.

The simulation results indicate a very close harmonic solution for either cubic

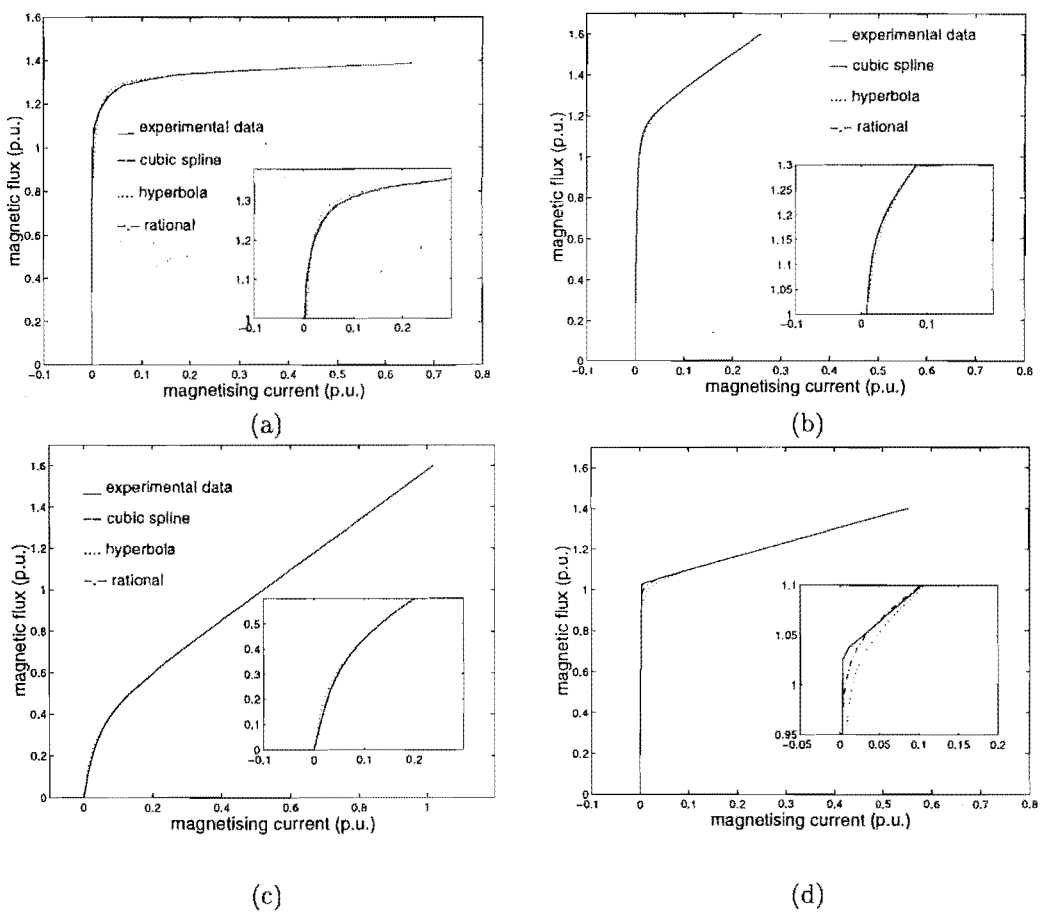

Figure 4.11 Comparison of interpolating curves

spline, rational-fration, hyperbola or four piecewise linear approximations approaches to represent the magnetising characteristic. The fundamental, third, fifth and seventh harmonic voltages, magnitude and phase angle, are illustrated in Figures 4.12(a) to (h). This performance is similar for the harmonic currents, illustrated in Figures 4.13(a) to (h).

4.7 CONCLUSIONS

For power transformer with smooth knee region magnetising characteristic, an accurate reproduction of the entire curve is essential for a rigorous harmonic analysis of power systems with resonance problems. For this type of magnetising characteristic, two and three piecewise linear approximations can be rather inadequate, yielding results with a large margin of error.

The approach based on SVD technique to determine the rational-fraction and hyperbola coefficients is extremely simple and efficient. About ten points of the experimental curve, evenly distributed, is sufficient to determine excellent interpolating curves. However, for the rational-fraction the order of the numerator and denominator equation must be known, while for the hyperbola the slope of the unsaturated region must be given.

The cubic spline is a very simple, efficient and extremely accurate way to reproduce any type of magnetising characteristic. It can be extended to represent hysteresis and is suitable for harmonic domain algorithm based on convolutions [Smith 1995].

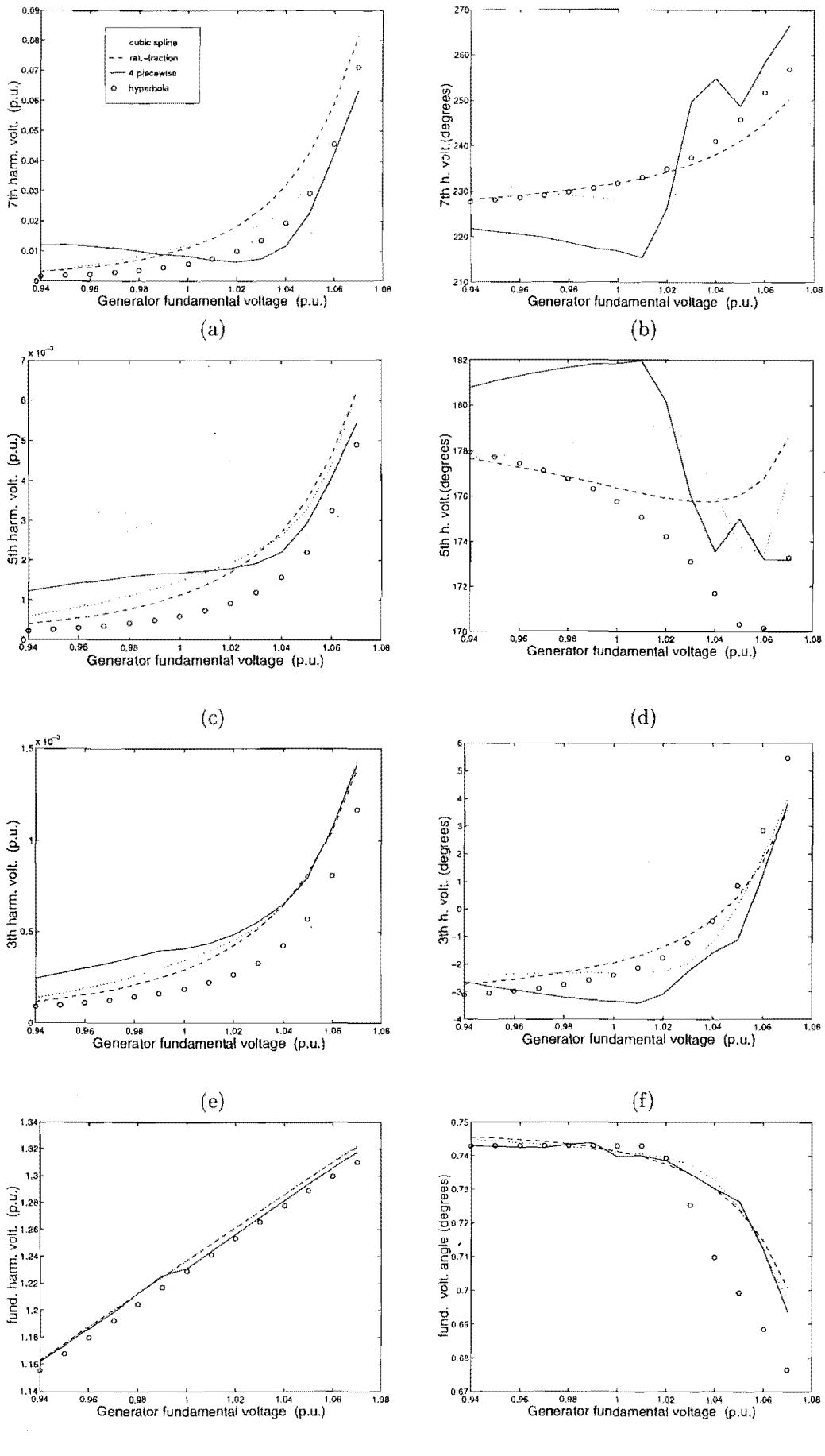

Figure 4.12 Harmonic voltages bus 3, phase A

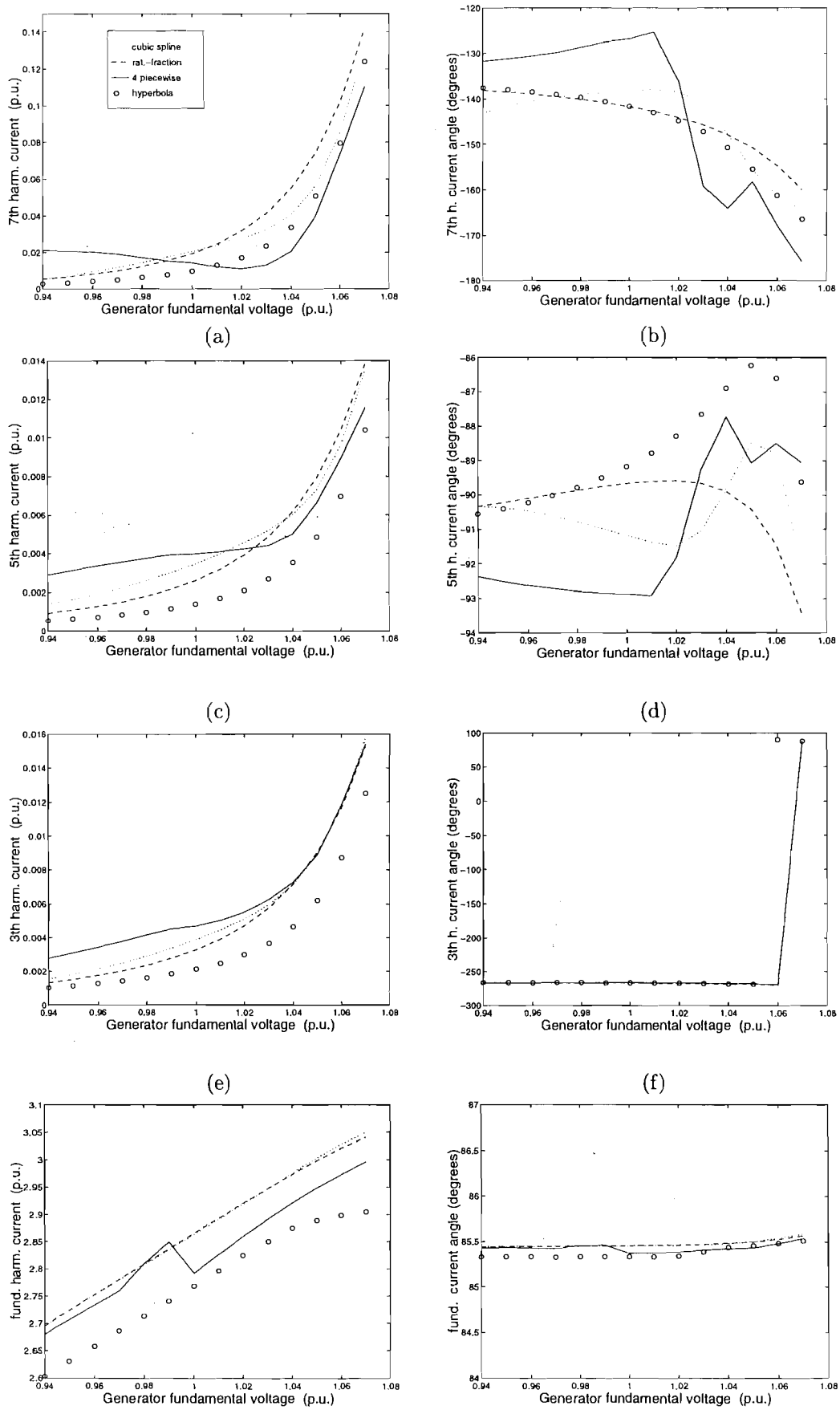

Figure 4.13 Magnesiting currents

Chapter 5

HARMONIC MODEL FOR THREE-LIMB TRANSFORMERS

5.1 INTRODUCTION

When determining the harmonic impedances of a network, or performing harmonic penetration studies from given harmonic current injections, the transformers are rarely represented as harmonic sources, i.e. their inherent magnetisation non-linearities are ignored on the assumption that the transformers have been designed to operate within the linear region of the magnetising characteristics. Such an assumption may have been reasonable in earlier less competitive times. Recent transformer designs tend to operate very close to the limit of the linear characteristics and, even under small overexcitation, their contribution to the harmonic content can not be ignored.

An important contribution to rectify the problem was made by Dommel [Dommel *et al.* 1986], where both magnetic and electric circuits are solved sequentially. In that model the non-linear magnetic reluctances are represented in the electric circuit as voltage-dependent harmonic current sources, calculated from the magnetising characteristic, and the solution is achieved through a Gauss-Seidel iterative procedure.

An alternative proposal has been made by Semlyen [Semlyen *et al.* 1987a] to solve both circuits simultaneously through a unified Newton-type iterative procedure. The transformer magnetic circuit is represented in the form of a Norton harmonic equivalent obtained by linearisation of the magnetising characteristic in the harmonic domain. The unified approach proposed for single-phase transformers, has been extended by Medina [Medina and Arrillaga 1992] to the multi-limb transformers considering individual magnetising characteristics for each branch. A generic linearised equation is derived for the magnetic branches and with the aid of a connection matrix (describing the magnetic branch connections), a generalised formulation for the magnetic equivalent circuit of a multi-limb transformer is obtained in the form of an electrical Norton equivalent.

The extension of the single loop core formulation to a multi-limb core is not straightforward. The nodal magnetising current equations obtained with the help of the connection matrix do not provide unambiguous information of the flux distribu-

tion in the various branches of a saturated multi-limb core. Besides magnetising its corresponding winding branch, each magnetising current contributes to the magnetisation of the remaining iron core branches. Our attempts to match steady-state and Time Domain results with the Harmonic Domain simulation programs have shown good agreement for the single-phase transformer model but considerable discrepancies for the multi-limb model. In general, the distortion levels predicted by the multi-limb case in the Harmonic Domain were larger than those obtained using Time Domain formulation.

The present contribution improves the Harmonic Domain model with the addition of the nodal magnetising flux balance ($\sum \phi = 0$) to the nodal magnetising current formulation thus providing important missing information about the magnetic circuit.

5.2 MODIFIED HARMONIC DOMAIN ALGORITHM

The basic structure of the Harmonic Domain algorithm described in Chapter 3 has been modified as illustrated in the block diagram of Figure 5.1. Block α and β, enclosed in dotted lines, represent the main modifications to the three-limb transformer model proposed in this work. Block α replaces the assumed linear distribution of the magnetic fluxes by a Newton flux distribution iterative procedure. Block β replaces the Norton equivalent developed in reference [Medina and Arrillaga 1992] by a more accurate Norton equivalent proposed in this work. These two blocks are described in the next sections.

5.2.1 Derivation of the Norton equivalent

An accurate determination of the magnetising currents of the multi-limb transformer should involve the complete magnetic circuit. The solution is not straightforward due to the non-linearities of the magnetic reluctances, which are functions of the magnetic material and branch geometries. The yokes, zero-sequence flux paths and for a five limb transformer, the outer branches, have magnetising characteristics considerably different from that of the winding branches, as shown by Dick and Watson [Dick and Watson 1981].

The magnetic equivalent circuit must be described as a function of the branch fluxes and reluctances, and the magnetic circuit equations obtained by applying the magnetic circuit laws

$$\sum Ni = \sum \mathcal{R}\phi \tag{5.1}$$

for any closed path (N being the number of turns), and

$$\sum \phi = 0 \tag{5.2}$$

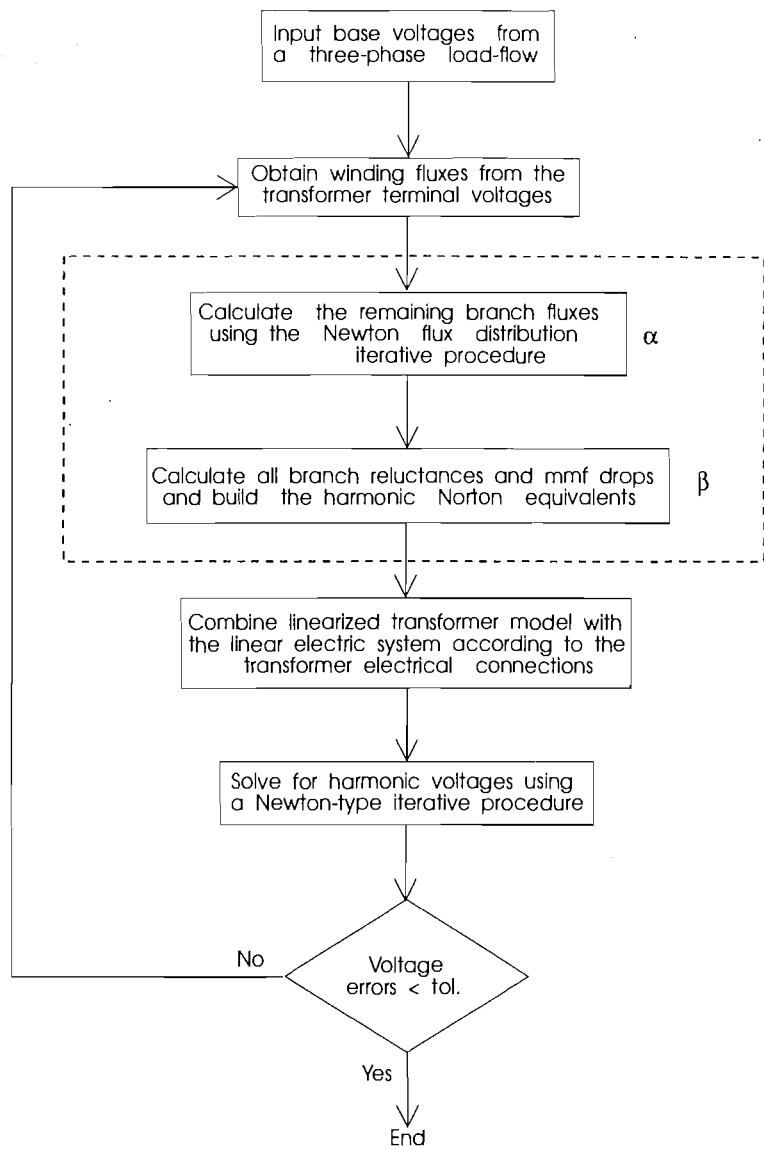

Figure 5.1 HDA flow diagram

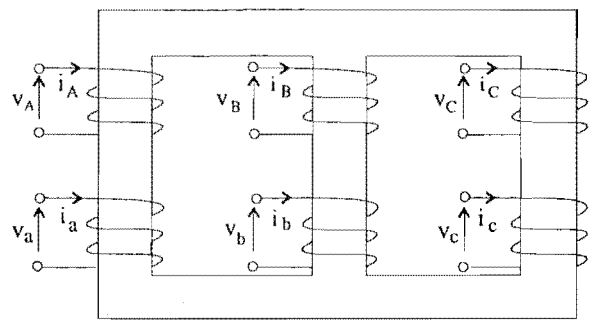

Figure 5.2 Three-phase three-limb core transformer

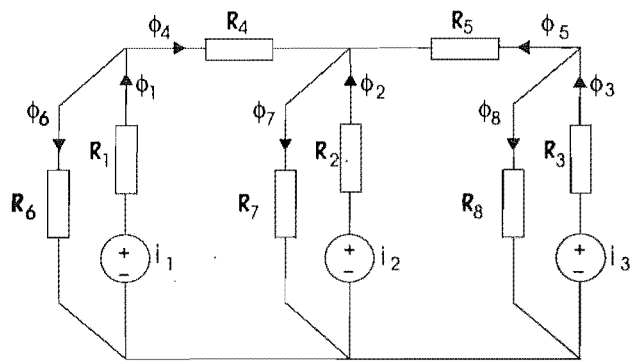

Figure 5.3 Magnetic equivalent circuit

at any junction.

For the case of the three-limb transformer shown in Figures 5.2 and 5.3, the winding flux values ϕ_1 to ϕ_3 can be calculated according to Faraday's law ($\phi_s = \frac{1}{N}\int v_s.dt$). Therefore, the magnetic equivalent circuit will have eight unknown variables, i.e. three magnetising currents i_1,i_2 and i_3 and five fluxes, ϕ_4 to ϕ_8. Five basic equations can be derived from the first magnetic circuit law

$$i_1 = f_1(\phi_1) + f_6(\phi_6) \tag{5.3}$$

$$i_2 = f_2(\phi_2) + f_7(\phi_7) \tag{5.4}$$

$$i_3 = f_3(\phi_3) + f_8(\phi_8) \tag{5.5}$$

$$i_1 - i_2 = f_1(\phi_1) + f_4(\phi_4) - f_2(\phi_2) \tag{5.6}$$

$$i_2 - i_3 = f_2(\phi_2) - f_5(\phi_5) - f_3(\phi_3) \tag{5.7}$$

where the branch mmf drop across each branch reluctance has been represented by the corresponding magnetising characteristic $i = f(\phi)$. The other three necessary equations are obtained from the second magnetic circuit law

$$\phi_1 - \phi_4 - \phi_6 = 0 \tag{5.8}$$

$$\phi_2 + \phi_4 + \phi_5 - \phi_7 = 0 \tag{5.9}$$

$$\phi_3 - \phi_5 - \phi_8 = 0 \tag{5.10}$$

Applying a Taylor's expansion to equations (5.3) to (5.10) about a base operating point, and truncating after the first order yields

$$\begin{aligned} i_1 &= f_1(\phi_{1b}) + f_6(\phi_{6b}) + \\ &\quad \mathcal{R}_{1b}(\phi_1 - \phi_{1b}) + \mathcal{R}_{6b}(\phi_6 - \phi_{6b}) \qquad (5.11) \\ i_2 &= f_2(\phi_{2b}) + f_7(\phi_{7b}) + \\ &\quad \mathcal{R}_{2b}(\phi_2 - \phi_{2b}) + \mathcal{R}_{7b}(\phi_7 - \phi_{7b}) \qquad (5.12) \\ i_3 &= f_3(\phi_{3b}) + f_8(\phi_{8b}) + \\ &\quad \mathcal{R}_{3b}(\phi_3 - \phi_{3b}) + \mathcal{R}_{8b}(\phi_8 - \phi_{8b}) \qquad (5.13) \\ i_1 - i_2 &= f_1(\phi_{1b}) + f_4(\phi_{4b}) - f_2(\phi_{2b}) + \\ &\quad \mathcal{R}_{1b}(\phi_1 - \phi_{1b}) + \mathcal{R}_{4b}(\phi_4 - \phi_{4b}) - \\ &\quad \mathcal{R}_{2b}(\phi_2 - \phi_{2b}) \qquad (5.14) \\ i_2 - i_3 &= f_2(\phi_{2b}) - f_5(\phi_{5b}) - f_3(\phi_{3b}) + \\ &\quad \mathcal{R}_{2b}(\phi_2 - \phi_{2b}) - \mathcal{R}_{5b}(\phi_5 - \phi_{5b}) - \\ &\quad \mathcal{R}_{3b}(\phi_3 - \phi_{3b}) \qquad (5.15) \end{aligned}$$

where the subscript b denotes the base values and the magnetic reluctance $\mathcal{R}_{kb}$ is the derivative of the magnetising characteristic $i_k = f_k(\phi_k)$ with respect to the base flux ϕ_{kb} ($\mathcal{R}_{kb} = f'(\phi_{kb})$, $k = 1, 2, ..., 8$). Adding equations (5.8) to (5.10) to this set of linearised equations and expressing them in matrix form, with the magnetising currents and ϕ_4 to ϕ_8 as functions of the winding fluxes, leads to

$$\left[\ H\ \right] \begin{bmatrix} i_1 \\ i_2 \\ i_3 \\ \phi_4 \\ \phi_5 \\ \phi_6 \\ \phi_7 \\ \phi_8 \end{bmatrix} = \begin{bmatrix} \mathcal{R}_{1b}\phi_1 - a_1 \\ \mathcal{R}_{2b}\phi_2 - a_2 \\ \mathcal{R}_{3b}\phi_3 - a_3 \\ \mathcal{R}_{1b}\phi_1 - \mathcal{R}_{2b}\phi_2 - a_4 \\ \mathcal{R}_{2b}\phi_2 - \mathcal{R}_{3b}\phi_3 - a_5 \\ \phi_1 \\ \phi_2 \\ \phi_3 \end{bmatrix} \qquad (5.16)$$

where

$$\left[\ H\ \right] = \begin{bmatrix} 1 & & & & & -\mathcal{R}_{6b} & & \\ & 1 & & & & & -\mathcal{R}_{7b} & \\ & & 1 & & & & & -\mathcal{R}_{8b} \\ 1 & -1 & & -\mathcal{R}_{4b} & & & & \\ & 1 & -1 & & \mathcal{R}_{5b} & & & \\ & & & 1 & & 1 & & \\ & & & -1 & -1 & & 1 & \\ & & & & 1 & & & 1 \end{bmatrix} \tag{5.17}$$

$$\begin{aligned} a_1 &= \mathcal{R}_{1b}\phi_{1b} + \mathcal{R}_{6b}\phi_{6b} - f_1(\phi_{1b}) - f_6(\phi_{6b}) \\ a_2 &= \mathcal{R}_{2b}\phi_{2b} + \mathcal{R}_{7b}\phi_{7b} - f_2(\phi_{2b}) - f_7(\phi_{7b}) \\ a_3 &= \mathcal{R}_{3b}\phi_{3b} + \mathcal{R}_{8b}\phi_{8b} - f_3(\phi_{3b}) - f_8(\phi_{8b}) \\ a_4 &= \mathcal{R}_{1b}\phi_{1b} + \mathcal{R}_{4b}\phi_{4b} - \mathcal{R}_{2b}\phi_{2b} - f_1(\phi_{1b}) - \\ &\quad f_4(\phi_{4b}) + f_2(\phi_{2b}) \\ a_5 &= \mathcal{R}_{2b}\phi_{2b} - \mathcal{R}_{5b}\phi_{5b} - \mathcal{R}_{3b}\phi_{3b} - f_2(\phi_{2b}) + \\ &\quad f_5(\phi_{5b}) + f_3(\phi_{3b}) \end{aligned}$$

Equation (5.16) produces the following expressions for the magnetising currents

$$\begin{bmatrix} i_1 \\ i_2 \\ i_3 \end{bmatrix} = \begin{bmatrix} d_{11} & \dots & \dots & \dots & \dots & \dots & d_{18} \\ d_{21} & \dots & \dots & \dots & \dots & \dots & d_{28} \\ d_{31} & \dots & \dots & \dots & \dots & \dots & d_{38} \end{bmatrix} \begin{bmatrix} \mathcal{R}_1\phi_1 - a_1 \\ \mathcal{R}_2\phi_2 - a_2 \\ \mathcal{R}_3\phi_3 - a_3 \\ \mathcal{R}_1\phi_1 - \mathcal{R}_2\phi_2 - a_4 \\ \mathcal{R}_2\phi_2 - \mathcal{R}_3\phi_3 - a_5 \\ \phi_1 \\ \phi_2 \\ \phi_3 \end{bmatrix}$$

where d_{ij} are the elements of the inverse of matrix [H]. This matrix equation can be re-arranged in the form

$$\begin{bmatrix} i_1 \\ i_2 \\ i_3 \end{bmatrix} = \begin{bmatrix} k_{11} & k_{12} & k_{13} \\ k_{21} & k_{22} & k_{23} \\ k_{31} & k_{32} & k_{33} \end{bmatrix} \begin{bmatrix} \phi_1 \\ \phi_2 \\ \phi_3 \end{bmatrix} + \begin{bmatrix} i_{n1} \\ i_{n2} \\ i_{n3} \end{bmatrix}$$

or

$$\tilde{i}_s = [K]\,\tilde{\phi}_s + \tilde{i}_{ns} \tag{5.18}$$

where $s = 1, 2, 3$.

The interface with the external electrical system is made by relating the magnetising currents to the winding voltages. In the harmonic domain and per unit form Faraday's law is expressed by

$$v_s = jhw\phi_s \tag{5.19}$$

Finally, substitution of equation (5.19) into equation (5.18) yields

$$\tilde{i}_s = [Y]\tilde{v}_s + \tilde{i}_{ns} \tag{5.20}$$

where

$$[Y] = [K]Diag\{jhw\}^{-1}$$

and

$$i_{ns} = -a_1 d_{s1} - a_2 d_{s2} - a_3 d_{s3} - a_4 d_{s4} - a_5 d_{s5}$$

where $s = 1, 2, 3$.
The elements of matrix $[K]$ are defined below

$$\begin{aligned} k_{s1} &= d_{s1}\mathcal{R}_{1b} + d_{s4}\mathcal{R}_{1b} + d_{s6} \\ k_{s2} &= d_{s2}\mathcal{R}_{2b} - d_{s4}\mathcal{R}_{2b} + d_{s5}\mathcal{R}_{2b} + d_{s7} \\ k_{s3} &= d_{s3}\mathcal{R}_{3b} - d_{s5}\mathcal{R}_{3b} + d_{s8} \end{aligned}$$

where $s = 1, 2, 3$.

Equation (5.20) is the Norton harmonic equivalent representation of the magnetic circuit; [Y] is a matrix of Norton harmonic admittances and i_{ns} a vector of Norton harmonic current injections. Although the formulation has been derived for a three-phase three-limb transformer, it can be easily extended to multi-limb transformers with any core configuration.

5.2.2 The Newton-Raphson flux distribution iterative procedure

The derivation of the harmonic Norton equivalents described in the previous section has been based on the assumption that all magnetic fluxes are known. However, only the winding fluxes can be directly obtained by integrating the transformer terminal voltages. The remaining fluxes are function of the winding fluxes and branch reluc-

tances, which being non-linear, impose an additional problem to be solved. It has been suggested in the EMTP manual[Dommel 1986] a very simple procedure for an approximate evaluation of the yoke and zero-sequence fluxes. Assuming a linear distribution of the winding fluxes among the yoke branches and zero-sequence flux paths, these fluxes are defined as follows:

$$\begin{aligned}
\phi_4(t) &= 0.9[0.508\phi_1(t) - 0.5\phi_2(t) - 0.9\phi_3(t)] \\
\phi_5(t) &= 0.9[-0.9\phi_1(t) - 0.5\phi_2(t) + 0.508\phi_3(t)] \\
\phi_6(t) &= \phi_1(t) - \phi_4(t) \\
\phi_7(t) &= \phi_4(t) + \phi_2(t) + \phi_5(t) \\
\phi_8(t) &= \phi_3(t) - \phi_5(t)
\end{aligned}$$

The EMTP suggested procedure has been used in the transformer model proposed by Medina and Arrillaga[1992], i.e. it has been implemented in the HDA algorithm to determine the yoke and zero-sequence flux values for each incremental time of a complete cycle discretised in 512 samples. Based on their respective magnetising characteristics, the discrete flux waveforms are then used to derive the corresponding branch magnetising current and reluctance waveforms. By means of a complex discrete Fourier transform (FFT version) these waveforms are solved in the frequency domain and the harmonic coefficients are used to build the harmonic Norton equivalents.

The accuracy of the HDA solution depends largely on an adequate evaluation of the harmonic Norton equivalents, which is entirely based on the branch fluxes and magnetising characteristics. The margin of error introduced by adopting the EMTP linear approximation for flux distribution has not been evaluated yet as more precise yoke and zero-sequence flux values for comparisons were not available. These fluxes can only be accurately determined by solving the complete non-linear magnetic circuit, i.e. equations (5.3) to (5.10). Matrix equation (5.16) expresses this set of equations in a linearized form and thus a solution based on the Newton-Raphson method is possible with the Jacobian matrix defined by matrix [H](equation (5.17)).

Expressing equations (5.3) to (5.10) in a compact form,

$$F(\tilde{x}) = \tilde{0}$$

where

$$\tilde{x} \stackrel{def}{=} \begin{bmatrix} i_1 & i_2 & i_3 & \phi_4 & \phi_5 & \phi_6 & \phi_7 & \phi_8 \end{bmatrix}^T \tag{5.21}$$

a Newton-type iterative procedure is proposed with the main steps summarized as follows:

1. Integrate the transformer terminal voltages determined at the last HDA iteration to obtain the winding fluxes ϕ_1, ϕ_2 and ϕ_3.

2. Estimate the starting values $\tilde{x}_b$. The magnetising currents i_b are derived by associating the winding fluxes with their respective magnetising characterisitics; the yoke and zero sequence fluxes (ϕ_b) are defined from the winding fluxes using the EMTP linear approximation for flux distribution.

3. Determine the yoke and zero-sequence flux path reluctances $\mathcal{R}_b$ ($\mathcal{R}_b = f'(\phi_b)$) and form the Jacobian matrix $[H_b]$.

4. Determine function F at the point $\tilde{x}_b$ ($\mathrm{F}(\tilde{x}_b)$).

5. Calculate the change $\Delta\tilde{x}_b$ and replace $\tilde{x}_b$ by $\tilde{x}_{b+1}$,

$$\begin{aligned} \Delta\tilde{x}_b &= -[H_b]^{-1}F(\tilde{x}_b) \\ \tilde{x}_{b+1} &= \tilde{x}_b + \Delta\tilde{x}_b \end{aligned}$$

6. If the criterion for convergence has not been met and the iterative process is yet to continue, then another iteration is performed from step 3; otherwise, the process is stopped.

The proposed Newton-Raphson flux distribution (FD) iterative procedure has been implemented in the time domain, i.e. the iterative procedure is performed for each incremental time of a complete discrete cycle of the variables x . After convergence, the Fast Fourier transform is then applied to the time domain solution to determine its harmonic complex coefficients, which are required to build the harmonic Norton equivalents.

As the transformer magnetic non-linearities have been appropriately taken into consideration, the FD iterative procedure yields accurate yoke and zero-sequence fluxes which can be used as a reference to validate the results obtained with different procedures such as the one suggested in the EMTP manual.

Obviously, the FD algorithm requires additional computation as compared with the EMTP suggested procedure; at each HDA iteration, the former requires a complete Newton-Raphson procedure, while the latter requires only the substitution of the flux values in a set of linear equations. To reduce computational time, at each iteration of the HDA algorithm, the Jacobian matrix $[F]$ is kept constant after it has been evaluated for the first FD iteration.

It must be pointed out that an exact solution for both magnetic and electric circuit can only be obtained if the FD algorithm is used to determine yoke and zero-sequence fluxes; the magnetising currents are determined when the HDA converges,

while the yoke and zero-sequence fluxes are exactly determined by the FD algorithm (at each HDA iteration). By using the EMTP suggested procedure, the HDA solution does not necessarily satisfy the whole magnetic circuit, as the yoke and zero-sequence fluxes are determined by a linear approximation.

5.2.3 The harmonic electromagnetic model

Considering the three-phase three-limb core transformer illustrated in Figure 5.2, the primitive electric parameters for the six coils terminals are represented by the following matrix equation [Chen and Dillon 1974]

$$\begin{bmatrix} i_A \\ i_a \\ i_B \\ i_b \\ i_C \\ i_c \end{bmatrix} = \begin{bmatrix} y_p & -y_m & y'_l & y''_l & y'_l & y''_l \\ -y_m & y_p & y''_l & y'''_l & y''_l & y'''_l \\ y'_l & y''_l & y_p & -y_m & y'_l & y''_l \\ y''_l & y'''_l & -y_m & y_s & y''_l & y'''_l \\ y'_l & y''_l & y'_l & y''_l & y_s & -y_m \\ y''_l & y'''_l & y''_l & y'''_l & -y_m & y_s \end{bmatrix} \begin{bmatrix} v_A \\ v_a \\ v_B \\ v_b \\ v_C \\ v_c \end{bmatrix} \tag{5.22}$$

where

y_p, y_s	:	Self primary and secondary leakage admittances, respectively
y_m	:	Mutual leakage admittance between primary and secondary coils on the same limb
y'_l	:	Mutual leakage admittance between primary coils
y''_l	:	Mutual leakage admittance between primary and secondary coils on different limbs
y'''_l	:	Mutual leakage admittance between secondary coils

A composite harmonic electromagnetic transformer model can be derived by an adequate combination of electric and magnetic transformer models.

An approximate π equivalent model can be derived by assuming an equal distribution of the magnetising branch (harmonic Norton equivalent) between primary and secondary transformer terminals. This assumption had been used in the past and suggested more recently [Dommel 1975]; it yields an accurate solution for most of power system studies. It has also been adopted in previous harmonic domain transformer models [Acha *et al.* 1989] [Medina and Arrillaga 1992], but its validity for harmonic analysis has not been investigated.

The exact allocation of the harmonic Norton equivalents in the electric system requires knowledge of the primary and secondary transformer leakage reactances as well as the external system impedance. In this Chapter, they are distributed between primary and secondary terminals proportionally to the factors α and β, which are detailed described in the next Chapter. This results in the following π harmonic electromagnetic equivalent transformer model

$$\begin{bmatrix} i_A \\ i_a \\ i_B \\ i_b \\ i_C \\ i_c \end{bmatrix} = \begin{bmatrix} Y \end{bmatrix} \begin{bmatrix} v_A \\ v_a \\ v_B \\ v_b \\ v_C \\ v_c \end{bmatrix} + \begin{bmatrix} \alpha I_{n1} \\ \beta I_{n1} \\ \alpha I_{n2} \\ \beta I_{n2} \\ \alpha I_{n3} \\ \beta I_{n3} \end{bmatrix} \tag{5.23}$$

where

$$\begin{bmatrix} Y \end{bmatrix} = \begin{bmatrix} y_p + \alpha y_{11} & -y_m & y'_l + \alpha y_{12} & y''_l & y'_l + \alpha y_{13} & y''l \\ -y_m & y_p + \beta y_{11} & y''_l & y'''_l + \beta y_{12} & y''_l & y'''_l + \beta y_{13} \\ y'_l + \alpha y_{21} & y''_l & y_p + \alpha y_{22} & -y_m & y'_l + \alpha y_{23} & y''_l \\ y''_l & y'''_l + \beta y_{21} & -y_m & y_s + \beta y_{22} & y''_l & y'''_l + \beta y_{23} \\ y'_l + \alpha y_{31} & y''_l & y'_l + \alpha y_{32} & y''_l & y_s + \alpha y_{33} & -y_m \\ y''_l & y'''_l + \beta y_{31} & y''_l & y'''_l + \beta y_{32} & -y_m & y_s + \beta y_{33} \end{bmatrix}$$

In practice the self and mutual leakage admittances (y_p, y_s, and y_m) are approximately equal to the leakage admittance y_l, obtained by a short-circuit test [Chen and Dillon 1974].

The primitive parameters of equation (5.23) are transformed to nodal quantities by the use of connection matrix, which mathematically represents the transformer electrical configuration. The nodal equations for the the most commonly used trans-

former connections are derived in Chapter 6.

5.3 TEST SYSTEM AND RESULTS

As the main purpose of the proposed algorithm is the transformer model, the rest of the test system, shown in Figure 5.4, has been kept very simple. It consists of a grounded-Star/grounded-Star transformer connected to an infinite source via either a series inductance or a parallel resonant circuit.

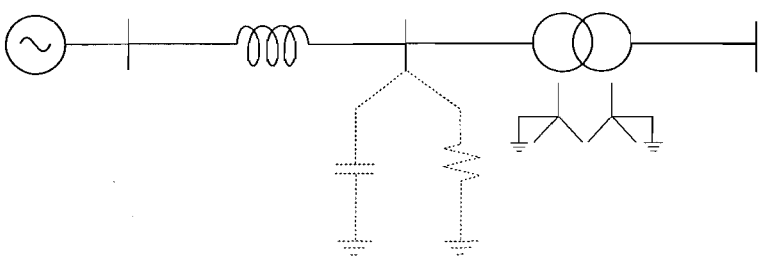

Figure 5.4 Test System

The slope of the unsaturated and saturated regions of the experimental magnetising characteristics given in reference[Dick and Watson 1981] have been used to derive the two straight lines magnetising characteristics adopted for the simulations of this Chapter. The magnetising characteristics associated with the winding, yoke branches and zero-sequence flux paths are represented by curves 1, 2 and 3 of Figure 5.5, respectively, and their hyperbola parameters are described in Appendix B.

The HDA simulations involved the first 15 harmonics and convergence was checked using a tolerance of 0.0001 (p.u.) for the harmonic voltages.

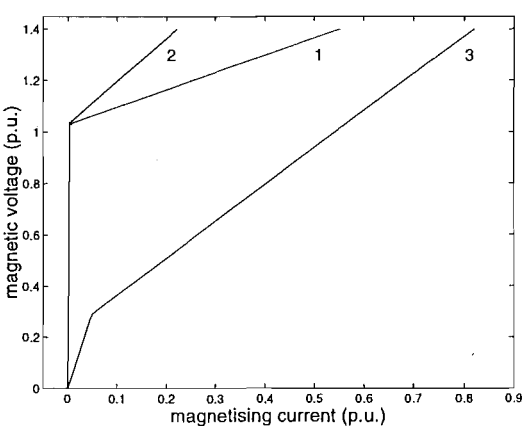

Figure 5.5 Magnetising Characteristics

For verification purposes, the test system was also analysed using the EMTDC program [EMTDC 1988] with the proposed Norton equivalent, adapted to the instan-

taneous form as described in Appendix C. The dynamic simulations using a $50\mu s$ time step, were run for one cycles to ensure a reasonable steady-state before the results were compared.

5.3.1 Example 1

In this case, an inductance $X_l = 0.1$ (p.u.) is connected between the infinite source, specified as 1.1 (p.u.), and the transformer. The results of the HDA simulation are shown in Figure 5.6. Figures 5.6.(a) and 5.6.(b) illustrate the magnetising current waveforms and their spectrum, respectively. The corresponding voltage waveforms at the transformer primary side and their harmonic spectrum are illustrated in Figure 5.6.(c) and 5.6.(d). Although the voltage distortions caused by the magnetising currents are within 1.0% of the fundamental, it should be pointed out that the individual harmonic levels permitted by legislation are usually of this order [Arrillaga and Arnold 1990].

Of course, the magnitude of the harmonic voltages are affected by the overvoltage levels and by the frequency-dependent network impedances. By increasing the infinite bus source up to 1.2 (p.u.) or the serie reactance up to 1.0 (p.u.) distortion levels of up to 4% have been calculated, which are considerably lower than those predicted by the earlier model[Medina and Arrillaga 1992].

In all simulations, the flux distribution iterative procedure and HDA algorithm have achieved convergence within 4 iterations.

5.3.2 Example 2

In this case, the circuit in dotted line of Figure 5.4 is added to the system. A parallel capacitive-inductive circuit is tuned to resonate at the third harmonic and a shunt resistance provides some damping. The inductance, capacitance and resistance values are 0.1(p.u.), -0.9(p.u.), 1.0 (p.u.) respectively.

Figure 5.7.(a) illustrates the waveforms of the current flowing through the inductance obtained with HDA and EMTDC solutions and 5.7.(b) the harmonic content. The transformer primary side voltage waveforms and harmonic content are shown in Figures 5.7.(c) and 5.7.(d) (only phase A results are shown). Almost a perfect match is achieved for the voltage waveforms, the difference between the two solutions is indistinguishable in Figure 5.7.(c). In this case, the third harmonic voltage is nearly 7%.

The results indicate very good agreement between the HDA and EMTDC solutions, specially considering the difficulty of the case analysed. The maximum magnitude differences is 0.003 (p.u.) for the voltages and 0.009 for the currents, both occurring at the third harmonic . The HDA solution has been achieved in 4 iterations.

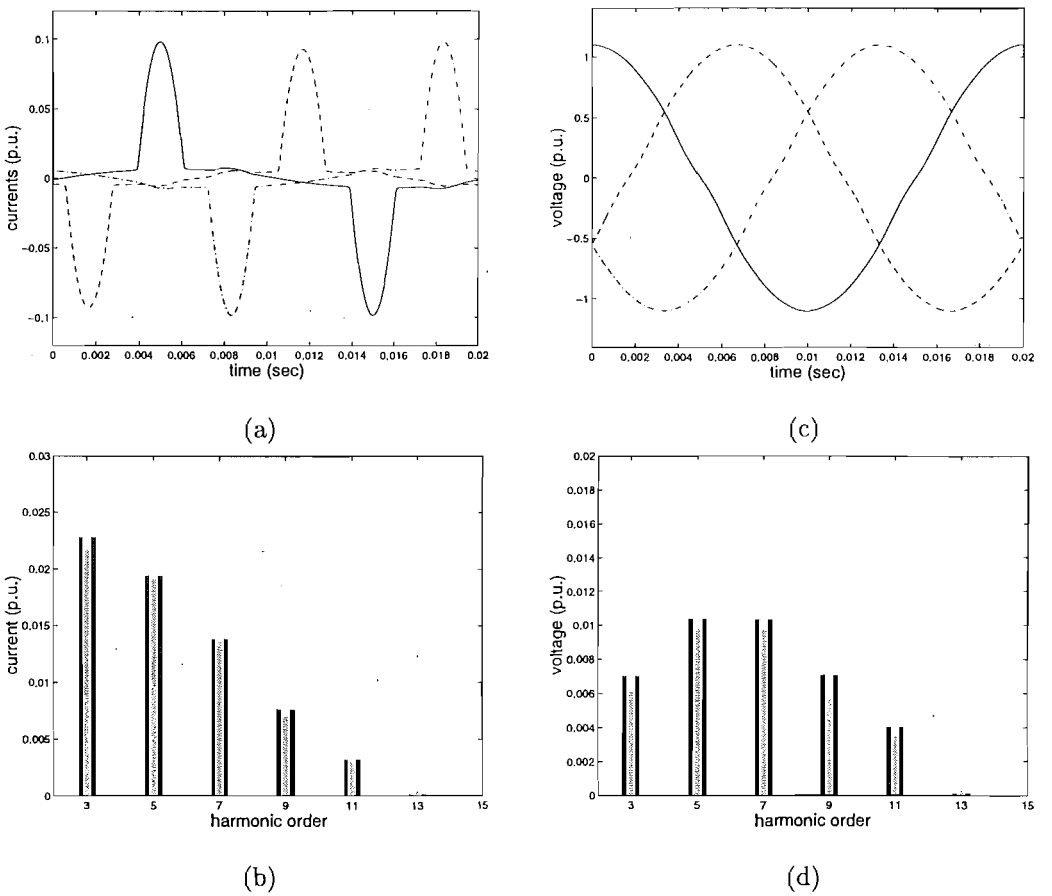

Figure 5.6 HDA simulations - *Example* 1

5.3.3 Comparison between EMTP approximation and FD iterative procedure

Using the test system of *Example* 1, several simulations have been carried out with the HDA program using the Flux Distribution (FD) iterative procedure and the EMTP linear approximation for flux distribution - from now on referred to as HDA/FD and HDA/EMTP algorithms, respectively. Figures 5.8.(a) to (d) illustrate the yoke and zero-sequence path flux (ϕ_4 and ϕ_6) waveforms and harmonic content, obtained by the two algorithms. Having taken into account the saturation and interphase magnetic couplings, the harmonic solution obtained using the FD procedure accurately defines a flat-topped yoke flux waveform and a zero-sequence path flux with two maxima within one-half waveform. The magnetising currents are also more precisely calculated, as it is shown in Figure 5.8.(e) (phase A). The second and smaller maxima in the current waveform, which comprises the higher order harmonics (notably the 5th and the 7th), is not so prominent, particularly in this example where the transformer is slightly saturated. The voltage waveforms at the primary side of the transformer, illustrated in Figure 5.8.(g), do not show distinguishible differences, although the solution based on the FD procedure yields 5th and 7th harmonic voltages slightly larger(Figure 5.8.(h)).

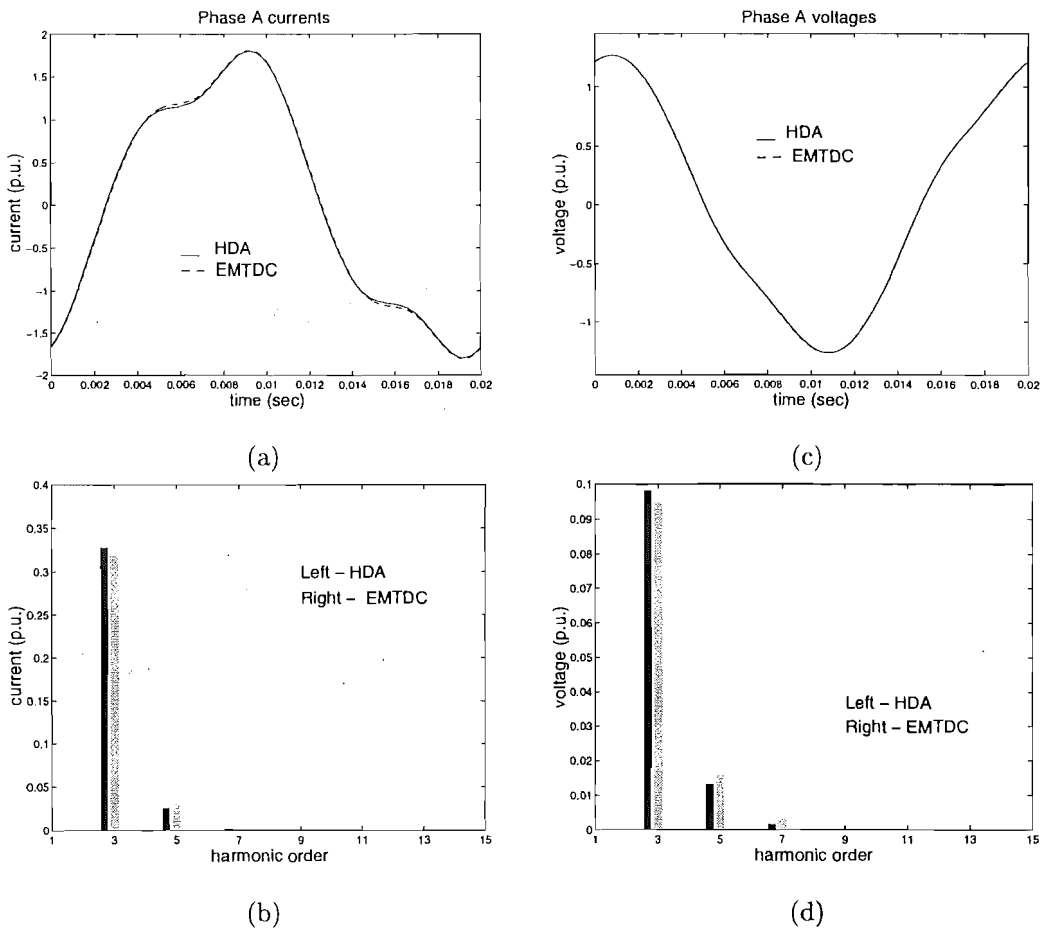

Figure 5.7 HDA and EMTDC soluions - *Example* 2

Another simulation has been carried out considering a larger value for the zero-sequence path reluctances by reducing the slope m_1 of the unsaturated region of this path from to 6.0 to 1.0. The three-phase currents, waveform and harmonic content, calculated by the HDA/FD algorithm are shown in Figure 5.9(a) and (b), respectively, and by the HDA/EMTP, in Figure 5.9(c) and (d).

In this case, the differences between the two procedures are more evident; the second maxima in the current waveforms are more prominent than that of the previous case. Although through the 'air' path (i.e. air, oil and transformer tank) flow mainly the zero-sequence fluxes, when the main and yoke branches saturate, part of other harmonic fluxes, such as fundamental, fifth and seventh, will also flow through this path as the saturated iron core reluctance is larger than the 'air' path. By increasing the 'air' reluctance, the portion of non-triplen harmonic fluxes that would flow through the 'air' in case of saturation, will remain in the core . Consequently, with higher levels of fundamental, fifth and seventh harmonic fluxes, the core goes deeper into saturation, which results in higher level of harmonic distortion.

Having assumed a linear distribution of fluxes, the saturation effects can not be

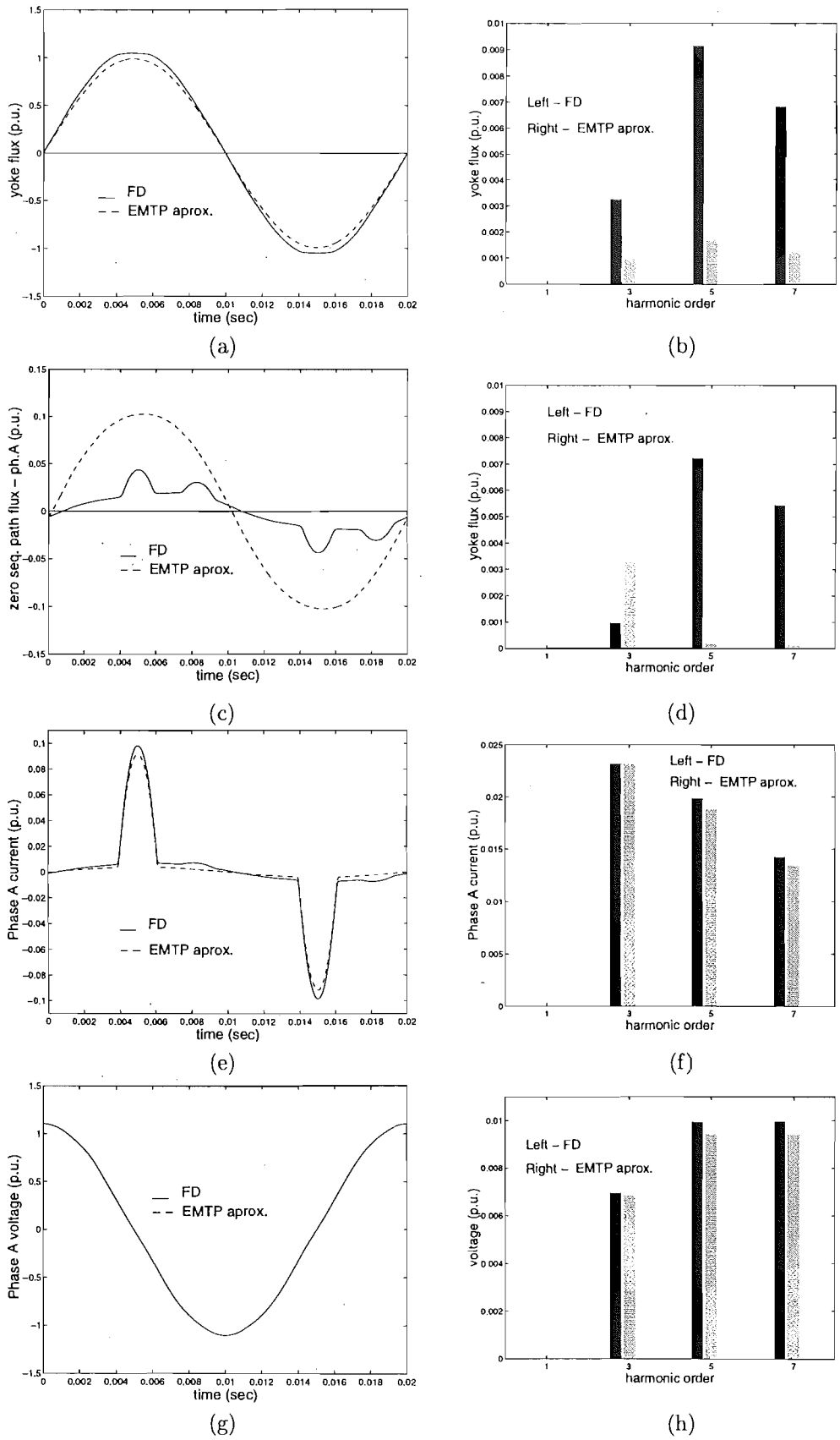

Figure 5.8 Comparison between HDA/FD and HDA/EMTP solutions

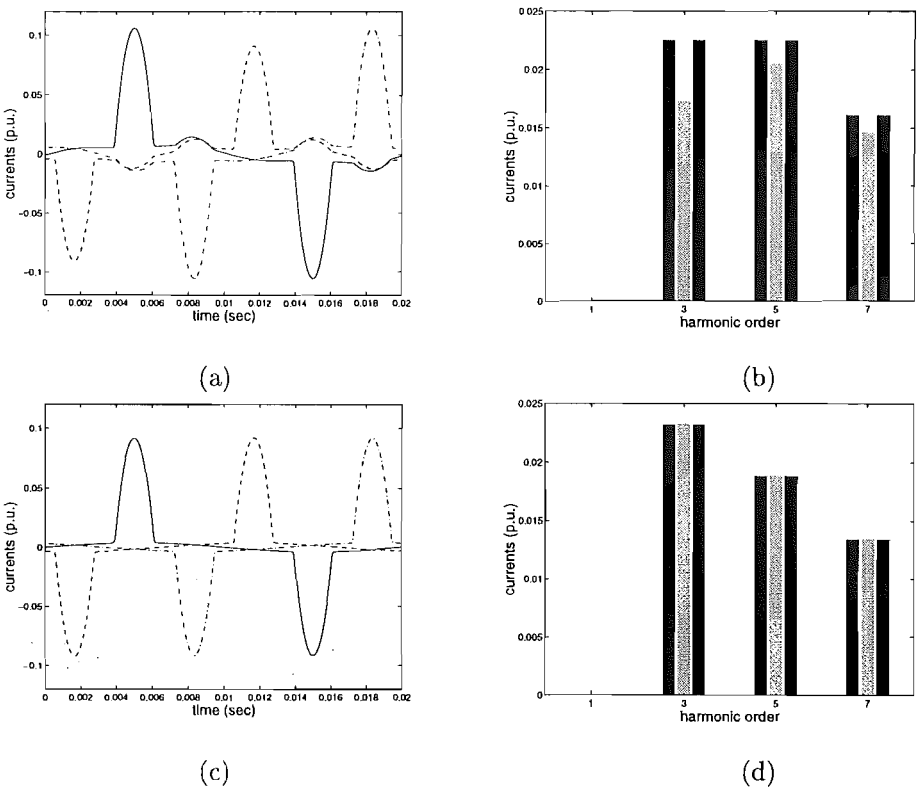

Figure 5.9 Current waveforms and harmonic content for $m_1 = 1.0$

exactly determined with the EMTP approximation. Thus, as the zero-sequence path reluctance increases the differences between the two solutions increase for the 5th and 7th harmonics (increasing the second maxima in the current waveforms).

Due to the interphase magnetic couplings, phase B current must be smaller than those of phase A and C. This effect could be adequately calculated by the HDA/FD algorithm, while a solution based on the EMTP linear approximations could not detect it, at least for this level of saturation.

In order to have a better perspective of the accuracy level of these two approaches, a sensitivity analysis has been carried out by simulating several cases either varying the zero-sequence flux path's reluctance or the generator voltage.

5.3.3.1 Sensitivity analysis varying the reluctance of the zero-sequence flux path

Considering *Example* 1 test sytem and a generator voltage equal to 1.1 (p.u.), the first set of simulations consisted of 25 cases derived by reducing the slope of the unsaturated region of the zero-sequence flux path from its original value ($m_1 = 6.0$), at the rate of 0.2. The harmonic voltage and current magnitudes determined by HDA/FD and HDA/EMTP algorithms, phase A and B, are illustrated in Figures 5.8(a), (b), (c) and (d), respectively (phase A results are on the left side).

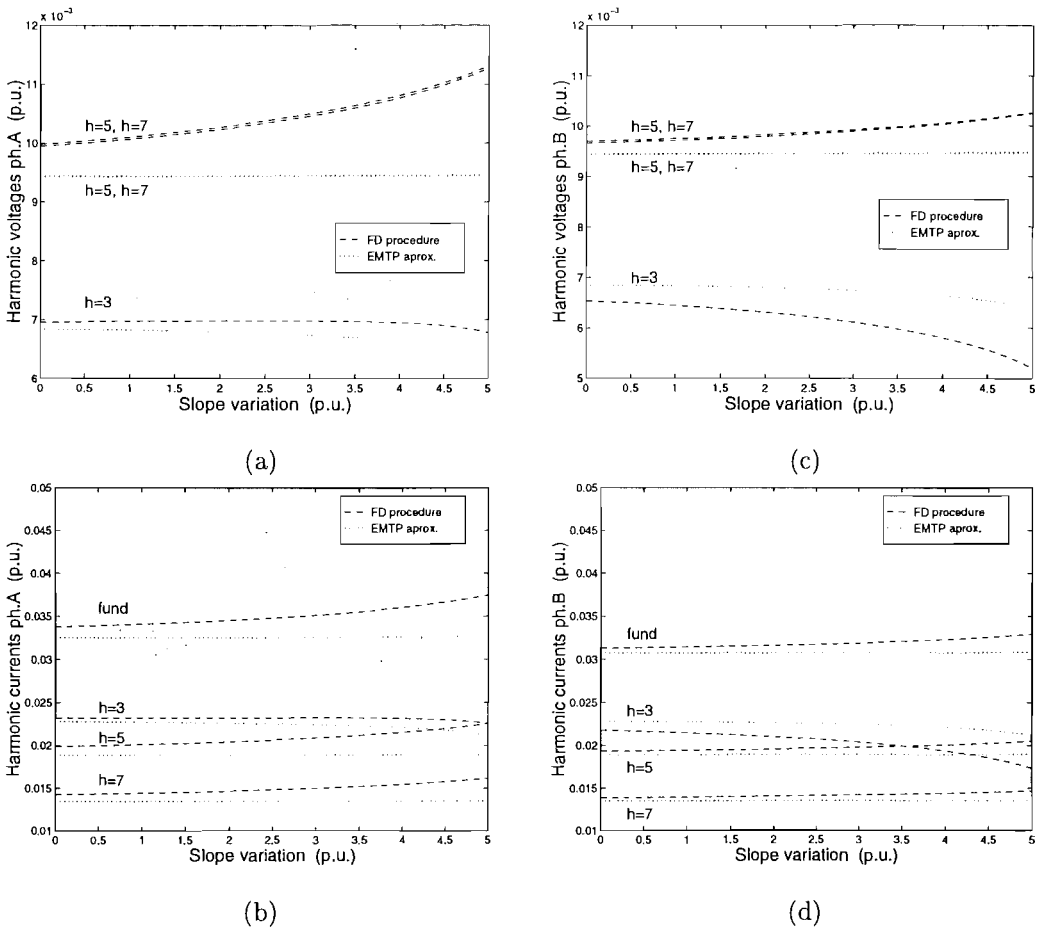

Figure 5.10 HDA simulations varying the slope m_1, v=1.1(p.u.)

As the zero-sequence flux path reluctance increases, the third harmonic voltages and currents reduce while the fundamental, fifth and seventh increase. However, as the transformer is not in deep saturation and the system impedance is relatively small, the differences between the two solutions are not significant.

5.3.3.2 Sensitivity analysis varying the generator voltage

Considering the previous test system and increasing the generator voltage from 1.1 (p.u) at the rate of 0.02 (p.u), another two sets of 14 simulations have been carried out for the same test system; the first set with the slope of the zero-sequence path m_1 equal to 6.0 (small zero-sequence flux path's reluctance) and the second, m_1 equal to 1.0 (large zero-sequence flux path's reluctance). The results are summarised in Figures 5.11 (a) to (d), phase A only.

With $m_1 = 6.0$, the harmonic voltage and current magnitudes obtained with the two approaches are illustrated in Figures 5.11 (a) and (b) (left side figures), respectively, and they show very close agreement. With $m_1 = 1.0$, the harmonic currents

(Figure 5.11 (c)) also show good agreement, except small differences for the cases with generator voltages between 1.1 (p.u.) to 1.15 (p.u.). These differences are more clearly observed for the harmonic voltages, illustrated in Figure 5.11 (d). At low level of saturation, the differences between both solutions are more accentuated. When the transformer is slightly saturated, the EMTP linear approximation erroneously determines a larger value for the fundamental frequency flux flowing through the 'air' (see Figure5.8(c)), and therefore, with a small value of fundamental flux remaining in the core, the harmonic distortion are very small. The algorithm quickly converges, without achieving the exact solution.

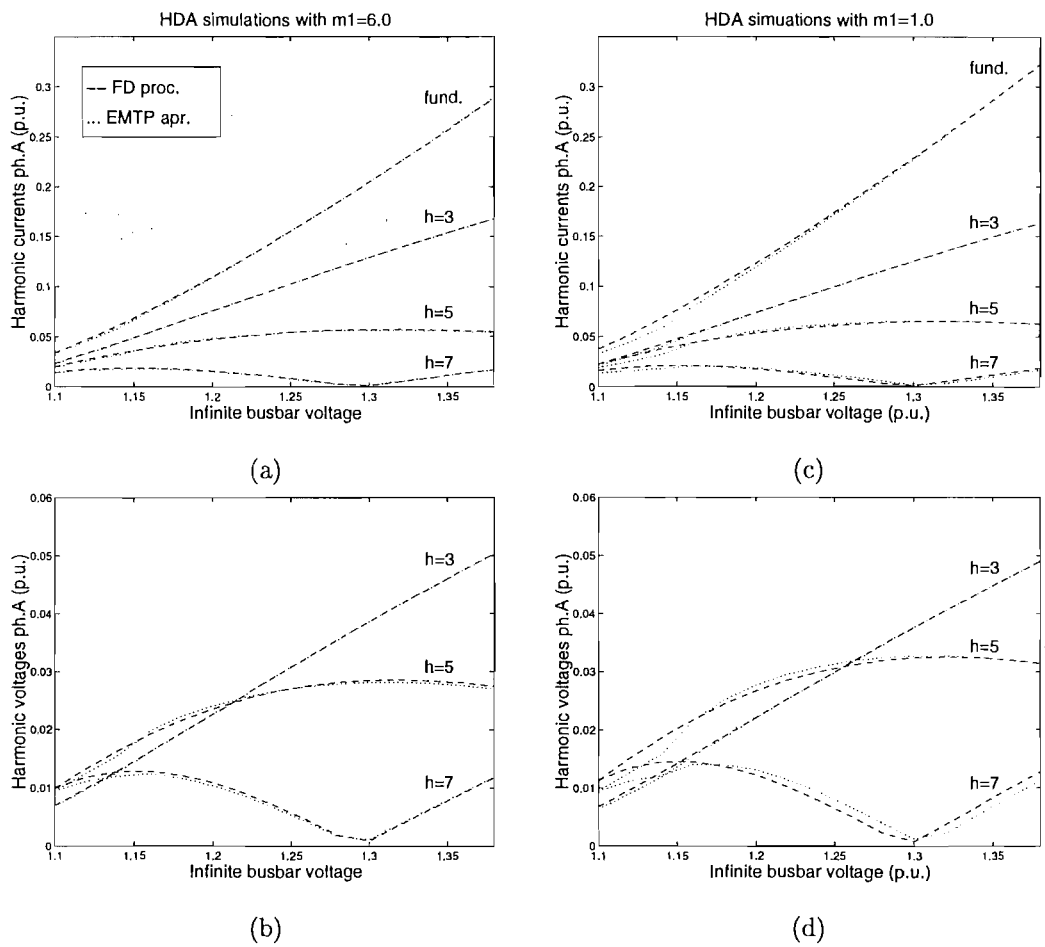

Figure 5.11 Harmonic currents and voltages phase A - cases varying the gen. voltage

5.3.3.3 Sensitivity analysis in resonant systems

Finally, two set of simulations have been carried out considering *Example* 2, i.e. the third harmonic resonant circuit, and the Jaguara-Taquaril resonant test system described earlier. Each set of simulations has been defined by varying the zero-sequence flux path reluctance as in Section 5.3.3.1.

Firstly, *Example* 2 test system has been simulated with an applied voltage of 1.1 (p.u.) and the third harmonic voltage and current magnitudes of busbar 2, phase A, are illustrated in Figure5.12(a) and (b), respectively. The HDA/FD and HDA/EMTP solutions closely match for small values of zero-sequence reluctance, which corresponds to the slope variations from 0.0 to 1.0, i.e m_1 values reduced from 6.0 to 5.0. For a slope variation above 1.0, the differences are distinguishable, but still small. The third harmonic voltage and current differences achieve the maximum value of 0.003 and 0.01 (p.u), respectively.

The same simulations have been carried out for the Jaguara-Taquaril test system, considering an applied voltage of 0.95 (p.u.). The seventh harmonic voltage and current magnitudes are illustrated in Figures 5.12 (c) and (d), respectively. In this case the differences are more significant, achieving a maximum value about 0.02 (p.u) for the voltages and 0.135 (p.u.) for the currents, for a slope variation equal to 5.0.

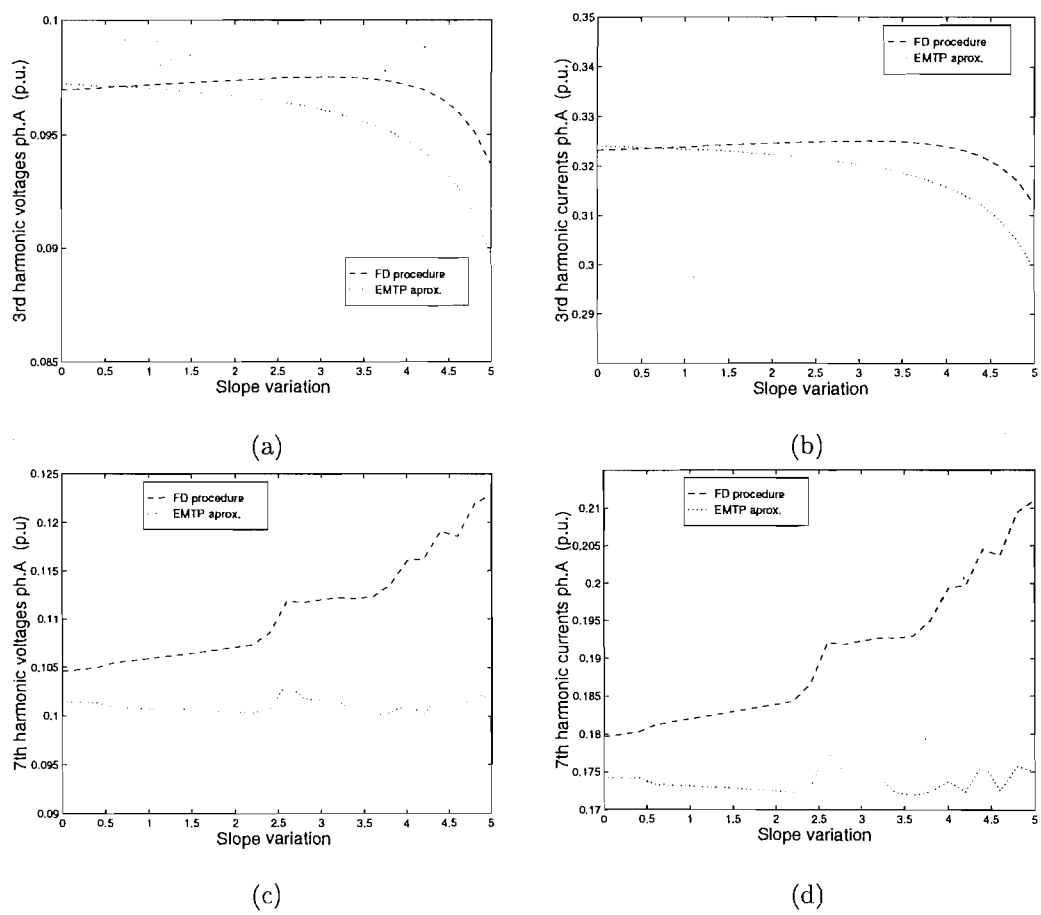

Figure 5.12 Harmonic currents and voltages in resonant systems

5.4 JAGUARA-TAQUARIL TEST SYSTEM

Fields measurements on the Jaguara-Taquaril transmission circuit [Cunha and Dommel 1973] are the one of few practical data on harmonic voltage distortions due to transformer saturation available in the literature. It has been used as benchmark to validate time and harmonic domain transformer models [Dommel *et al.* 1983] [Enrique Acha Daza 1988], although due to the restrictions on the field data available (e.g. a combined generator and transformer linear impedance is given) a perfect match between measurements and simulation results is not expected.

The time and harmonic intervalidation has been done by superposing the measured voltage waveform with those obtained from the simulation results and the adequacy of the transformer model checked through a visual comparison of these waveforms. The latter has assumed a two slope magnetising characteristic instead of a five slope characteristic described by Cunha, which may have introduced additional innacuracy to the results. This aspect will be detailed investigated in Chapter 4.

A quantitative comparison has been done in this work by scanning the voltage waveform shown in [Cunha and Dommel 1973], with subsequent transformation to a xy data file amenable to FFT analysis. HDA simulations have been carried out considering five slope magnetising characteristic and including frequencies up to the 7th harmonic. To assess the influence of the cross-coupling between frequencies, which is explicitly represented in the Harmonic Domain, an additional simulation has been done including frequencies up to the 15th harmonic.

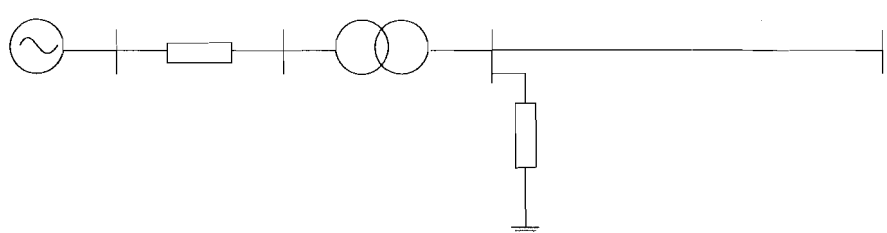

Figure 5.13 Jaguara-Taquaril test system

Figure 5.14 illustrates the scanned experimental voltage waveform and those obtained with the HDA simulations including frequencies up to the 7th and to the 15th harmonic. The harmonic spectrum of each of these curves are shown in Figure 5.15. As a perfect match is not expected, the results indicate a close agreement, similar to those obtained by Acha [1988]. Small even harmonics are present in the experimental voltage due to the slight distortion process of reproduction of the waveform.

It is interesting to note, that the cross-coupling between higher frequencies has a smaller effect upon the harmonic solution than that reported earlier [Medina and Arrillaga 1992]: the HDA solution considering harmonics up to the 15th predicted a

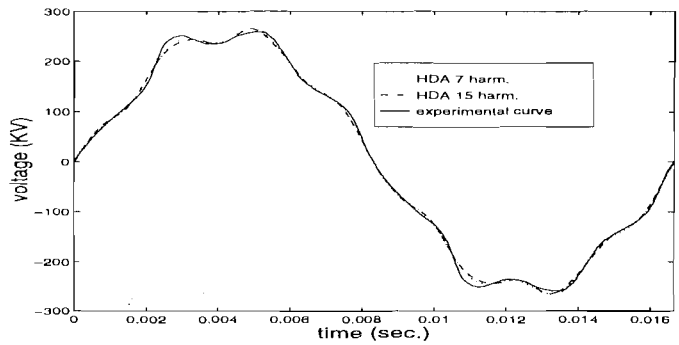

Figure 5.14 Comparison between HDA and experimental curve voltage waveforms

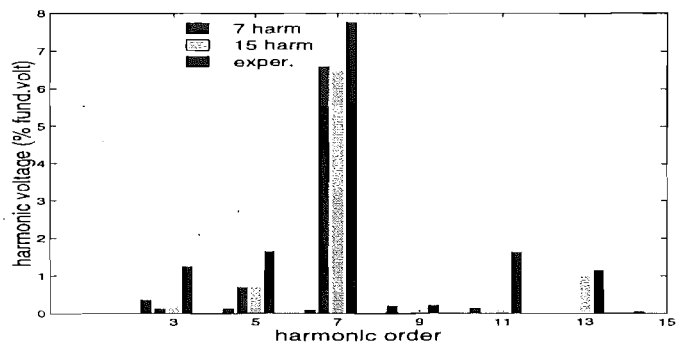

Figure 5.15 Comparison between HDA and experimental curve harmonic spectrum

slight smaller 7th harmonic voltage, with additonal 11th and 13th harmonic voltages, compared with the HDA solution with 7 harmonics. Besides, the overall harmonic solutions obtained here are much closer to the field measurements than those predicted by Medina.

5.5 CONCLUSIONS

An accurate Norton equivalent to represent the nodal magnetising currents has been derived by incorporating the magnetic circuit laws into the formulation and providing detailed representation of saturation in the different magnetic branches. A Newton-Raphson iterative procedure has also been presented to calculate the non-linear distribution of the magnetic fluxes, required to adequately evaluate the harmonic Norton equivalents.

Several cases have been analysed indicating that the improved accuracy achieved with this procedure is relatively small as compared with the EMTP approximation in most of the cases, except in resonant systems. Taking into account the additional computational time , this procedure is only recommended when a rigorous harmonic analysis is required.

The linearized harmonic transformer model has also been adapted to the instan-

taneous form and implemented in the EMTDC program. A comparison between the harmonic and time domain technique has been made. The results up to the 15th harmonic of HDA and EMTDC solutions have shown excellent agreement, thus increasing the confidence in the potential of the harmonic domain technique.

It should be noted, however, that the effectiveness of the algorithm depends on the availability of accurate transformer data, currently not provided by the manufacturers. Also, fields tests to measure harmonic distortion caused by magnetising currents of multi-limb saturated transformers are needed so that a more conclusive corroboration of the mathematical formulation may be made.

Chapter 6

DIVISION OF THE NORTON HARMONIC EQUIVALENTS

6.1 INTRODUCTION

The complete harmonic electromagnetic transformer model derived in the previous Chapter has been based on the use of superposition, with the transformer electric circuit represented by a linear admittance matrix and the nonlinear magnetic circuit represented in a linearised form by means of harmonic Norton equivalents. The latter are divided between primary and secondary transformer terminals proportionally to the factors α and β, which leads to a π-equivalent transformer representation. The accuracy of the proposed model will depend on the realistic determination of these two factors and this aspect is discussed in this Chapter.

The transformer behaviour can be understood using the coupled-circuit method, i.e. by self and mutual inductances. Very accurate formulae available are available for the calculation of these two inductances. However, because of the presence of the iron core, both the self and mutual inductances are variable. Further, their numerical values are very close, which may result in ill-conditioned equations.

In order to overcome the mathematical restrictions imposed by the self and mutual inductances, a transformer model based on the concept of leakage reactances and a magnetising branch was introduced by Steinmetz [Steinmetz 1895], early in this century. By dividing the magnetic flux distribution into two components (mutual and leakage fluxes) this method separates the transformer linear and nonlinear components (if a linear flux leakage path is assumed). The magnetising branch is placed between the primary and secondary leakage reactances, which results in a T-equivalent transformer representation as illustrated in Figure 6.1.

Mathematical formulae for the magnetising current distribution between primary and secondary sides based on the T-equivalent circuits were derived[Dahl 1925b]. However, the difficulty is to obtain the primary and secondary leakage reactances either experimentally or mathematically [Dahl 1925a] [Boyajian 1925] [Dommel 1975]. The latter procedure requires a detailed knowledge of the transformer windings, and

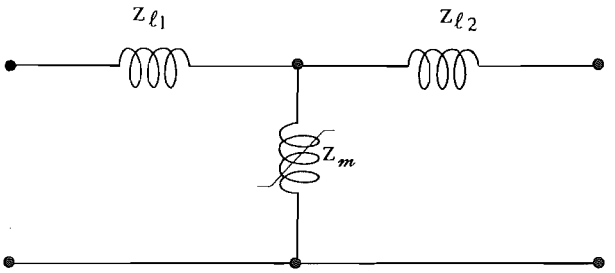

Figure 6.1 T-equivalent transformer model

inevitably, laborious calculations for accurate solutions. In fact, no formula is totally free from error due to the nonlinear distribution of the magnetic fluxes, and only the finite elements technique provides exact information. On the other hand, the total leakage reactance can be easily obtained by short-circuit test, and taking advantage of the availability of this data, Steinmetz transformer's model has been developed further to a π equivalent circuit, as illustrated in Figure 6.2.

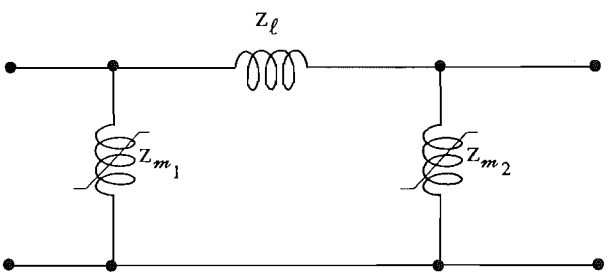

Figure 6.2 π-equivalent transformer model

Both, T and π-equivalent circuits are mathematically equivalent to each other and equally valid [Blume *et al.* 1959], for a given value of magnetic branch reactance. While the division of the total leakage reactance into primary and secondary leakages reactances is avoided with the π-equivalent representation, the division of the magnetising branch between the transformer terminals, is introduced instead. However, for most of the steady-state power system analysis (i.e. fundamental frequency studies), the core nonlinearities do not play an important role, and therefore, an equal division of the magnetising branch between the transformer terminals [Chen and Dillon 1974] [Dommel 1975] is a perfectly adequate approximation.

This approximation has been used in the previous transformer models developed in the harmonic domain [Acha *et al.* 1989] [Medina and Arrillaga 1992]. However, the adequacy of an equal distribution of the magnetising branch for transformers operating in the saturation region has not been thoroughly investigated and it may be inadequate at harmonic frequencies. In the absence of meaningful field test results, the validation approach used in this Chapter consists of sensitivity analysis to assess the level of

inaccuracy introduced by the assumption.

The extension of this approximation to three-phase harmonic transformer models requires additional consideration. The transformer electrical configuration imposes restrictions upon the zero sequence harmonic currents and voltages, which must be taken into account in the π-equivalent circuit. It will be shown in this Chapter that equal distribution of the magnetising branch is rather inadequate for some transformer electrical configurations, such as star-connected windings with neutral unearthed, which so far has not been pointed out in the literature.

6.2 SINGLE-PHASE TRANSFORMER

Conventional transformer theory leads to the following two equations representing the single-phase unit of Figure 6.3 (winding resistances neglected) [Connely 1965].

$$v_p = \left(L_p - L_m \frac{N_p}{N_s}\right) \frac{di_p}{dt} + \frac{L_m}{N_s}\left(N_p \frac{di_p}{dt} - N_s \frac{di_s}{dt}\right) \tag{6.1}$$

$$v_s = -\left(L_s - L_m \frac{N_s}{N_p}\right) \frac{di_s}{dt} + \frac{L_m}{N_p}\left(N_p \frac{di_p}{dt} - N_s \frac{di_s}{dt}\right) \tag{6.2}$$

where
L_s, L_p and L_m are the self primary, self secondary and mutual inductances, respectively.

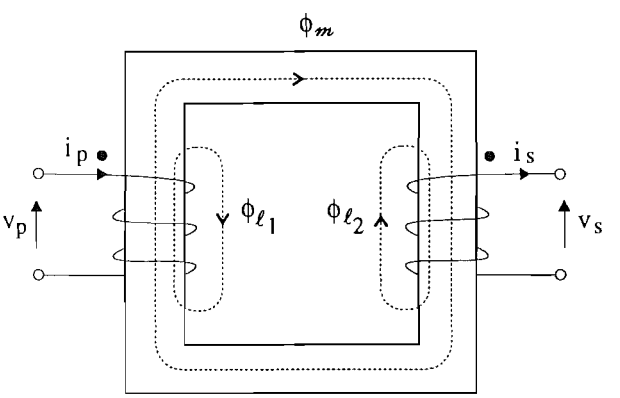

Figure 6.3 Flux distribution in a single-phase transformer

The first term of equation (6.1) represents the e.m.f. induced in the primary by its corresponding leakage flux. This voltage is equal to that which be dropped across an inductance of value

$$L_1 = \left(L_p - L_m \frac{N_p}{N_s}\right) \tag{6.3}$$

called primary leakage inductance. Similar consideration for the secondary side leads to the definition of the secondary leakage inductance,

$$L_2 = \left(L_p - L_m \frac{N_p}{N_s} \right) \tag{6.4}$$

The second term of equation (6.1) (or equation (6.2)) represents the e.m.f induced by the resultant mutual fluxes due to the primary and secondary combined[Connely 1965]. This term would lead to a mutual (non-linear) inductance connected across the primary and/or secondary windings.

From the above considerations, a T-equivalent transformer representation as illustrated in Figure 6.4 can be derived. The induced e.m.f.'s can be represented by a linear shunt reactance for transformers operating in the linear region (Steinmetz model), or by a voltage-dependent current source [Dommel *et al.* 1986] or by harmonic Norton equivalents [Semlyen *et al.* 1988]. Note that the primary and secondary leakage reactances have constant values as the core nonlinearity has been entirely restricted to the reactance of the mutual inductance, x_m.

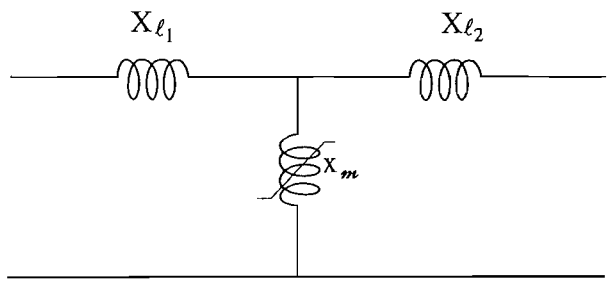

Figure 6.4 T-equivalent transformer model

L_1 and L_2 , defined in equations (6.3) and (6.4), express the difference between two nearly equal quantities. To determine them mathematically requires detailed information about the transformer design, particularly regarding the windings. Difficulties are also met to determine them by practical measurements. Some attempts have been made in the past, but the suggested experimental methods are either only applicable for three-phase bank of identical transformers [Dahl 1925a], or transformers with 1:1 ratio [Boyajian 1925]. As an example, Dahl's method is illustrated in Figure 6.5.

The principle of this method consists of applying a sinusoidal voltage on a YΔ connected bank of transformers, so that the third harmonic component of the magnetising current will be confined to the delta where it appears as circulating current. By simultaneously measuring the third harmonic current and the third harmonic e.m.f producing it, the primary and secondary leakage reactances can be determined. However, the three-phase voltages must be purely sinusoidal and the three transformers identical in order to avoid zero sequence harmonic currents due to unbalanced conditions.

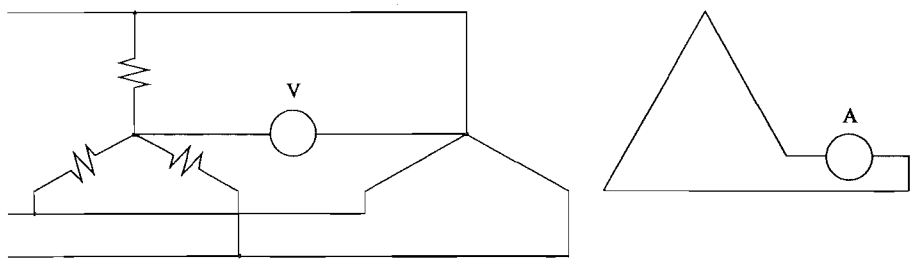

Figure 6.5 Dahl's diagram of connections for leakage impedance test

More recently, some values of these two reactances have been determined [Szabados 1981],[Szabados 1979], however the experimental method not clearly described.

On the other hand, the total leakage reactance is easily and accurately determined by a short-circuit test. Taking advantage of the availability of this data, a π-equivalent circuit, mathematically equivalent to the T transformer representation, can alternatively be derived as described next.

6.3 α AND β FACTORS

Consider the electric circuit of Figure 6.6, where the transformer is represented by the exact T-equivalent model, with the magnetising branch represented by a voltage-dependent current source i_m.

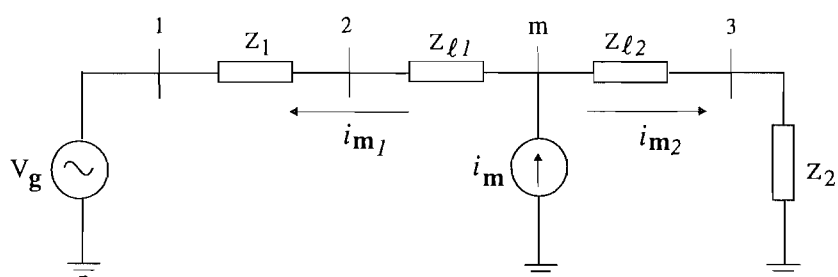

Figure 6.6 T-equivalent transformer model

The harmonic components of the magnetising current i_m will split between primary and secondary circuits in inverse proportion to their corresponding impedances

$$i_{m_2} = \frac{(z_1 + z_{l_1})}{z_{tot}} i_m$$

$$i_{m_1} = \frac{(z_{l_2} + z_2)}{z_{tot}} i_m$$

where

$$z_{tot} = z_1 + z_2 + z_{l_1} + z_{l_2}$$

and

i_{m_1} : Magnetising current flowing in the primary

i_{m_2} : Magnetising current flowing in the secondary

A π-equivalent transformer representation, as shown in Figure 6.7, can be derived from the previous circuit by considering that the current sources i_p and i_s must be such that the currents flowing through the primary and secondary circuits in both cases are identical.

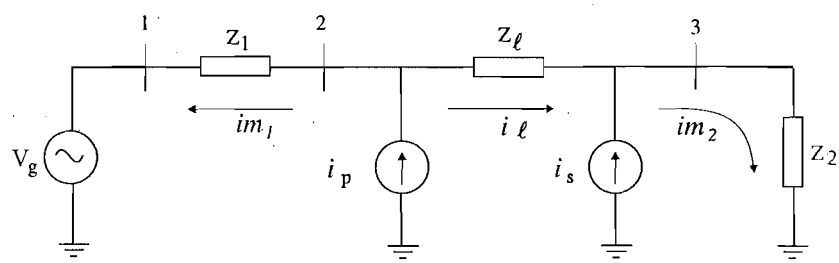

Figure 6.7 π-equivalent transformer model

With this restriction, solving the electric circuit yields

$$i_{m_p} = \left[\frac{(z_1 + z_l)(z_{l_2} + z_2)}{z_l z_{tot}} - z_2\frac{(z_{l_1} + z_1)}{z_{tot} z_l}\right] i_m$$
$$i_{m_s} = \left[\frac{(z_1 + z_{l_1})(z_l + z_2)}{z_l z_{tot}} - z_1\frac{(z_{l_2} + z_2)}{z_{tot}}\right] i_m$$

or

$$i_{m_p} = \alpha i_m$$
$$i_{m_s} = \beta i_m$$

where

$$\alpha = \left[\frac{(z_1 + z_l)(z_{l_2} + z_2)}{z_l z_{tot}} - z_2\frac{(z_{l_1} + z_1)}{z_{tot} z_l}\right] \tag{6.5}$$

$$\beta = \left[\frac{(z_1 + z_{l_1})(z_l + z_2)}{z_l z_{tot}} - z_1 \frac{(z_{l_2} + z_2)}{z_{tot}} \right] \tag{6.6}$$

are the harmonic distribution factors.

From the above equations it can be seen that the division of the magnetising currents between the transformer terminals is defined by the primary and secondary leakage reactances and also external system impedances. They may be different for each harmonic, specially if the circuit has capacitances, and they are certainly different from the value 0.5 (i.e. equal distribution approximation). The greatest difference would correspond the resonance condition on either side of the transformer.

6.3.1 Example

To assess the errors involved when using an *approximated* π-equivalent circuit, several simulations have been carried out with a single-phase T- and π-equivalent harmonic transformer models. The test system is the same described in Chapter 5, with a load impedance added to the secondary side equal to 2.0 (p.u).

Ten sets of simulations have been carried out with the T-equivalent model using values of primary and secondary leakages reactances given by

$$\begin{aligned} z_{l_1} &= (1-k)z_l \\ z_{l_2} &= kz_l \end{aligned}$$

with k=0, 0.1, 0.2,..., 1.0, and one case using the π-equivalent circuit with α= β=0.5. For each case the generator voltage was varied from 0.95(p.u.) to 1.3 (p.u), in ten steps.

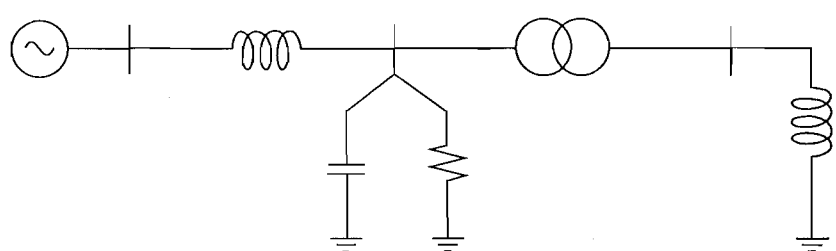

Figure 6.8 Test system

The results are plotted in Figures 6.9(a) and (b) for the third harmonic currents flowing through the generator and load impedances, respectively. Similarly, Figures 6.9(c) and (d) show the primary and secondary third harmonic voltages, respectively. The approximate π-equivalent circuit produced results wich are almost the average of the two extreme cases considered for the T-equivalent model, i.e. k=0.0 and k=1.0.

However, a closer look at the results indicate otherwise. For instance, the third harmonic voltages obtained with a particular generator voltage equal to 1.1 (p.u.) is 0.08 (p.u.) for the π-equivalent circuit, whereas the range of values for the T-equivalent is 0.06 to 0.12 (p.u). In percentage of the fundamental voltage these results are approximately 7.2, 5.5 and 11%, respectively, and these differences may not be considered negligible in rigorous harmonic analysis.

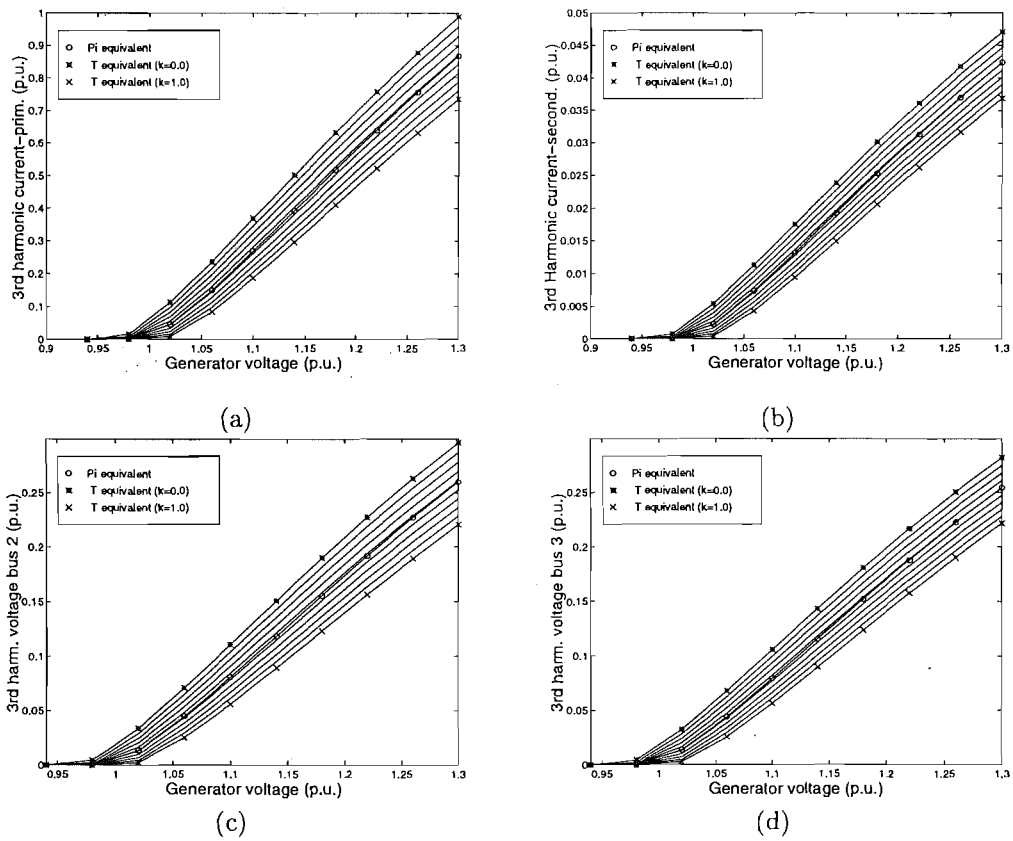

Figure 6.9 Third harmonic currents and voltages

6.4 THREE-PHASE π-EQUIVALENT PRIMITIVE MODEL

Difficulties arise in modelling three-phase transformers based on T-equivalent circuit representation [Chen and Dillon 1974], and therefore, the adequacy of the *approximated* π-equivalent three-phase transformer model cannot be verified by means of comparisons and sensitivity analysis, as it has been done for the single-phase transformer model.

In balanced three-phase systems, the distribution of the zero sequence harmonics may be partially or totally defined by the transformer electrical connections, independently from the external system. These relevant restrictions are:

- Zero sequence harmonic voltages cannot appear between lines (but they can appear between line and neutral).
- Zero sequence harmonic currents can only flow in the lines if the transformer windings are Y-connected, with the neutral grounded.
- In Δ-connected transformers, the zero sequence harmonic currents are restricted to the closed delta path.

The three-phase harmonic π-equivalent transformer model has been derived by superimposing the harmonic Norton equivalents on the transformer primitive electric parameters, according to the factors α and β. Subsequently, by means of connectivity matrix, the transformer windings electrical configuration is taken into account.

If primary and secondary windings are star-grounded connected, the errors involved assuming equal distribution of the harmonic Norton equivalents are the same as those for a single-phase transformer. However, this is not the case with delta and ungrounded-star connected transformers. As the superposition of the magnetic and electric circuits has been made at the stage of primitive parameters, when the connectivity matrix is applied, the portion of the zero sequence harmonic magnetising currents assigned to each side and defined by the α and β factors, will be confined to these sides if they are delta or ungrounded-connected. This implies that, if from these factors a distribution of the zero sequence harmonic magnetising currents violates the restrictions defined by the transformer connection, the algorithm has no means to correctly redistribute them along the iterative process.

The inadequacy of an equal distribution of the harmonic Norton equivalents is more evident for the ungrounded-star connection. In this case, no zero sequence harmonic currents can flow at all, i.e. the connection has the effect of introducing infinite zero sequence harmonic impedances. If any portion of the zero sequence harmonic magnetising currents is allocated to the ungrounded-star connected side, the algorithm will diverge on the first iteration because it will have zero sequence harmonic current sources being injected into an infinite impedance.

From the above discussion, it is evident that, the distribution of the magnetising currents must be determined previously to the superposition of the magnetic and electric circuits, that is, the zero sequence harmonic transformer connection restrictions must be taken into account to determine α and β factors.

Osborne's third harmonic transformer model

A simple equivalent circuit for three-phase transformers has been proposed [Osborne 1915], which facilitates the theoretical understanding of the triplen harmonic effects associated with the transformer behaviour. The circuit, illustrated in Figure 6.10, is applicable to all connections and harmonics and it has been experimentally corroborated [Morgan *et al.* 1933].

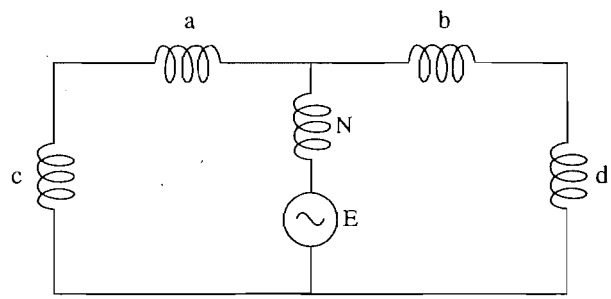

Figure 6.10 Osborne's transformer equivalent circuit

To consider the third harmonic circuit in isolation, the shunt leg of the T contains a third harmonic generator in series with the no-load impedance N. The voltage E of this fictitious generator is the third harmonic component of the e.m.f. which exist in the terminal voltage of the transformer when the third harmonic component of the magnetising current is supressed by the transformer connection. The mutual impedance N is the ratio of third harmonic voltage to the current of the same frequency which would exist in the magnetising current if it had no external impedance to overcome (no-load impedance). The series reactances a and b are the primary and secondary leakage reactances. If the primary winding are star-connected with ungrounded neutral, c is equal to infinite and no third harmonic currents can flow. If the neutral is grounded, c is equal to the third harmonic primary external system impedance (including the neutral impedance, if any) and third harmonic currents will flow in the circuit. If the windings are delta connected, c is equal to zero, providing a closed path for the third harmonic currents. Similar considerations applied to d, for corresponding secondary winding connections.

Osborne's third harmonic circuit is similar to the T-equivalent single-phase transformer described in Section 6.3. Therefore, triplen harmonic α and β factors for three-phase transformers can be accurately determined using equations similar to (6.5) and (6.6). (The shunt leg can also be represented by an equivalent current source in paral-

lel with the no-load impedance[Szabados 1981], which facilitates the correlation of this circuit with Norton harmonic equivalents used in this work).

If the three-phase system is unbalanced or with zero sequence harmonic sources, the transformer electrical connection will impose restrictions not only upon the triplen harmonics, but on *all* zero-sequence harmonics. In this case, an accurate determination of α and β factors can only be done by means of symmetrical components.

Zero-sequence component transformer model

Zero-sequence node admittance models for the most commonly used three-phase transformer connections have already been derived earlier[Chen and Dillon 1974] and are illustrated in Figure 6.11. However, these models are not complete as the magnetising branch has not been taken into account.

Considering that Osborne's third harmonic transformer model is valid for any harmonic, it can also be extended to the zero-sequence harmonic component transformer models described above. Thus, α_{h_0} and β_{h_0} factors can be accuretely determined by equations similar to (6.5) and (6.6). These factors would still have to be transformed to phase components before becoming applicable to the three-phase harmonic transformer model proposed in this work. Again, accurate determination of these factors requires the knowledge of primary and secondary leakage reactances.

6.5 CONCLUSIONS

It has been demonstrated through sensitivity analysis that an equal distribution of the magnetising branches is not a good approximation, at harmonic frequencies, for single phase transformers. For accurate solutions, this distribution must be determined for each frequency. This can be determined mathematically, provided that the primary and secondary leakage transformer reactances are known, through distribution factors called α and β.

A theoretical investigation has been done to verify the adequacy of this approximation with reference to three-phase transformers. It has been shown that an equal distribution of the harmonic Norton equivalent is inadequate for star-connected transformer windings.

Moreover, for three-phase systems, an accurate determination of the distribution factors α and β can be achieved using a symmetrical components circuit representation, with the formulation of the single-phase transformer. Again, the knowlege of the primary and secondary leakage reactances is required for this purpose.

The correct determination of α and β is also required to represent the magnetic circuit response to the electric restriction imposed by the star connection. This aspect is considered further in the next Chapter.

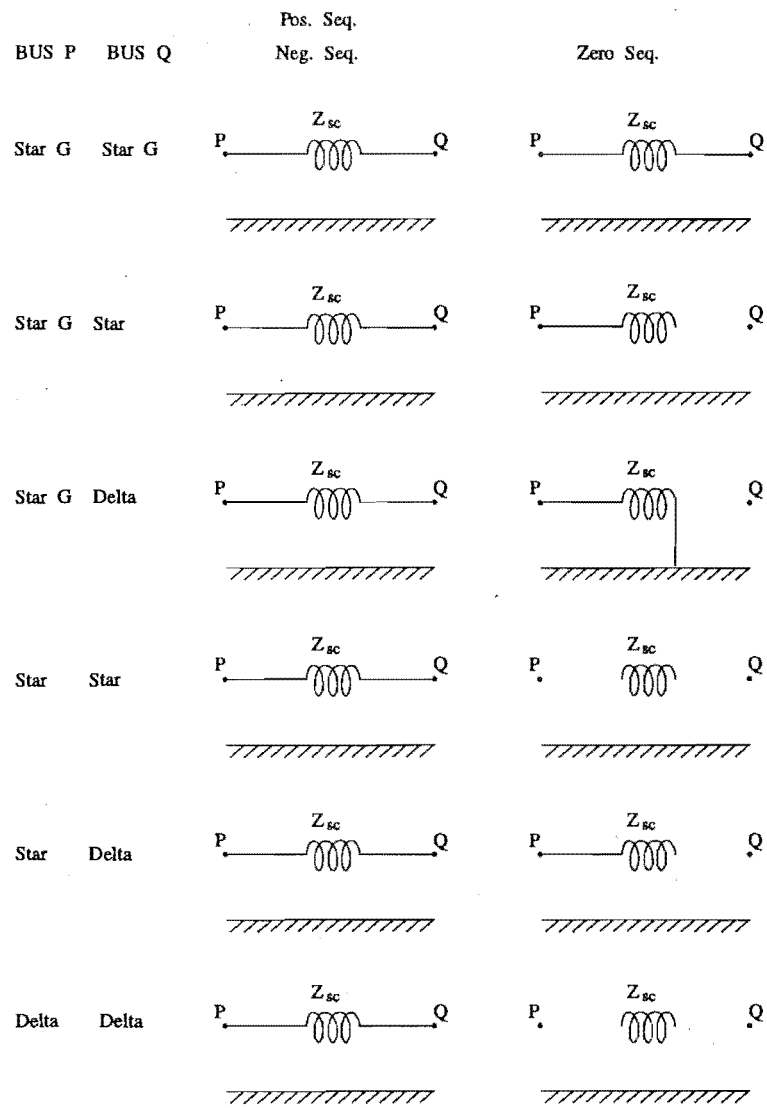

Figure 6.11 Zero-sequence component model for the six most common connections of three-phase transformers

Chapter 7

TRANSFORMER CONNECTION MODELS

7.1 INTRODUCTION

Transformer models with increasing levels of detail have been proposed in the literature in recent years. However, little attention has been paid to the modelling of different electrical winding configurations. As discussed in Chapter 2, the flow of zero sequence harmonic currents can be totally or partially controled by the transformer electrical connection. Thus, its adequate representation is a requirement for accurate electromagnetic transformer models.

Star-connected transformer windings with ungrounded neutrals may give rise to large zero sequence harmonic voltages when operating under saturation conditions. Difficulties arise when representing this type of winding configuration as the the neutral voltage is a function of the transformer iron core geometry and magnetic properties. The AC system connected to other star-grounded connected windings also affects the harmonic response of the transformer.

Electromagnetic models for the most commonly used transformer electrical winding configurations are proposed in this Chapter. Due to the lack of field tests data, the adequacy of the proposed models are verified by means of sensitivity analysis, and practical experience reported in literature [Stigant *et al.* 1941].

7.2 THREE-PHASE ELECTROMAGNETIC TRANSFORMER MODELS

Harmonic nodal three-limb transformer models for different transformer electrical connections can be derived with the use of connectivity matrices and the primitive electromagnetic harmonic transformer model derived in Chapter 5.

By definition, connectivity matrices relate the branch parameters of the primitive (unconnected) electric circuit to the nodal parameters of the actual (connected) electric circuit (see [Arrillaga and Arnold 1990]).

In a primitive circuit, the relationship between voltages and currents can be expressed in a generic form as follows

$$\tilde{i}_{prim} = [Y]_{prim}\tilde{v}_{prim} \tag{7.1}$$

while the relationships between the voltages and currents of a primitive circuit and those of an actual circuit are

$$\tilde{v}_{prim} = [C]^t\tilde{V}_{node} \tag{7.2}$$

$$\tilde{I}_{node} = [C]\tilde{i}_{prim} \tag{7.3}$$

where the subscripts *prim* and *node* denote primitive and nodal parameters, respectively, and [C] is the connectivity matrix.

Substitution of equations (7.1) and (7.2) into (7.3) results

$$\tilde{I}_{node} = [Y]_{node}\tilde{V}_{node} \tag{7.4}$$

where

$$\tilde{Y}_{node} = [C][Y]_{prim}[C]^t \tag{7.5}$$

The connectivity matrices for the most commonly used transformer electrical connections are presented next. (The voltage and current subscripts in equations 7.6 to 7.11 correspond to those of Figure 5.2).

Star-Star connection

$$\begin{bmatrix} v_1 \\ v_2 \\ v_3 \\ v_4 \\ v_5 \\ v_6 \end{bmatrix} = \begin{bmatrix} 1 & & & & & -1 & \\ & 1 & & & & -1 & \\ & & 1 & & & -1 & \\ & & & 1 & & & -1 \\ & & & & 1 & & -1 \\ & & & & & 1 & -1 \end{bmatrix} \begin{bmatrix} V_A \\ V_B \\ V_C \\ v_a \\ v_b \\ v_c \\ V_N \\ v_n \end{bmatrix} \tag{7.6}$$

Star-Delta connection

$$\begin{bmatrix} v_1 \\ v_2 \\ v_3 \\ v_4 \\ v_5 \\ v_6 \end{bmatrix} = \begin{bmatrix} 1 & & & & & -1 \\ & 1 & & & & -1 \\ & & 1 & & & -1 \\ & & & 1 & -1 & \\ & & & & 1 & -1 \\ & & & -1 & & 1 \end{bmatrix} \begin{bmatrix} V_A \\ V_B \\ V_C \\ v_a \\ v_b \\ v_c \\ V_N \end{bmatrix} \tag{7.7}$$

Delta-Delta connection

$$\begin{bmatrix} v_1 \\ v_2 \\ v_3 \\ v_4 \\ v_5 \\ v_6 \end{bmatrix} = \begin{bmatrix} 1 & -1 & & & & \\ & 1 & -1 & & & \\ -1 & & 1 & & & \\ & & & 1 & -1 & \\ & & & & 1 & -1 \\ & & & -1 & & 1 \end{bmatrix} \begin{bmatrix} V_A \\ V_B \\ V_C \\ v_a \\ v_b \\ v_c \end{bmatrix} \tag{7.8}$$

For transformer windings star-connected with grounded-neutral, the column corresponding to the neutral voltage should be removed in equations (7.6) and (7.7).

Based on equations (7.2) and (7.3) and (7.5), harmonic nodal three-limb transformer models for these electrical winding configurations have been derived and are represented by equations (7.9), (7.10) and (7.11). Extra consideration has to be taken for star-delta connection if the analysis is carried out in per unit system: with both primary and secondary nominal voltages being 1.0 (p.u.), the transformer model for this connection requires an effective turns ratio of $\sqrt{3}$ [Laughton 1968] [Chen and Dillon 1974].

$$
\begin{bmatrix} I_A - \alpha I_{n1} \\ I_B - \alpha I_{n2} \\ I_C - \alpha I_{n3} \\ I_a - \beta I_{n1} \\ I_b - \beta I_{n2} \\ I_c - \beta I_{n3} \\ I_N + \beta I_{n1} + \beta I_{n2} + \beta I_{n3} \\ I_n + \alpha I_{n1} + \alpha I_{n2} + \alpha I_{n3} \end{bmatrix} =
$$

$$
\begin{bmatrix}
y_l + \alpha y_{11} & y_l' + \alpha y_{12} & y_l' + \alpha y_{13} & -y_l & y_l'' & y_l'' & -y_l - 2y_l' \\ & & & & & & -\alpha y_{11} - \alpha y_{12} \\ & & & & & & -\alpha y_{13} \\
y_l' + \alpha y_{21} & y_l + \alpha y_{22} & y_l' + \alpha y_{23} & y_l'' & -y_l & y_l'' & -y_l - 2y_l' \\ & & & & & & -\alpha y_{21} - \alpha y_{22} \\ & & & & & & -\alpha y_{23} \\
y_l' + \alpha y_{31} & y_l' + \alpha y_{32} & y_l + \alpha y_{33} & y_l'' & y_l'' & -y_l & -y_l - 2y_l' \\ & & & & & & -\alpha y_{31} - \alpha y_{32} \\ & & & & & & -\alpha y_{33} \\
-y_l & y_l'' & y_l'' & y_l + \beta y_{11} & y_l''' + \beta y_{12} & y_l''' + \beta y_{13} & y_l - 2y_l'' \\
y_l'' & -y_l & y_l'' & y_l''' + \beta y_{21} & y_l + \beta y_{22} & y_l''' + \beta y_{23} & y_l - 2y_l'' \\
y_l'' & y_l'' & -y_l & y_l''' + \beta y_{31} & y_l''' + \beta y_{32} & y_l + \beta y_{33} & y_l - 2y_l'' \\
-y_l - 2y_l' & -y_l - 2y_l' & -y_l - 2y_l' & y_l - 2y_l'' & y_l - 2y_l'' & y_l - 2y_l'' & 3y_l + 6y_l' \\
-\alpha y_{11} - \alpha y_{21} & -\alpha y_{12} - \alpha y_{22} & -\alpha y_{13} - \alpha y_{23} & & & & +\alpha y_{11} + \alpha y_{12} + \alpha y_{13} \\
-\alpha y_{31} & -\alpha y_{32} & -\alpha y_{33} & & & & +\alpha y_{21} + \alpha y_{22} + \alpha y_{23} \\ & & & & & & +\alpha y_{31} + \alpha y_{32} + \alpha y_{33} \\
y_l - 2y_l'' & y_l - 2y_l'' & y_l - 2y_l'' & -y_l - 2y_l''' & -y_l - 2y_l''' & -y_l - 2y_l''' & -3y_l + 6y_l'' \\
 & & & -\beta y_{11} - \beta y_{21} & -\beta y_{12} - \beta y_{22} & -\beta y_{13} - \beta y_{23} & \\
 & & & -\beta y_{31} & -\beta y_{32} & -\beta y_{33} &
\end{bmatrix}
$$

$$
\begin{bmatrix} y_l - 2y_l'' \\ y_l - 2y_l'' \\ y_l - 2y_l'' \\ -y_l - 2y_l''' \\ -\beta y_{11} - \beta y_{12} - \beta y_{13} \\ -y_l - 2y_l''' \\ -\beta y_{21} - \beta y_{22} - \beta y_{23} \\ -y_l - 2y_l''' \\ -\beta y_{31} - \beta y_{32} - \beta y_{33} \\ 3y_l + 6y_l'' \\ \\ \\ 3y_l + 6y_l''' \\ +\beta y_{11} + \beta y_{12} + \beta y_{13} \\ +\beta y_{21} + \beta y_{22} + \beta y_{23} \\ +\beta y_{31} + \beta y_{32} + \beta y_{33} \end{bmatrix}
\begin{bmatrix} V_A \\ V_B \\ V_C \\ V_a \\ V_b \\ V_c \\ V_N \\ V_n \end{bmatrix}
$$

Connection : Star − Star (7.9)

$$
\begin{bmatrix}
I_A - \alpha I_{n1} \\
I_B - \alpha I_{n2} \\
I_C - \alpha I_{n3} \\
I_a - \beta I_{n1} + \beta I_{n3} \\
I_b + \beta I_{n1} - \beta I_{n2} \\
I_c + \beta I_{n2} - \beta I_{n3} \\
I_N + \alpha I_{n1} + \\
\alpha I_{n2} + \alpha I_{n3}
\end{bmatrix}
=
\begin{bmatrix}
y_l + \alpha y_{11} & y_l' + \alpha y_{12} & y_l' + \alpha y_{13} & -y_l - y_l'' & y_l + y_l'' & 0 & -y_l - 2y_l' \\
 & & & & & & -\alpha y_{11} - \alpha y_{12} \\
 & & & & & & -\alpha y_{13} \\
-y_l' + \alpha y_{21} & y_l + \alpha y_{22} & y_l' + \alpha y_{23} & 0 & -y_l - y_l'' & y_l + y_l'' & -y_l - 2y_l' \\
 & & & & & & -\alpha y_{21} - \alpha y_{22} \\
 & & & & & & -\alpha y_{23} \\
y_l' + \alpha y_{31} & y_l' + \alpha y_{32} & y_l + \alpha y_{33} & y_l + y_l'' & 0 & -y_l - y_l'' & -y_l - 2y_l' \\
 & & & & & & -\alpha y_{31} - \alpha y_{32} \\
 & & & & & & -\alpha y_{33} \\
-y_l - y_l'' & 0 & y_l + y_l'' & 2y_l - 2y_l''' & -y_l + y_l''' & -y_l + y_l''' & 0 \\
 & & & +\beta y_{11} - \beta y_{31} & -\beta y_{11} + \beta y_{31} & +\beta y_{32} - \beta y_{33} & \\
 & & & -\beta y_{13} + \beta y_{33} & +\beta y_{12} - \beta y_{32} & -\beta y_{12} + \beta y_{13} & \\
y_l + y_l'' & -y_l - y_l'' & 0 & -y_l + y_l''' & 2y_l - 2y_l''' & -y_l + y_l''' & 0 \\
 & & & -\beta y_{11} + \beta y_{21} & +\beta y_{11} - \beta y_{21} & +\beta y_{12} - \beta y_{22} & \\
 & & & +\beta y_{13} - \beta y_{23} & -\beta y_{12} + \beta y_{22} & -\beta y_{13} + \beta y_{23} & \\
0 & y_l + y_l'' & -y_l - y_l'' & -y_l + y_l''' & -y_l + y_l''' & 2y_l - 2y_l''' & 0 \\
 & & & -\beta y_{21} + \beta y_{31} & +\beta y_{21} - \beta y_{31} & \beta y_{22} - \beta_{32} & \\
 & & & +\beta y_{23} - \beta y_{33} & -\beta y_{22} + \beta y_{32} & -\beta y_{23} + \beta y_{33} & \\
-y_l - 2y_l' & -y_l - 2y_l' & -y_l - 2y_l' & 0 & 0 & 0 & 3y_l + 6y_l'' \\
-\alpha y_{11} - \alpha y_{21} & -\alpha y_{12} - \alpha y_{22} & -\alpha y_{13} - \alpha y_{23} & & & & +\alpha y_{11} + \alpha y_{12} + \alpha y_{13} \\
-\alpha y_{31} & -\alpha y_{32} & -\alpha y_{33} & & & & +\alpha y_{21} + \alpha y_{22} + \alpha y_{23} \\
 & & & & & & +\alpha y_{31} + \alpha y_{32} + \alpha y_{33}
\end{bmatrix}
\begin{bmatrix}
V_A \\ V_B \\ V_C \\ V_a \\ V_b \\ V_c \\ V_N
\end{bmatrix}
$$

Connection : Star − Delta (7.10)

$$
\begin{bmatrix} I_A - \alpha I_{n1} + \alpha I_{n3} \\ I_B + \alpha I_{n1} - \alpha I_{n2} \\ I_C + \alpha I_{n2} - \alpha I_{n3} \\ I_a - \beta I_{n1} + \beta I_{n3} \\ I_b + \beta I_{n1} - \beta I_{n2} \\ I_c + \beta I_{n2} - \beta I_{n3} \end{bmatrix} =
$$

$$
\begin{bmatrix}
\begin{matrix} y_l - y_l' \\ +\alpha y_{11} - \alpha y_{31} \\ -\alpha y_{13} - \alpha y_{33} \end{matrix} &
\begin{matrix} -y_l + y_l' \\ -\alpha y_{11} + \alpha y_{31} \\ -\alpha y_{12} + \alpha y_{32} \end{matrix} &
\begin{matrix} -y_l + y_l' \\ +\alpha y_{13} - \alpha y_{33} \\ +\alpha y_{12} - \alpha y_{32} \end{matrix} &
-2y_l - 2y_l'' & y_l + y_l'' & y_l + y_l'' \\
\begin{matrix} -y_l + y_l' \\ -\alpha y_{11} + \alpha y_{21} \\ +\alpha y_{23} - \alpha y_{13} \end{matrix} &
\begin{matrix} 2y_l - 2y_l' \\ \alpha y_{11} - \alpha y_{21} \\ -\alpha y_{12} + \alpha y_{22} \end{matrix} &
\begin{matrix} -y_l + y_l' \\ \alpha y_{12} - \alpha y_{22} \\ +\alpha y_{23} - \alpha y_{13} \end{matrix} &
y_l + y_l'' & -2y_l - 2y_l'' & y_l + y_l'' \\
\begin{matrix} -y_l + y_l' \\ -\alpha y_{21} + \alpha y_{31} \\ +\alpha y_{33} - \alpha y_{23} \end{matrix} &
\begin{matrix} -y_l + y_l' \\ \alpha y_{32} - \alpha y_{22} \\ -\alpha y_{21} + \alpha y_{31} \end{matrix} &
\begin{matrix} 2y_l - 2y_l' \\ -\alpha y_{32} + \alpha y_{22} \\ +\alpha y_{33} - \alpha y_{23} \end{matrix} &
y_l + y_l'' & y_l + y_l'' & -2y_l - 2y_l'' \\
-2y_l - 2y_l'' & y_l + y_l'' & y_l + y_l'' &
\begin{matrix} 2y_l - 2y_l''' \\ +\beta y_{11} - \beta y_{31} \\ -\beta y_{13} + \beta y_{33} \end{matrix} &
\begin{matrix} -y_l + y_l''' \\ -\beta y_{11} + \beta y_{31} \\ +\beta y_{12} - \beta y_{32} \end{matrix} &
\begin{matrix} -y_l + y_l''' \\ +\beta y_{13} - \beta y_{33} \\ +\beta y_{12} + \beta y_{32} \end{matrix} \\
y_l + y_l'' & -2y_l - 2y_l'' & y_l + y_l'' &
\begin{matrix} -y_l - y_l''' \\ -\beta y_{11} + \beta y_{21} \\ -\beta y_{13} + \beta y_{23} \end{matrix} &
\begin{matrix} 2y_l - 2y_l''' \\ +\beta y_{11} - \beta y_{21} \\ -\beta y_{12} + \beta y_{22} \end{matrix} &
\begin{matrix} -y_l + y_l''' \\ +\beta y_{12} - \beta y_{22} \\ -\beta y_{13} + \beta y_{23} \end{matrix} \\
y_l + y_l'' & y_l + y_l'' & -2y_l - 2y_l'' &
\begin{matrix} -y_l + y_l''' \\ -\beta y_{21} + \beta y_{31} \\ -\beta y_{23} + \beta y_{33} \end{matrix} &
\begin{matrix} -y_l + y_l''' \\ -\beta y_{22} - \beta y_{32} \\ -\beta y_{21} + \beta y_{31} \end{matrix} &
\begin{matrix} 2y_l - 2y_l''' \\ +\beta y_{22} - \beta_{32} \\ -\beta y_{23} + \beta y_{33} \end{matrix}
\end{bmatrix}
\begin{bmatrix} V_A \\ V_B \\ V_C \\ V_a \\ V_b \\ V_c \end{bmatrix}
$$

Connection : Delta – Delta (7.11)

7.2.1 Neutral nodes in transformer star connection

An extra node appears in the mathematical formulation for star-connected transformer windings with ungrounded neutral, i.e. the neutral nodes in equations (7.9) and (7.10), which can be eliminated by Kron reduction. For simplicity of mathematical derivations, the transformer nodal matrix equations have been generically re-defined as follows.

$$\begin{bmatrix} i_p \\ i_n \end{bmatrix} = \begin{bmatrix} A & B \\ C & D \end{bmatrix} \begin{bmatrix} v_p \\ v_n \end{bmatrix} \tag{7.12}$$

where the subscript p and n indicate the phase (primary and secondary) and neutral nodes variables, respectively. Eliminating v_n results

$$\tilde{i}_{p_{red}} = [Y_{red}]\tilde{v}_p \tag{7.13}$$

where

$$[Y_{red}] = [A] - [B][D]^{-1}[C] \tag{7.14}$$

$$\tilde{i}_{p_{red}} = \tilde{i}_p - \left([B][D]^{-1}\right)\tilde{i}_n \tag{7.15}$$

and

$$\tilde{v}_n = [D]^{-1}\left(\tilde{i}_n - [C]\right)\tilde{v}_p \tag{7.16}$$

with the subscript *red* denoting *reduced* variables.

Equation (7.13) still requires further considerations in order to taken into account the electric circuit restriction imposed by the connection, i.e. the sum of the currents to or from the neutral point must be zero, and the consequent magnetic circuit counter-reaction to this restriction. A careful analysis of the factors α_h and β_h associated to the Norton harmonic equivalents is of fundamental importance.

Consider first the simplest case, i.e. the three-phase system is symmetrical and only the transformer linear electric circuit is represented, i.e. α_h and β_h equal to zero for all harmonics, then

$$\begin{aligned} \tilde{i}_n &= 0 \\ \tilde{v}_n &= 0 \end{aligned} \tag{7.17}$$

and the transformer model becomes

$$\tilde{i}_{p_{red}} = [Y_{red}]\tilde{v}_p \tag{7.18}$$

where

$$\tilde{i}_{p_{red}} = i_p$$

Equation (7.18) represents the classical three-phase linear transformer model proposed earlier [Laughton 1968], [Chen and Dillon 1974].

Including now the magnetic circuit in this analysis (i.e., considering α_h and β_h different from zero), comes

1. Due to the nonlinear magnetising characteristic, for an applied sinusoidal voltage at the transformer terminals, harmonic frequencies of magnetising currents are required.

2. Due to the electric circuit restriction associated with star-connected windings, the triplen harmonic magnetising currents required by the iron core can not flow in the electric circuit.

Both requirements must be satisfied and therefore, they must be included in the mathematical formulation. In doing so, the triplen harmonic effects derived from both requirements (discussed in Chapter 2) will be adequately reproduced.

The magnetising currents are defined by the Norton harmonic equivalents, i.e.

$$\tilde{i} = \tilde{i}_n + [Y_n]\tilde{v} \tag{7.19}$$

The triplen harmonic currents must be equal to zero in each phase in order to satisfy the electric circuit restriction. Thus, it results

$$\tilde{i}_{n3} = -[Y_{n3}]\tilde{v} \tag{7.20}$$

which must be included in the algorithm. The neutral voltages will not be zero, but determined by equation (7.16), which represents the magnetic circuit response. Note that the voltage applied to the transformer windings is defined by the difference between the phase and neutral nodal voltages,

$$\tilde{v} = \tilde{v}_p - \tilde{v}_n \tag{7.21}$$

If primary and secondary windings are both star-connected, the harmonic electromagnetic transformer model is already complete, i.e. defined by equations (7.13),(7.20) and (7.21). However, if the secondary is delta or grounded-star connected, further considerations must be taken. Quoting [Stigant *et al.* 1941](pp.700)

> *...the magnetising current will, wherever possible, take the shape required by the particular connections and conditions of service. In consequence of this, where it is not possible for the third harmonic component of the magnetising current to circulate in the primary, it will be transferred to the secondary by magnetic induction if the secondary is such as to allow circulation of the third harmonic to take place.*

The triplen harmonic currents flowing through the secondary windings, will produce a mmf on their own, which can reduce or increase the original third harmonic mmf produced by the primary windings, according to the secondary circuit impedance. This effect has been theoretically discussed in Chapter 2. The secondary circuit impedance consists of the load and transformer impedance (self and secondary leakage reactances) if star-grounded connected, or just the transformer impedance if delta-connected.

Assuming an extreme case, α equal to one and β equal to zero for all harmonics, it implies that the total magnetic circuit is allocated on the primary side. The third harmonic voltage arisen due to the primary star connected windings must be transferred to the secondary side, and this can be done by adding a third harmonic voltage source in each phase of the secondary, its value being equal to one third of the neutral voltage defined by equation (7.16). The third harmonic effects is not completely represented yet as the third harmonic currents that will flow on the secondary circuit will be incorrectly limited only by the third harmonic load impedance (β is equal to zero, thus no magnetising branch on the secondary side).

To fully and adequately describe the whole problem, a third harmonic magnetic impedance must be included on the secondary circuit (as in Osborne's circuit described in Chapter 6), its value being defined by dividing the neutral voltage v_n by the third harmonic current required by the iron core. Alternatively, the problem can be accurately represented by simply transferring the third harmonic currents, i.e. the harmonic Norton equivalents, to the secondary circuit. This is possible defining α equal to zero and β equal to one for the triplen harmonics.

Concluding, for star-delta or star-grounded connections, the transformer electromagnetic mathematical model is defined by equation (7.13), assuming α and β values for the triplen harmonic equal to zero and one, respectively.

It must be emphasized that equal distribution of the Norton harmonic equivalent between the primary and secondary transformer terminals is completely inadequate for this connection. The iterative process will be divergent as half the third harmonic current source (i_{n_3}) will be injected to the primary circuit, which has third harmonic impedance equal to infinite.

It also must be pointed out, that the triplen harmonic restrictions in symmetrical three-phase systems are extended to all zero-sequence harmonic frequencies for

the three-phase systems with asymmetries. In this case, an accurate representation requires the determination of the distribution factors based on symmetrical components representation of the electric circuit. This procedure has not been implemented in this work.

7.3 SIMULATION RESULTS

In order to validate the transformer electromagnetic model for star-star connection, secondary neutral ungrounded, several simulations have been carried out with the HDA program. The test system with a variable third harmonic load, illustrated in Figure 7.1, has been chosen in order to analyse the adequacy of the transformer electromagnetic model to represent the third harmonic effects. In all tests described in this section, the generator voltage is equal to 1.2 (p.u.), both generator and transformer leakage reactance equal to 0.1 (p.u.) and inductive load reactance equal to 10 (p.u.). A large value of load has been chosen in order to avoid considerable voltage drop other than the third harmonic. The magnetising characteristics are those defined by hyperbolae whose parameters are described in Appendix B, except if different curve parameters are explicitly defined in the text.

To assess the triplen harmonic effects, the first sets of simulations considered only the harmonic spectrum up to the third, and the three-phase bank of single-phase transformer model. The test system admittance values have been chosen arbitrarily, to emphasise the harmonic response of three phase transformers for different core configurations and external system impedances.

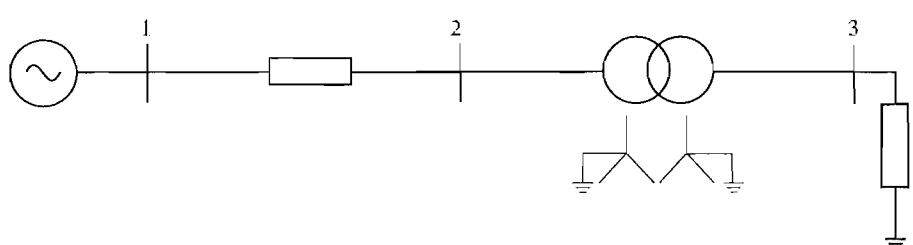

Figure 7.1 Test system

7.3.1 Test 1

Case (a) The first test consisted in simulating the test system with third harmonic shunt reactance x_{sh_3} equal to 5.0 (p.u.). The secondary circuit is then purely inductive, almost an open-circuit for all frequencies. In this case, a small third harmonic current will flow on the secondary, which results in a small demagnetising effect, i.e the original

third harmonic e.m.f. arisen due to the primary winding connection will be very little reduced.

Figures 7.2 (a), (c) and (e) illustrates the three-phase line-to-ground, neutral and line-to-neutral voltage waveforms at busbar 2, respectively. Their corresponding harmonic spectrum is illustrated in Figures (b), (d) and (f). As expected, the line-to-ground voltages are free from third harmonics, while the neutral voltage and consequently, the line-to-neutral voltages have prominent third harmonics. The latter, showing the characteristic peaked waveform.

Figures 7.3 (a), (c) and (e) illustrates the magnetic fluxes, the currents flowing in the primary (I_{12}) and the currents flowing through the shunt reactance x_{sh_3} (I_{30}), respectively. Their corresponding harmonic spectrum are illustrated in Figures 7.3 (b), (d) and (f). The flux waveforms are flat-topped with a third harmonic flux equal to one third of the the harmonic voltage. The currents flowing in the primary side are purely sinusoidal, while the currents flowing on the secondary circuit have third harmonic components.

Figures 7.4, 7.5 and 7.6 illustrates the composite waveform diagram (fundamental and third harmonics) for the secondary voltage, flux and current flowing in the secondary circuit, phase A, which clearly show the adequacy of the solution: all waveforms have the shape as described in literature [Stigant *et al.* 1941].

Case (b) In order to verify the adequacy of the algorithm for secondary capacitive load, a simulation has been carried out with x_{sh_3} equal to -100(p.u.). The results are shown in the form of composite waveform diagrams, illustrated in Figures 7.7, 7.8 and 7.9. Note that only the third harmonic current has a different phase from that of Case (a).

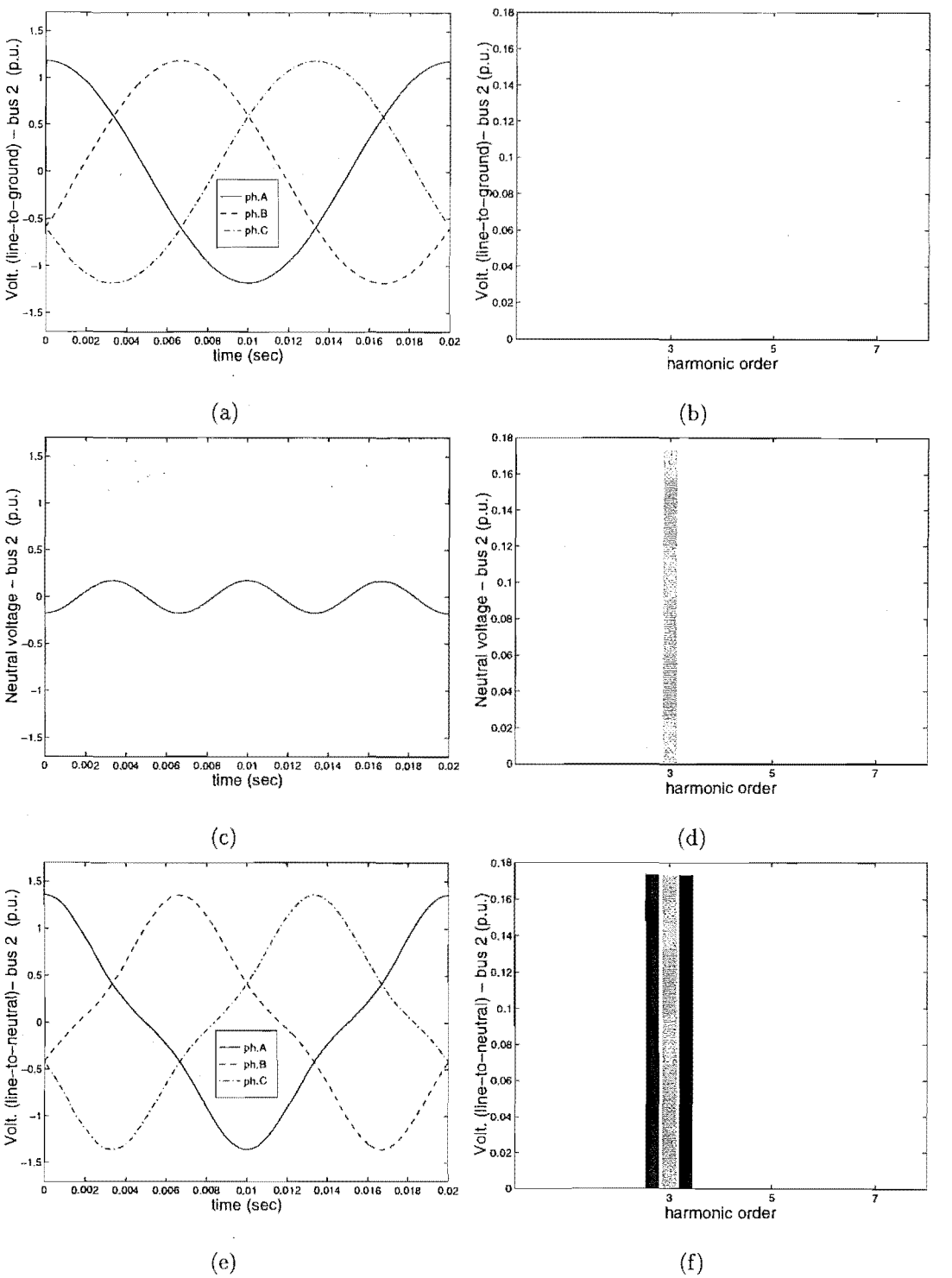

Figure 7.2 star/grounded-star connection: x_{l_3}=5.0(p.u.)

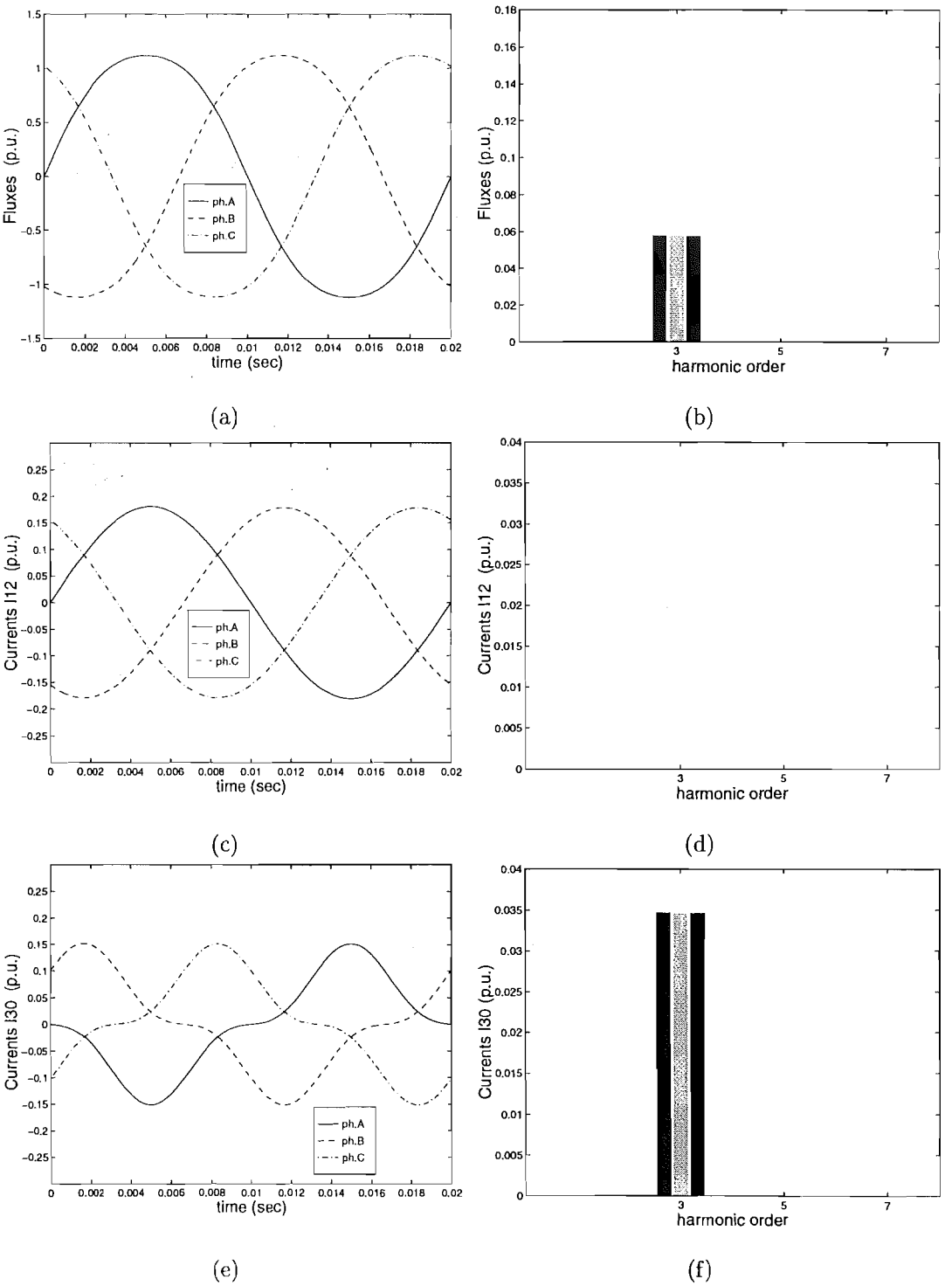

Figure 7.3 star/grounded-star connection: x_{l_3}=5.0(p.u.)

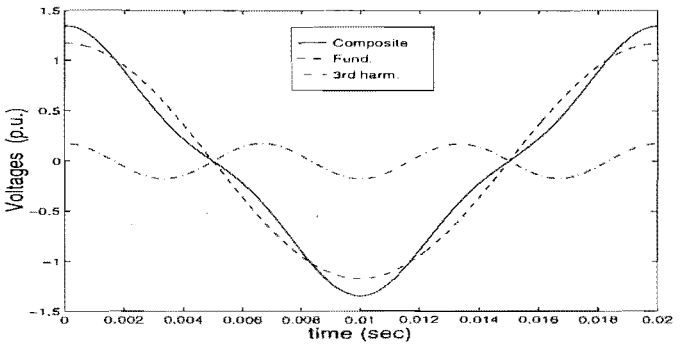

Figure 7.4 Voltages waveforms- x_{l_3}=5.0(p.u.)

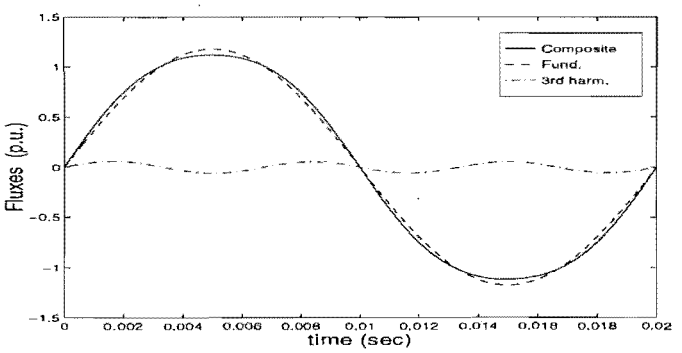

Figure 7.5 Fluxes waveforms- x_{l_3}=5.0(p.u.)

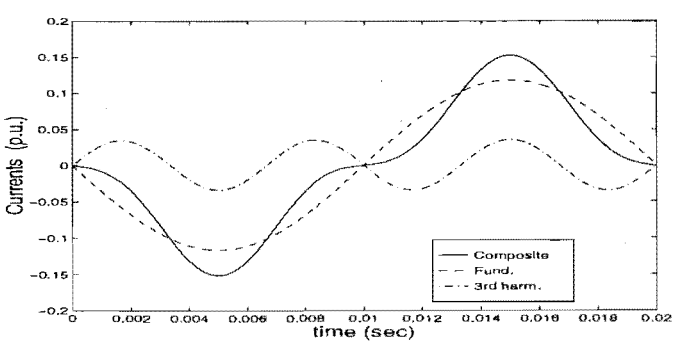

Figure 7.6 Currents waveforms: x_{l_3}=5.0(p.u.)

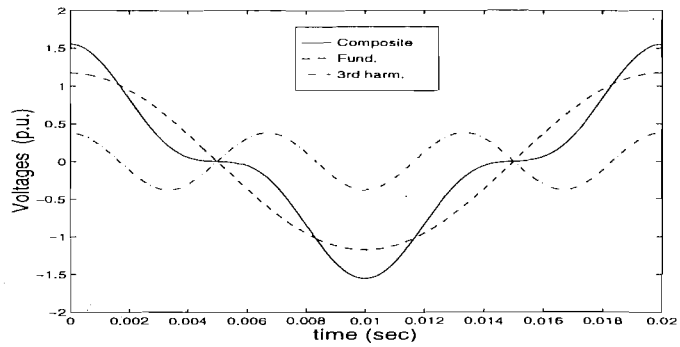

Figure 7.7 Voltages waveforms:x_{c_3}=-100.0(p.u.)

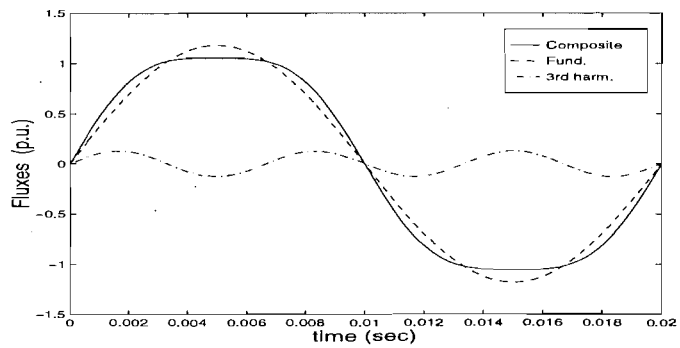

Figure 7.8 Fluxes waveforms :x_{c_3}=-100.0(p.u.)

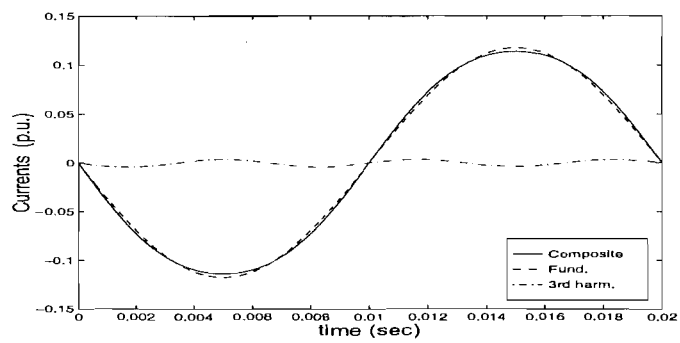

Figure 7.9 Currents waveforms :x_{c_3}=-100.0(p.u.)

7.3.2 Test 2

A set of 60 simulations has been carried out by varying the third harmonic shunt reactance x_{sh_3} from -100.0(p.u.) to 20.0(p.u.) and considering the harmonic spectrum up to the seventh. The range of x_{sh_3} variation has been chosen in order to verify the algorithm performance for capacitive, resonant and inductive secondary circuits. Equally division of the Norton harmonic equivalents between transformer primary and secondary windings are adopted for the non-triplen harmonic frequencies.

The secondary third harmonic voltage and current magnitudes (phase A) are illustrated in Figures 7.10(a) and (b), respectively, and their corresponding phase angle illustrated in Figures 7.10(c) and (d). For large capacitive values of x_{sh_3} (i.e. from -40j to -100(p.u.)), the third harmonic voltage will be about equal to the third harmonic e.m.f. produced on the primary windings (due to the restriction to the third harmonic magnetising currents dictated by the connection) as for these cases, the third harmonic secondary circuit can be considered as if it were open-circuit. Note that the third harmonic currents are very small in this region. However, as the magnitude of x_{sh_3} decrease and approximates to the transformer impedance, i.e. resonant condition, the third harmonic voltages and currents increase. This due to the fact that these currents do not have a proper phase to cause a demagnetising effect upon the original third harmonic e.m.f.. In fact, their corresponding m.m.f. and flux have the same phase as those produced on the primary side, thus intensifying the third harmonic effects.

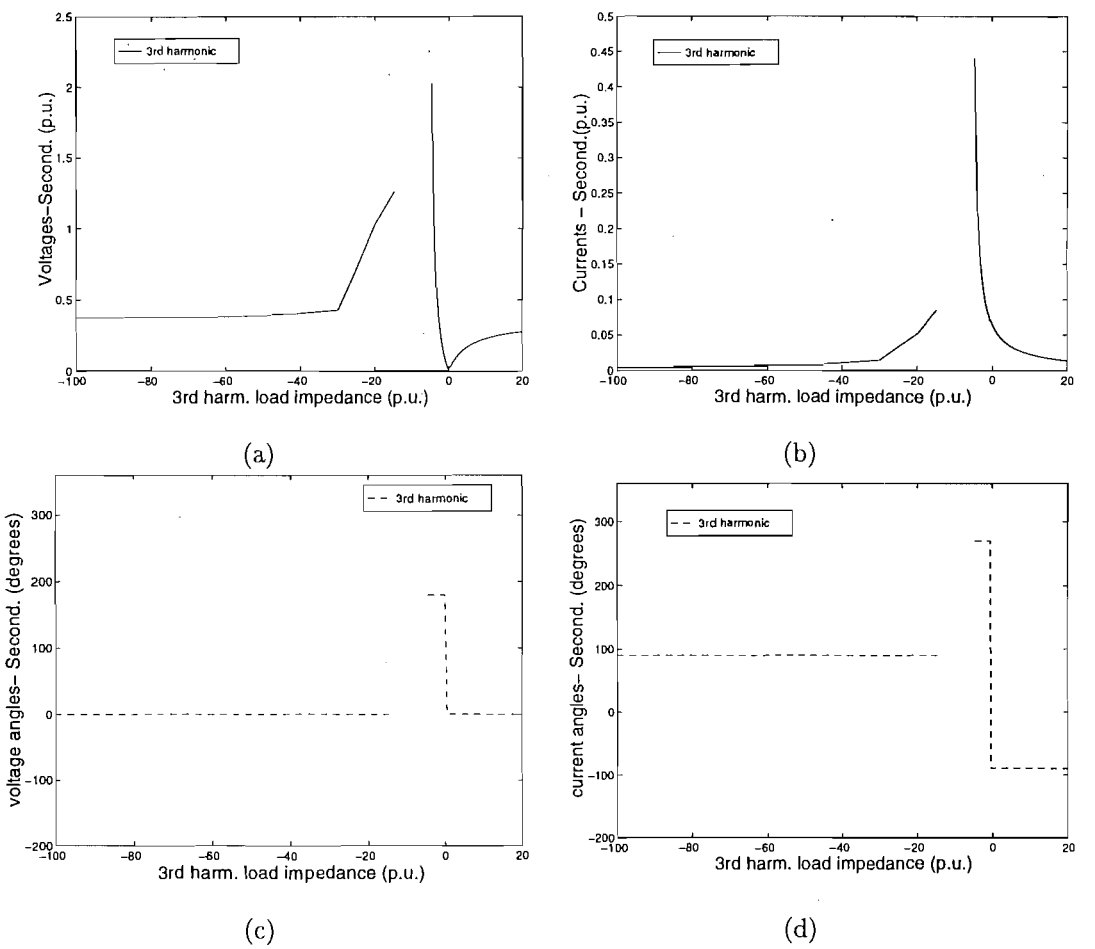

Figure 7.10 Third harmonic voltages and currents

For values close to the resonant point, the algorithm diverges (x_{sh_3} values between -15j to -5(p.u.)). However, after this region, as the x_{sh_3} approximates to zero (secondary third harmonic short circuit), the third harmonic voltages reduce drasti-

cally. It is important to note the voltage and current phase angle for this particular region.

Increasing x_{sh_3} from zero to 20(p.u.), the third harmonic voltage decreases, as for larger third harmonic inductive load the smaller will be the current on the secondary. Consequently, with smaller third harmonic current flowing through the transformer secondary windings, the smaller will be the demagnetising effect upon the original primary e.m.f.. Note that the voltage phase is again equal to zero, while the current phase is equal to -90 degrees.

The fifth and seventh harmonic voltage and current magnitudes, phase A, on the primary and secondary sides are illustrated in Figures 7.11 (a) to (d). From these figures is interesting to note that, although the Norton harmonic equivalents for these frequencies have been equally distributed, only a small fraction will flow through the secondary circuit as the fifth and seventh harmonic impedance on this side is much larger than the primary ones.

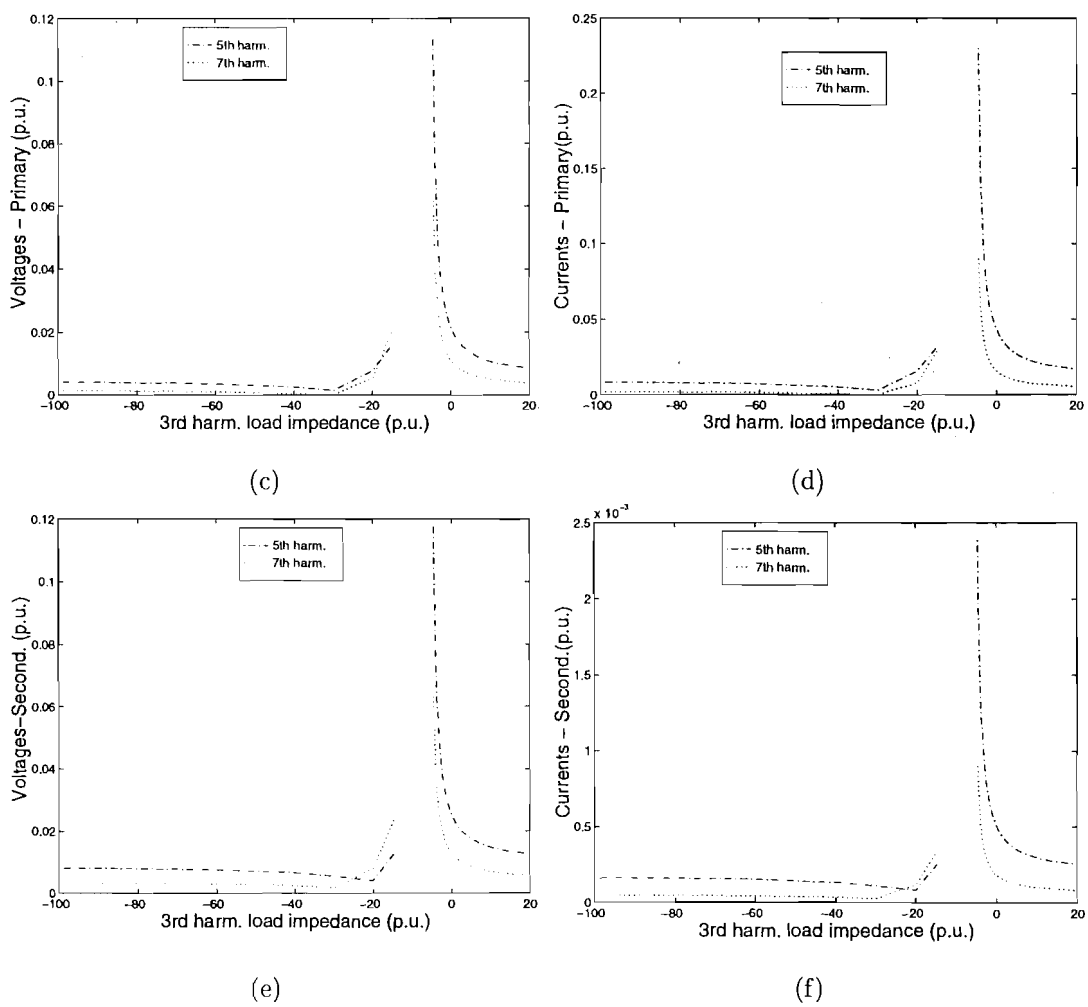

Figure 7.11 Fifth and seventh harmonic voltages and currents

The composite waveform diagrams for this range of x_{sh_3} where occurs a 90 degrees phase shift in third harmonic variables are illustrated in Figure in Figures 7.12, 7.13 and 7.12, considering the simulation results with x_{sh_3} equal to -2.0(p.u.).

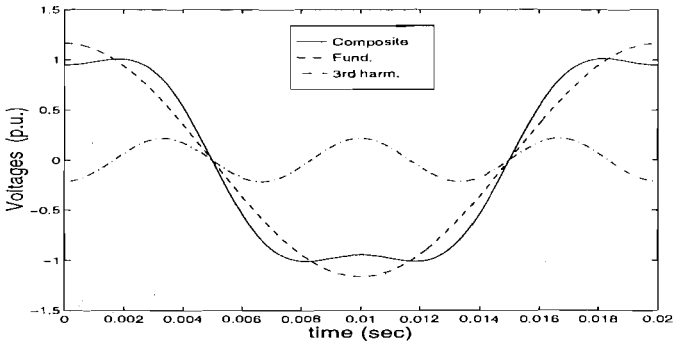

Figure 7.12 Voltages waveforms: x_{c_3}=-2.0(p.u.)

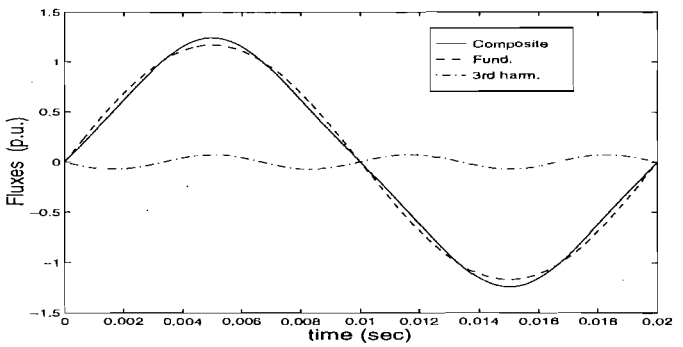

Figure 7.13 Fluxes waveforms: x_{c_3}=-2.0(p.u.)

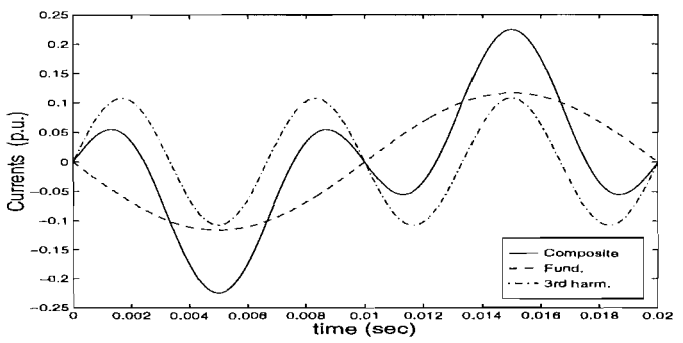

Figure 7.14 Currents waveforms: x_{c_3}=-2.0(p.u.)

The voltage waveforms associated with these three distinct secondary circuit harmonic responses are illustrated in Figures 7.15, 7.16 and 7.17, for several values of x_{sh_3}. Tridimensional figures for the entire range of 60 simulations are illustrated in Figure 7.18 (a), (b) and (c).

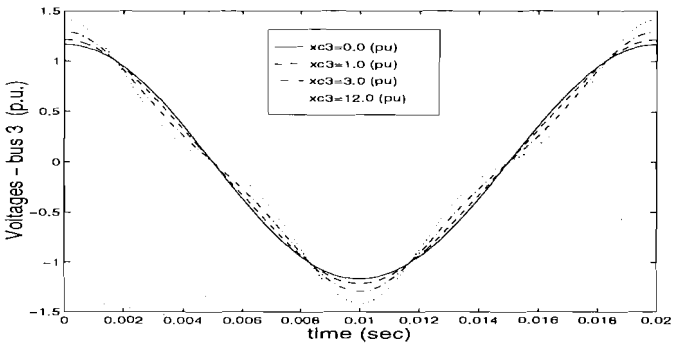

Figure 7.15 Inductive third harmonic load

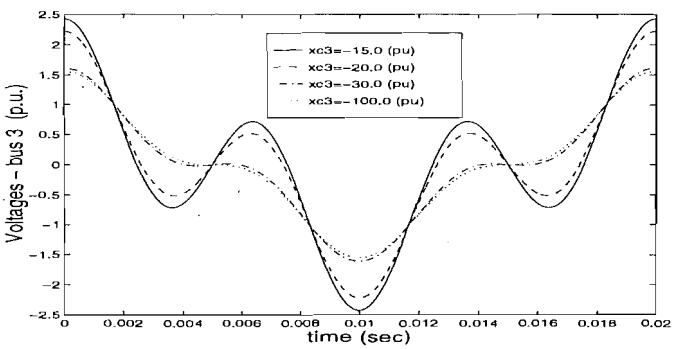

Figure 7.16 Capacitive third harmonic load-a

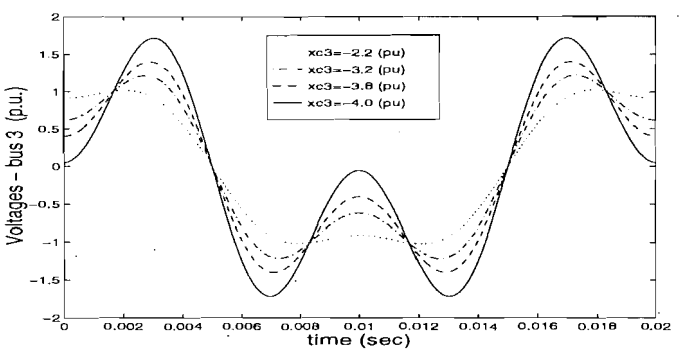

Figure 7.17 Capacitive third harmonic load-b

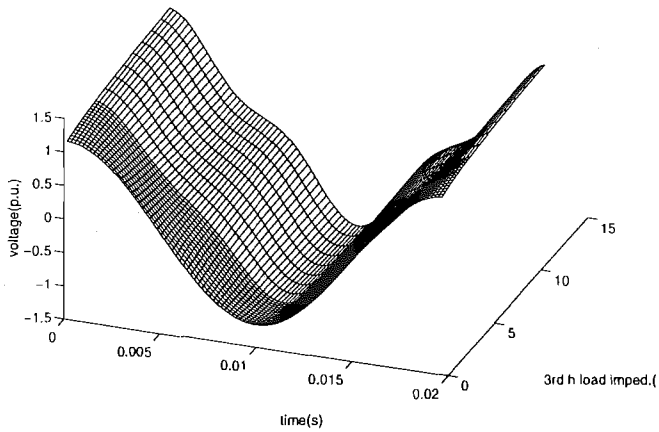

(a)

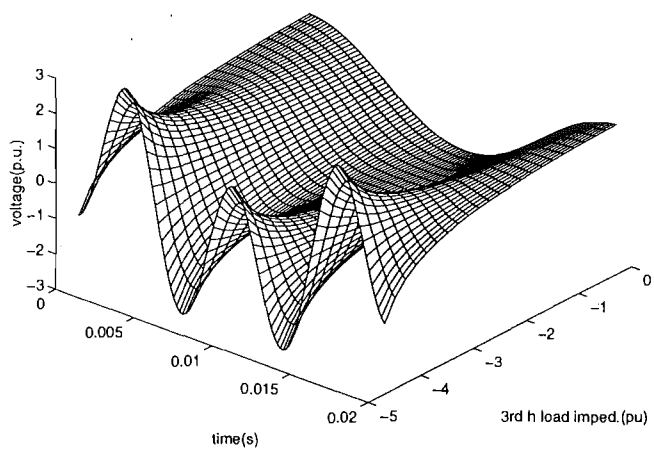

(b)

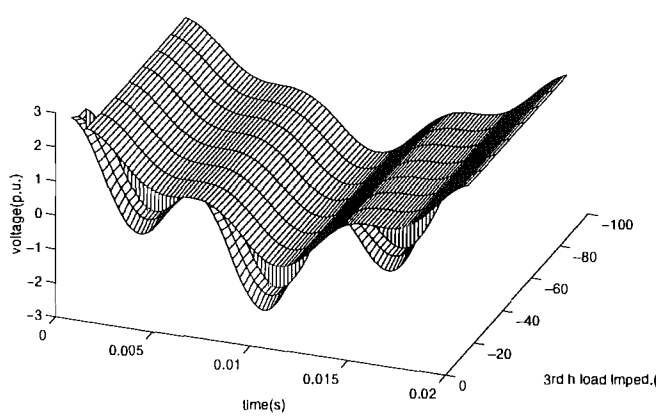

(c)

Figure 7.18 Third harmonic voltages for different x_{sh_3}

7.3.3 Test 3

The same set of 60 simulations has been performed using the three-limb electromagnetic model, using two different values for the slope of the zero-sequence flux path magnetising characteristic, i.e. m_1 equal to 6.0 and m_1 equal to 1.0. The purpose of these simulations is to verify the influence of the core geometry upon the transformer third harmonic response.

The three sets of simulation results regarding the third harmonic voltage and current magnitudes (phase A), are shown in Figure 7.19 (a) and (b), respectively. Their corresponding phase angles are illustrated in Figure 7.19 (c) and (d).

The same third harmonic effects that occurs for a three single-phase transformer, also occur for the three-limb core transformer. However, the latter, due to the core geometry, shows third harmonic effects very much reduced and the third harmonic resonant point closer to the origin.

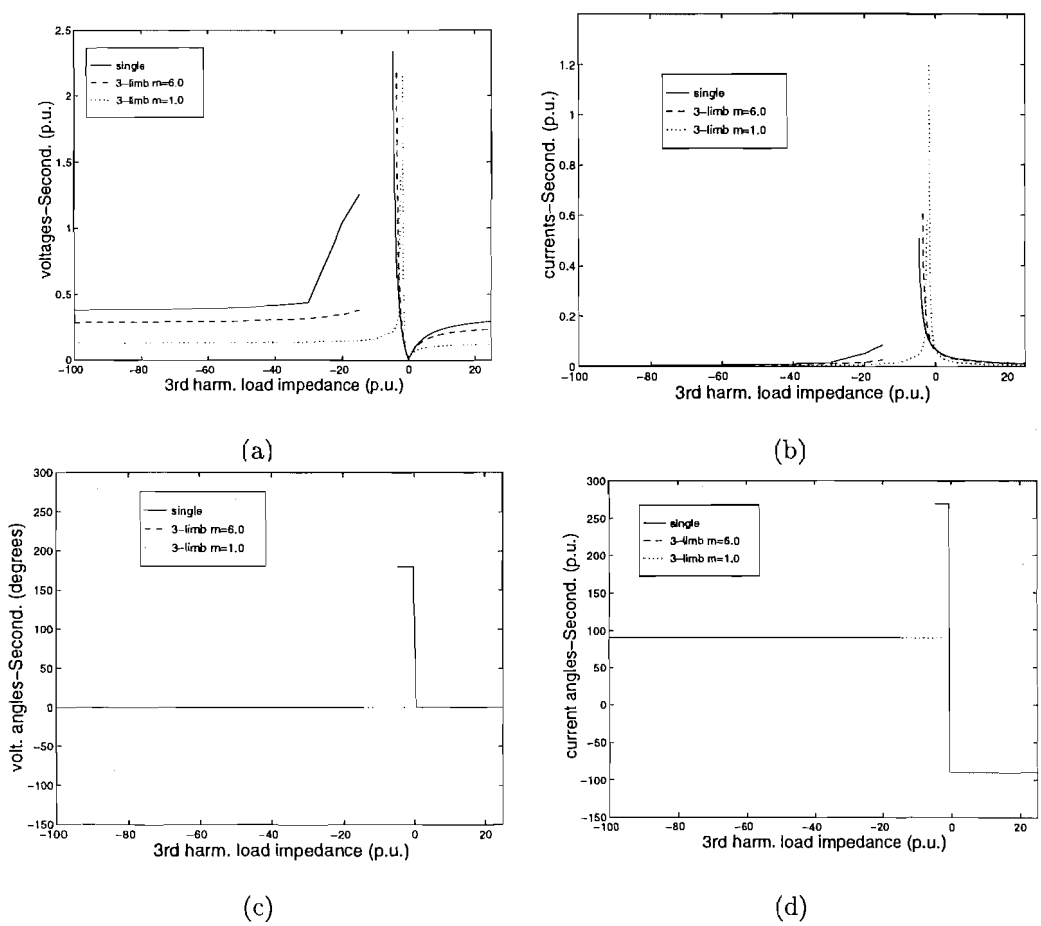

Figure 7.19 Comparisons between three-limb and three single-phase transformers

7.3.4 Test 4

Simulations have been carried out with the HDA program in order to verify the adequacy of the proposed models for Star-Star, with both neutral grounded, grounded Star-Delta and Star-Star with the secondary neutral grounded connections with the same test system and parameters, except that the third harmonic load impedance is fixed (i.e. equal to three times the fundamental impedance value).

Figure 7.20(a), (b) and (c) illustrate the three-phase currents flowing through the generator impedance using the grounded-Star/grounded-Star, grounded-Star/Delta and Star/grounded-Star connections, respectively. These preliminary results indicate adequacy of the proposed models, as the waveforms and harmonic content match with the experimental and theoretical information available in the literature [Stigant *et al.* 1941]. Small values of third harmonic current for grounded-Star/Delta and Star/grounded-Star connections are due to the asymmetry introduced by the core geometry (i.e. due to the yoke branches), therefore, not zero-sequence third harmonic currents.

The same case has been simulated again, considering the length of the yoke branch equal to zero to remove the core asymmetry. The results are illustrated in Figure7.21 (a) and (b), considering grounded-Star/Delta and grounded-Star/grounded-Star connections. As expected, all harmonics have the same magnitude in the three-phases and therefore, for the grounded-Star/Delta connected transformer no third harmonic currents flow in the primary. It should be pointed out that third harmonic currents could appear on the primary side for this connection as a closed path is also provided on this side with the transformer and generator neutrals grounded. The primary side circuit consists of the generator impedance and transformer primary leakage reactance (X_{l_1}), so, although X_{l_1} is not available, the total third harmonic impedance on the primary side will be larger than that of the secondary side. Thus, in this case, defining β_3 equal to 1.0, i.e. allocating all the magnetising current on the delta-connected side is a good approximation.

The voltage waveforms and harmonic content, magnitude and phase angle, of busbar 2 and 3 for the three transformer connections (grounded-star/grounded-star, grounded-star/Delta, ungrounded-star/ungrounded-star) are illustrated in Figures 7.22, 7.23 and 7.24 respectively. From the analysis of these curves, the effect of the transformer connection upon the zero-sequence harmonic voltages can be clearly verified. The thirty degrees differences between primary and secondary phase-angle voltages in a Star/Delta connection has also been correctly computed by the proposed model.

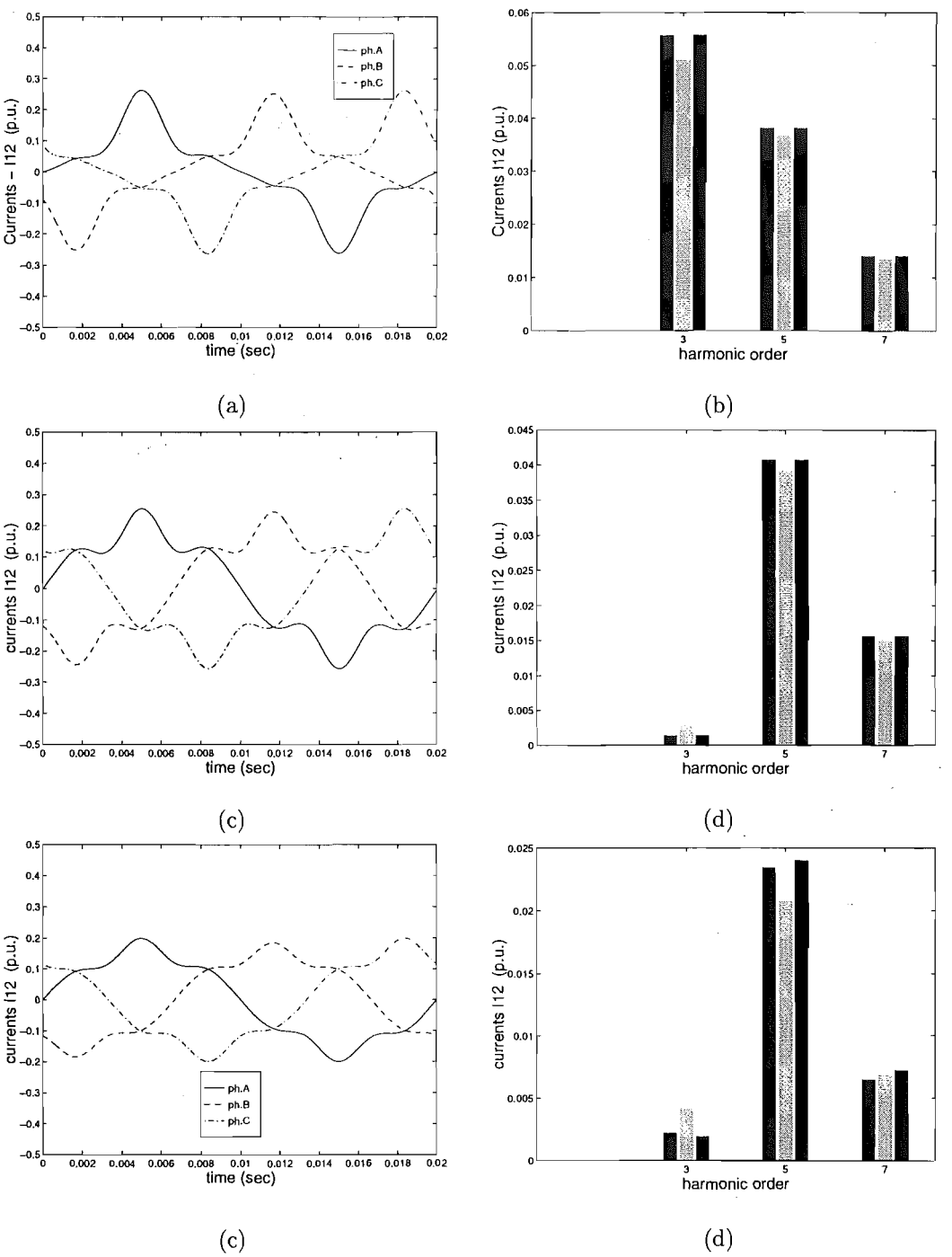

Figure 7.20 Comparisons: Currents flowing between nodes 1 and 2

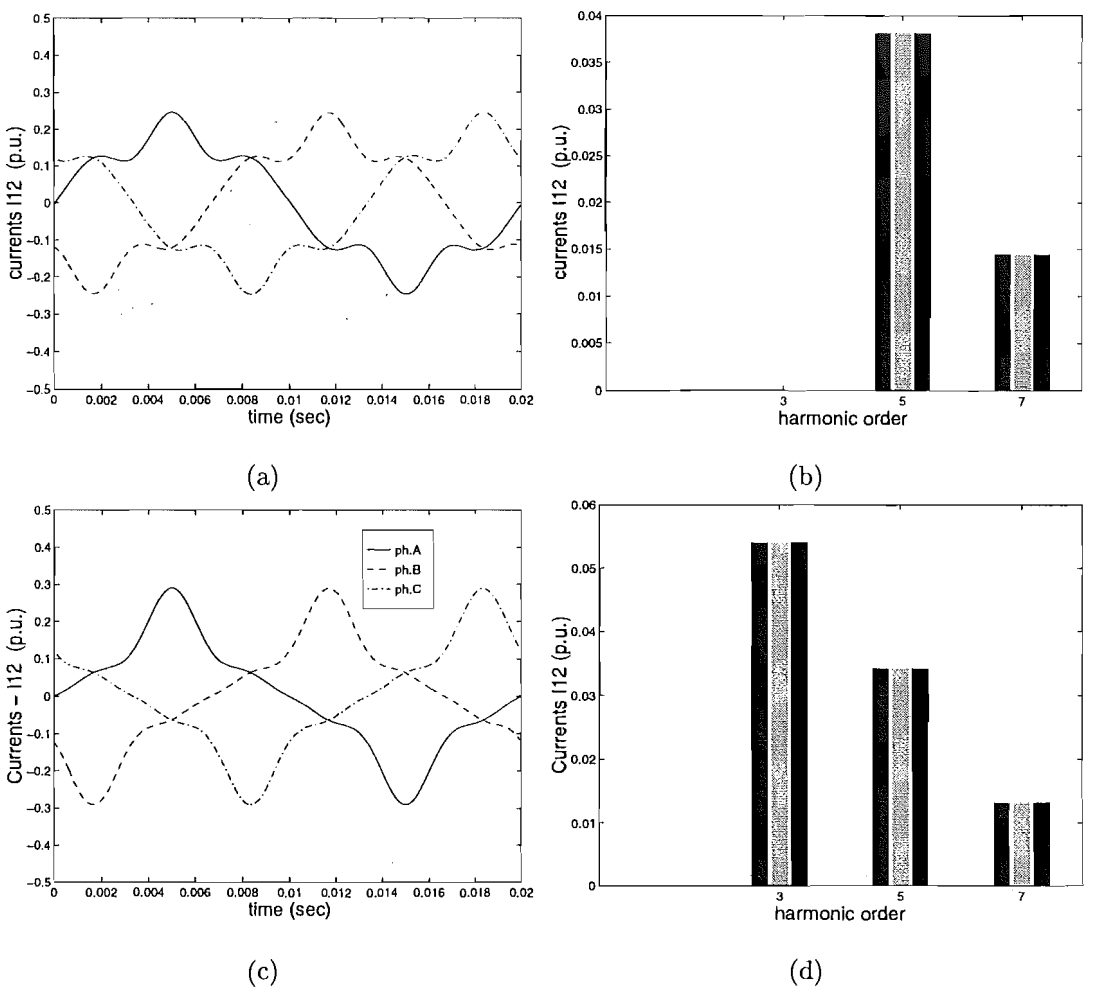

Figure 7.21 Currents flowing between nodes 1 and 2, considering yoke length equal to zero

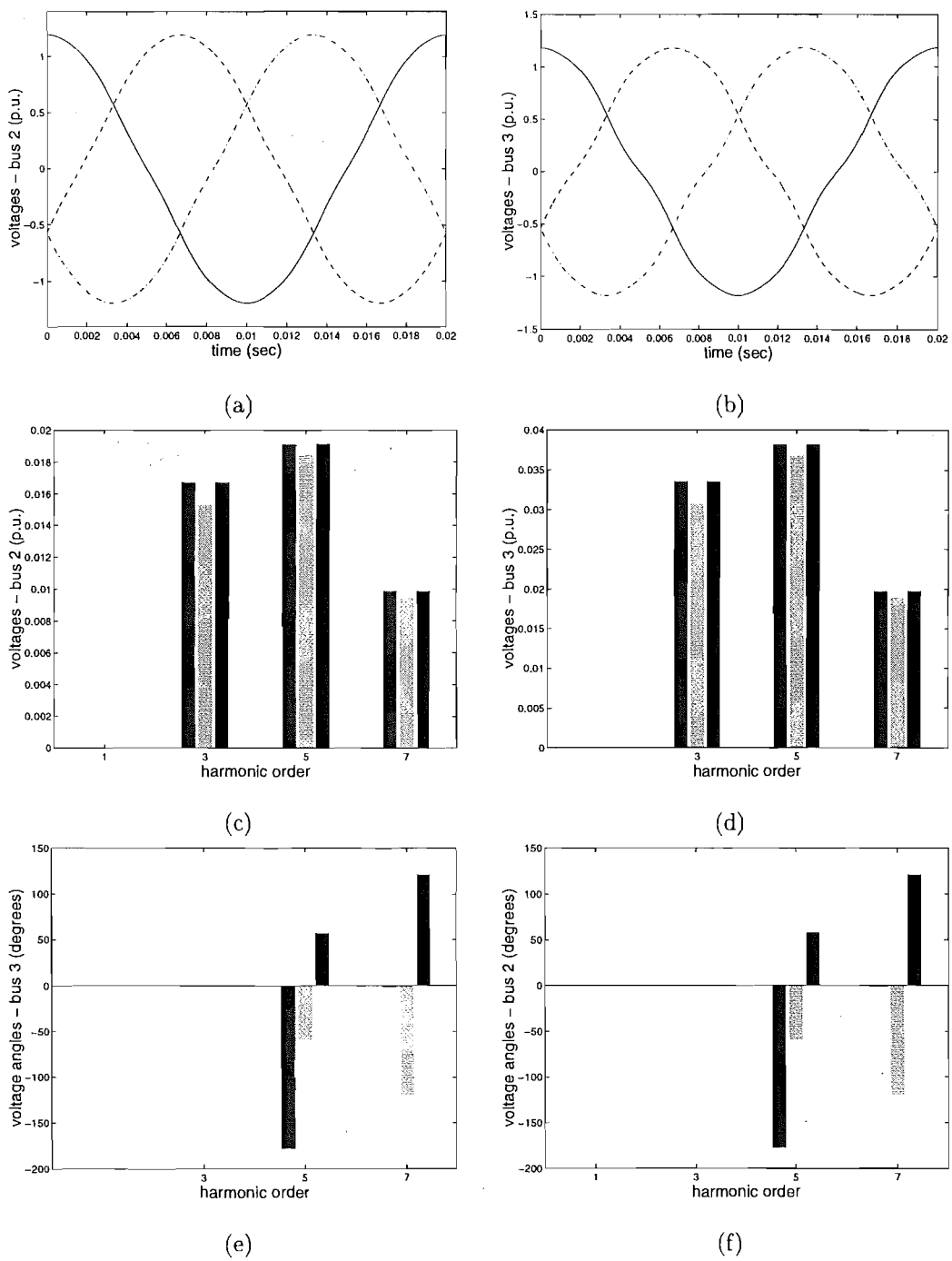

Figure 7.22 Grounded-star/ Grounded-star connection

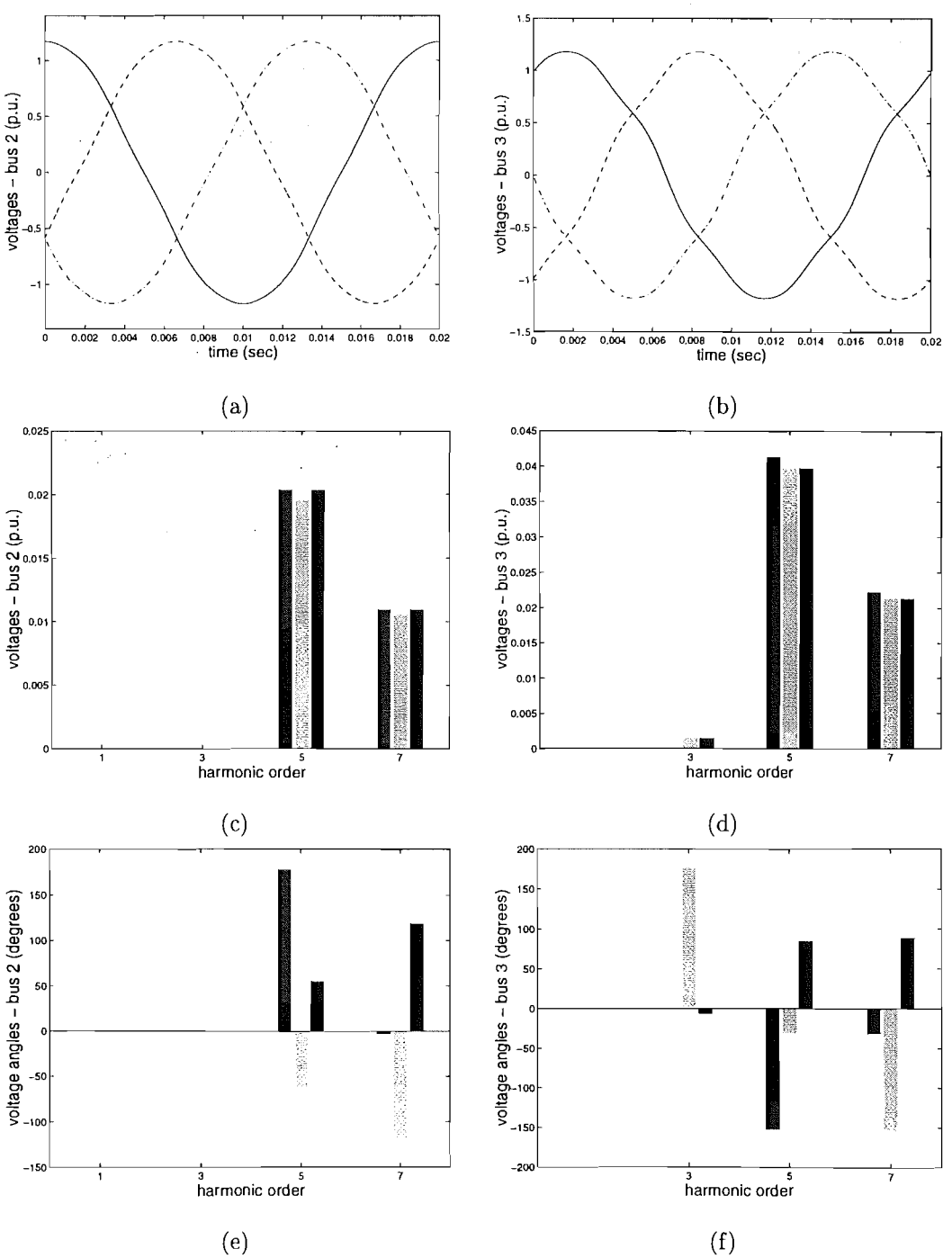

Figure 7.23 Grounded-star/ delta connection

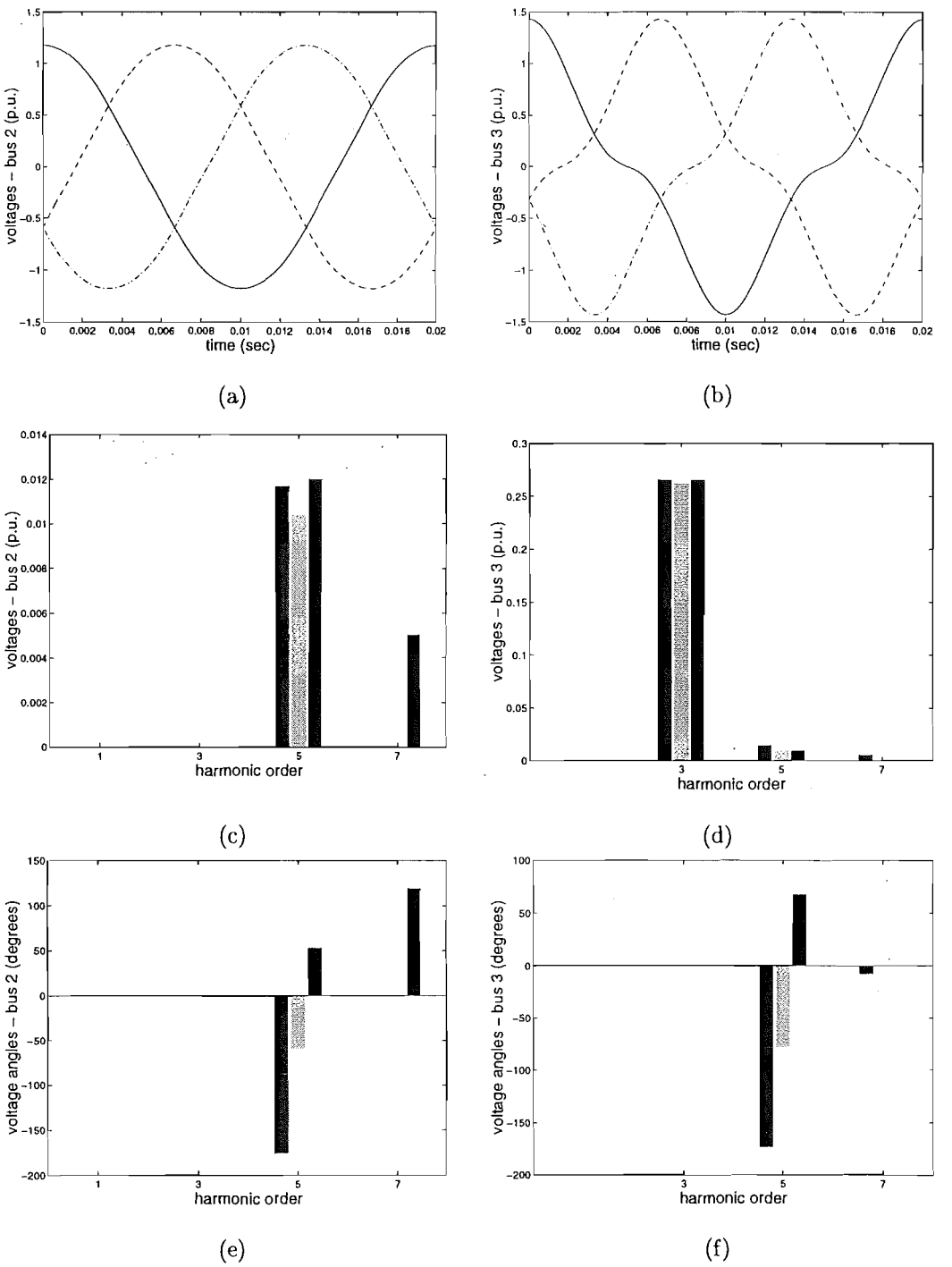

Figure 7.24 Grounded-star/ ungrounded-star connection

7.4 CONCLUSIONS

Harmonic three-phase three-limb electromagnetic transformer models for the most commonly used electrical configurations have been derived. Their adequacy has been verified through several simulations and the results match with the practical and theoretical knowledge available in the literature.

Due to the combined requirements of the magnetic and electric circuits, zero sequence harmonic voltages arise in the windings of star-connected transformers. This phenomenon has been adequately modelled with an appropriate distribution of the harmonic Norton equivalents between the transformer primary and secondary terminals and adequate determination of the neutral voltages.

Accurate evaluation of the distribution factors requires the knowledge of primary and secondary leakage reactances, rarely available in the literature, and the sequence component harmonic impedances of the primary and secondary external impedances. Due to the lack of some of the required information, for Star/Star-grounded connected transformers, allocating all the zero-sequence harmonic Norton equivalents on the grounded-Star connected windings has proven to be an adequate approximation. For similar reasons, for Star-grounded/Delta connected transformers, they should be placed on the delta side.

Chapter 8

CONCLUSIONS AND FUTURE WORK

8.1 CONCLUSIONS

With the increased use of power electronic devices, the operation of modern power systems is subjected more and more to harmonic voltages and currents. Moreover, modern transformers tend to operate very close to the limit of the linear characteristics and, even under small overexcitation, the harmonic content of their magnetising currents contribute to aggravate the problem.

Harmonic power system analysis, particularly at the planning stage, has become increasingly important as it constitutes a powerful tool for the adequate assessment and enhancement of power quality, and the impact of harmonic distortion upon system components. Accurate representation of power plant component non-linearities and the interaction with the electric network is of fundamental importance in rigorous harmonic studies. This work has concentrated on the development of detailed three-limb three-phase electromagnetic transformer models for steady-state harmonic analysis.

The influence of the external system impedance, transformer electrical and core configuration upon the overall transformer harmonic response has been analysed in Chapter 2, by means of phasor diagrams and sensitivity analysis. It has been shown that core configuration mainly affects the transformer zero sequence harmonic response. This requires accurate representation, particularly for power system operation conditions where zero sequence harmonics are of significance. These conditions arise with saturated star-connected transformers, system imbalance and/or other non-linear devices. In most cases, smaller harmonic voltages and currents are associated with the three-limb core transformer when compared with other core configurations. However, larger harmonic distortion may occur in capacitive circuits with grounded-star/grounded-star connected three-limb transformers, thus a general rule cannot be derived. It has also been shown that, for zero sequence harmonic frequencies, the external system impedance only affects the transformer harmonic response if it is star-connected with a grounded neutral.

In the Harmonic Domain, frequency dependent components can be accurately represented, and a unified steady state harmonic solution for the system is achieved through a Newton-Raphson iterative procedure. Based on a linearisation process in this domain, non-linear components are modeled in the form of Norton equivalents, with the cross-coupling between frequencies explicitly represented in the harmonic admittance matrix. The framework and application of the Harmonic Domain has been described in Chapter 3.

The main transformer non-linearity is in the magnetising characteristic, and therefore, its adequate mathematical representation is essential for the derivation of accurate electromagnetic transformer models. The adequacy of the most commonly used magnetising characteristic representations has been investigated in Chapter 4. It has been shown, that two and three piecewise linear segments approximation can lead to harmonic solutions with significant errors in resonant systems. On the other hand, four piecewise linear segments approximation, hyperbola as well rational-fraction representation result in very close harmonic solutions. Singular Value Decomposition technique has been explored, and has proven to be a better alternative to determine the parameters of rational-fraction and hyperbola equations than those proposed in the literature. In addition, cubic spline approximation has been investigated as an alternative to model the magnetising characteristic. It is a simple, efficient and accurate way to reproduce any type of magnetising characteristic, it can be extended to represent hysteresis and is suitable for the harmonic domain algorithm based on convolutions. With the exception of the two and three-piecewise linear segments approximations, the magnetising characteristic representation is a question of computational conveniences, as they all have similar levels of accuracy.

In Chapter 5, a detailed three-phase three-limb transformer model is proposed. It is a more accurate Harmonic Domain model as the nodal magnetising flux balance $\sum \phi = 0$ is incorporated into the formulation. A Newton-Raphson iterative procedure has also been presented to calculate the non-linear distribution of the fluxes among the various magnetic branches, as a basic step to derive the harmonic Norton equivalents. This approach is a more precise alternative than the commonly used EMTP linear procedure for flux distribution. However, gain accuracy is not significant, except in some cases of resonance, and is achieved at the expense of additional computation time.

The linearised harmonic transformer model has been adapted to the instantaneous form and implemented in the EMTDC program. A comparison between the harmonic and time domain techniques has been made and the results have shown excellent agreement, thus increasing the confidence in the potential of the Harmonic Domain technique.

Chapter 6 has demonstrated, through sensitivity analysis, that an equal distrib-

ution of the Norton equivalents between primary and secondary terminals is not a good approximation at harmonic frequencies. It has been shown that for accurate solutions, harmonic distribution factors should be used. These can be determined analytically, provided that the primary and secondary leakage transformer reactances are known. A theoretical investigation has shown the inadequacy of this approximation with reference to star-connected three-phase transformer models. The harmonic distribution factors can be derived based on sequence components impedances.

Finally, three-phase three-limb electromagnetic transformer models for the most commonly used electrical configurations have been derived. The zero sequence voltages associated with saturated star-connected transformers has been adequately modeled with an appropriate distribution of the harmonic Norton equivalents. The adequacy of the proposed models have been analysed through sensitivity analysis and comparisons with theoretical knowledge reported in the literature.

8.2 FUTURE WORK

The harmonic response of the transformer and other non-linear components is defined as a function of their intrinsic non-linearities, as well as their harmonic interaction with the external system. A detailed power converter model in the Harmonic Domain has been recently proposed[Smith 1995], and the incorporation of this component in the Harmonic Domain algorithm would allow the investigation of the mechanism of harmonic interaction between these two important power system components. The simultaneous representation of different sources of harmonics in the HD algorithm would result in a more powerful and efficient tool for harmonic power system analysis.

Positive frequency harmonic phasors have the advantage of allowing an unified solution of the entire system containing real valued unknowns (such is the case of systems containing power electronic devices), besides improving the algorithm computational efficiency. To implement the proposed three-limb transformer model with positive frequency harmonic phasors is straightforward. Harmonic calculations can be carried out either by means of convolutions, or frequency to time domain transformations with subsequent application of FFT. Investigation should be carried out to assess computational advantages in using one or the other approach for both converter and transformer models.

The proposed three-phase transformer models in the phase frame of reference suffer restrictions regarding the distribution of the transformer magnetising currents between primary and secondary terminals. This distribution has to be done based on the sequence component network and transformer impedances, this being essential for an accurate electromagnetic transformer model. Moreover, it has been shown that the converter model in sequence components displays a higher degree of sparsity in the

Jacobian matrix. A worthwhile area for future research is to explore the mathematical representation of transformer and other power plant components in this frame of reference.

Fields tests to measure harmonic distortion caused by magnetising currents of three-phase three-limb saturated transformers are needed in order to provide basis for comparisons and consequently, a more conclusive corroboration of the proposed mathematical formulations.

Appendix A

DATA FOR THE SOUTH ISLAND REDUCED SYSTEM

The relevant information for the three-phase test system [Densem *et al.* 1984] [Enrique Acha Daza 1988] used in Chapter 3 is as follows:

A.1 TRANSMISSION LINES

Earth resistivity: 100 (Ω-m)
The phase conductors of the first three transmission lines are arranged in a double circuit configuration and they are symmetrically placed around the vertical axis of the tower. There are two conductors per phase and the coordinates, taken from the center of the tower and the ground level, are given for one of the circuits.

A.1.1 Invercargill220-Manapouri220

Line length: 152.9 km
Conductor type: GOAT(30/3.71+7/3.71 ACSR)
Earth-wire typr: (7/3.05 Gehss)
Conductor coordinates (in meters)

Phase a	4.80	12.50
Phase b	6.34	18.00
Phase c	4.42	23.50
Earth-wire	0.00	29.00

A.1.2 Manapouri220-Tiwai220

Line length: 175.60 km
Type and coordinates of phase and earth-wire conductors are identical to those of line Invercargill-Manapouri220.

A.1.3 Invercargill220-Tiwai220

Line length: 24.3 km
Conductor type: GOAT(30/3.71+7/3.71 ACSR)
Earth-wire type: (7/3.05 Gehss)
Conductor coordinates (in meters)

Phase a	4.77	12.50
Phase b	6.29	17.95
Phase c	4.41	23.41
Earth-wire	1.52	28.26

A.1.4 Invercargill220-Roxburgh220

This line consists of two single-circuit lines of flat configuration having one conductor per phase. The coordinates are taken from the extreme left conductor and the ground level. Line length: 131.00 km
Conductor type: Zebra(54/3.18+7/3.18 ACSR)
Earth-wire(2) type: (7/3.05 Gehss)
Conductor coordinates (in meters)

Phase a	0.00	12.50
Phase b	6.47	12.50
Phase c	1.86	18.41
Earth-wire	11.08	18.41

Conductor coordinates of circuit two (in meters)

Phase a	22.94	12.50
Phase b	30.14	12.50
Phase c	37.34	12.50

A.2 GENERATORS

Generator	x''_d (p.u.)	$x''_0(p.u.)$
Manapouri1014	0.0370	0.0197
Manapouri2014	0.1480	0.0788
Manapouri3014	0.1480	0.0788
Roxburgh	0.0620	0.0323

A.3 TRANSFORMERS

Transformer	$x_l(p.u.)$
Manapouri220 Manapouri1014	0.02690
Manapouri220 Manapouri2014	0.10720
Manapouri220 Manapouri3014	0.10720
Invercarg033 Invercarg220	0.10290
Invercarg033 Invercarg220	0.10290
Roxburgh-220 Roxburgh1011	0.03820
Roxburgh-011 Roxburgh-220	0.07632
Roxburgh-011 Roxburgh-220	0.07632

A.4 LOADS

Load	P(MW)	Q(MVAR)
Roxburgh-011	90.0	54.0
Invercarg033	135.0	36.0

A.5 SYSTEM PARAMETERS

Base frequency:50 (Hz)

Base power: 100.0 (MVA)

Base voltage:220.0 (KV)

A.6 LOAD-FLOW SOLUTION

Bus	V(A)	Ang(A)	V(B)	Ang(B)	V(C)	Ang(C)
1	1.0050	0.0000	1.0050	-120.0000	1.0050	120.0000
2	1.0000	-2.5898	1.0031	-122.6669	1.0009	117.1622
3	0.9976	-4.1845	1.0023	-124.3120	0.9992	115.3990
4	1.0217	-3.9254	1.0239	-124.0922	1.0225	115.5809
5	1.0281	-1.9450	1.0296	-122.1463	1.0265	117.6984
6	1.0251	-3.6928	1.0267	-123.8719	1.0255	115.7990
7	0.9753	-6.1882	0.9801	-126.2967	0.9770	113.4020
8	0.9982	-8.0990	1.0006	-128.2467	0.9992	111.4148
9	0.9999	1.4468	0.9999	-118.5532	0.9999	121.4469
10	1.0160	-0.5355	1.0172	-120.6536	1.0151	119.2688
11	1.0011	1.4928	1.0011	-118.5702	1.0011	121.4298
12	1.0160	-0.5671	1.0180	-120.6759	1.0153	119.2809

Appendix B

PARAMATERS OF THE TEST SYSTEM

B.1 MAGNETISING CURVE PARAMETERS

Curve	m_1	m_2	*knee flux*	*knee curve*	b_1	b_2
1	292.38	0.67	1.037	0.0035	0.0	1.03
2	292.38	1.67	1.037	0.0035	0.0	1.03
3	6.00	1.44	0.050	0.2900	0.0	0.22

B.2 JAGUARA-TAQUARIL TRANSMISSION LINE

Phase conductors arranged in a horizontal configuration with 954 MCM-ACSR conductors per phase and $\frac{3}{8}''$ galvanised steel earth-wires. Relevant parameters are:
Line length: 398.00 km
Conductor type: 954 MCM-ACSR
Phase conductor height:13.18m
Phase spacing:8.5 m
Earth-wire(2) height: 22.97 m
Earth-wire spacing: 12.50 m
System base power: 100 MVA

Appendix C

EMTP TRANSFORMER NORTON EQUIVALENT

For the EMTP algorithm, the derived Norton equivalent formulation must be in instantaneous form and therefore some equations need to be re-written .
Considering a generic non-linear function $i_k = f(\phi_k)$, its linearized expression has the form $i_k(t) - i_k(t - \Delta t) = \mathcal{R}_k[\phi_k(t) - \phi_k(t - \Delta t)]$ where

$$\Delta t \to 0$$

and

$$\mathcal{R}_k = \frac{di_k}{d\phi_k}\bigg|_{\phi_k(t-\Delta t)}$$

Discretising per unit equation $v_s = \frac{d\phi_s}{dt}$ with trapezoidal integration yields $\tilde{\phi}_s(t) = \tilde{\phi}_s(t - \Delta t) + \frac{\Delta t}{2}\omega_0$

where ω_0 is the base angular frequency.

Finally, the Norton equivalent can be expressed by

$$\tilde{i}_{st} = [Y_t]\tilde{v}_s(t) + \tilde{i}_{nst} \quad \text{where}$$

$$[Y_t] = [K]\frac{\Delta t\omega_0}{2}$$

$$\tilde{i}_{nst} = [K][\frac{\Delta t\omega_0}{2}\tilde{v}_s(t - \Delta t) +$$

$$+\tilde{\phi}_s(t - \Delta t)] + \tilde{i}_{ns}$$

REFERENCES

ACHA, E. AND RICO, J.J. (1994), 'Harmonic domain modelling of non-linear power plant components', *ICHPS Conference, Bologna, Italy.*

ACHA, E., ARRILLAGA, J., MEDINA, A. AND SEMLYEN, A. (1989), 'General frame of reference for analysis of distortion in system with multiple transformer non-linearities', *Proc.IEE Pt.C*, Vol. 136, No. 5, September, pp. 271–278.

ARRILLAGA, J. (1981), *Harmonic monitoring*, UMIST, Manchester.

ARRILLAGA, J. AND ARNOLD, C.P. (1990), *Computer analysis of power system*, John Wiley and Sons.

ARRILLAGA, J. AND CALLAGHAN, C.D. (1989), 'Double-iterative algorithm for the analysis of power and harmonic flows at ac-dc convertor terminals', *Proceedings IEE*, Vol. 136, No. 6, pp. 319–324.

ARRILLAGA, J., BRADLEY, D.A. AND BODGER, P.S. (1985), *Power System Harmonics*, John wiley and Sons.

BISHOP, M.T., BARANOWSKI, J.F., HEATH, D. AND BENNA, S.J. (1996), 'Evaluating harmonic induced trnasformer heating', *IEEE transactions on power delivery*, Vol. 11, No. 1, January, pp. 305–309.

BLUME, L.F., BOYAJIAN, A., CAMILLI, G., LENNOX, T.C., MINNECI, S. AND MONTSINGER, V.M. (1959), *Transformer Engineering*, John Wiley and Sons, second ed.

BOYAJIAN, A. (1925), 'Resolution of transformer reactance', *A.I.E.E.*, June, pp. 805–820.

BRADLEY, D.A., MORFEE, P.J. AND WILSON, L.A. (1985), 'The New Zealand harmonic legislation', *Proceedings IEE*, Vol. 132, No. 4, July, pp. 174–184.

BRAUN, S.G. AND RAM, Y.M. (1987), 'Structural parameter identification in the frquency domain: The use of overdetermined systems', *Trans ASME*, Vol. 109, June, pp. 120–123.

C57 DISTRIBUTION, POWER AND REGULATING TRANSFORMERS STANDARDS (1990), *ieee Standard general requirements for liquid immersed-distribution, power, and regulating transformers*, IEEE inc., 1990 ed.

CHEN, M. AND DILLON, W. (1974), 'Power systems modeling', *Proceedings IEEE*, Vol. 62, No. 7, July, p. 901 to 915.

CIGRE WORKING GROUP 05 OF STUDY COMMITEE 12 (1983), 'An international survey on failures in large power transformers in service', *Electra*, No. 88, May.

CONNELY, F.C. (1965), *Transfomers: Their Priciples and Design for Light Electrical Engineers*, Sir Isaac Pitman and Sons Limited, fourth ed.

CUNHA, C.A.F. AND DOMMEL, H.W. (1973), 'Computer simulation of field tests on the 345 kv jaguara-taquaril line', *II Seminario Nacional de Producao e Transmissao de Energia Eletrica.* Belo horizonte-Brazil.

DAHL, O.G.C. (1925a), 'Separate leakage reactance of transformer windings', *A.I.E.E.*, June, pp. 785–791.

DAHL, O.G.C. (1925b), 'Transformer harmonics and their distribution', *A.I.E.E.*, June, pp. 792–804.

DENSEM, T.J., BODGER, P. AND ARRILLAGA, J. (1984), 'Three-phase transmission system modelling for harmonic penetration studies', *IEEE Transactions on Power Apparatus and Systems*, Vol. PAS-103, No. 2, pp. 310–317.

DICK, E. AND WATSON, W. (1981), 'Transformer models for transient studies based on field measurements', *IEEE Transactions on Power Apparatus and Systems*, Vol. PAS-100, No. 1, January, pp. 409 – 419.

DOMMEL, H. (1969), 'Digital computer solution of electromagnetic transients in single- and multiphase networks', *IEEE Transactions on Power Apparatus and Systems*, Vol. PAS-88, No. 4, April, pp. 388 – 399.

DOMMEL, H. (1975), 'Transformer models in the simulation of electromagnetic transients', *5th Power Systems Computation Conference, Cambridge, England*, Vol. 3.1/4, pp. 1–16.

DOMMEL, H. (1986), *[(Editor)]Electromagnetic Transients Program Reference Manual (EMTP Theory Book)*, Bonneville Power Administration.

DOMMEL, H.W., YAN, A. AND DE MARCANO, R.J.O. (1983), *Case studies for electromagnetic transients*, Technical Report, University of British Columbia, Department of Electrical Engineering, May.

DOMMEL, H.W., YAN, A. AND WEI, S. (1986), 'Harmonics from transformer saturation', *IEEE Trans. on Power systems*, Vol. PWRD-1, No. 2, April, pp. 209–215.

DUFFEY, C.K. AND STRATFORD, R.P. (1989), 'Update of harmonic standard ieee-519: Recommended practices and requirements for harmonic control in electric power systems', *IEEE Transactions on Industry and Applications*, Vol. 25, No. 6, November, pp. 1025–1033.

EL-SHERBINY, M.K. (1973), 'Representation of the magnetization characteristic by a sum of exponentials', *IEEE Transactions on Magnetics*, Vol. MAG-9, No. 1, March, pp. 60–61.

(1988), *[The EMTDC Users Manual]*, Manitoba Hydro, Canada.

ENRIQUE ACHA DAZA (1988), *Modelling of Power System trnasformers in the complex conjugate harmonic space*, PhD thesis, University of Canterbury.

FISHER, J. AND MOSER, H. (1956), 'Die nachbildung von magnetisierungskurven durch einfache algebraische oder traszendente funktionen', *Archiv fur Elektrotechnik*, Vol. 41, pp. 186–199.

GOLUB, G.H. AND LOAN, C.F. *Matrix Computations 2e*, The John Hopkins University Press.

GREVILLE, T.N. (1969), *Theory and Applications of Spline Functions*, Academic Press.

HATZIANTONIU, C., GALANOS, G.D. AND MILIAS-ARGILIS, J. (1988), 'An incremental transformer model for the study of harmonic overvoltages in weak ac/dc systems', *IEEE Transactions on Power Delivery*, Vol. 3, No. 3, July, pp. 1111–1121.

HWANG, J.H. AND LORD, W. (1976), 'Exponential series for bh curve modelling', *Proceedings IEE*, Vol. 123, No. 6, June, pp. 559–560.

IEEE TRANSMISSION AND DISTRIBUTION COMMITTEE (1993), 'Geomagntic disturbance effects on power systems', *IEEE Transactions on Power Delivery*, Vol. 8, No. 3, July, pp. 1206–1215.

IEEE WORKING GROUP ON POWER SYSTEM HARMONICS (1983), 'Power system harmonics: an overview', *IEEE Power Apparatus and SYstems*, Vol. PAS-102, No. 8, August, pp. 2455–2459.

LAUGHTON, M.A. (1968), 'Analsysis of unbalanced po.lyphase networks by the method pf phase co-ordinates;part1.system representation in phase frame of reference', *Proceedings IEE*, Vol. 115, No. 8, August, pp. 1163–1172.

LEE, K.H. AND SCHNEIDER, J.M. (1989), 'Rockport transient voltage monitoring system:analysis and simulation of recorded waveform', *IEEE Transactions on power delivery*, Vol. 4, No. 3, July, pp. 1794–1805.

MACFADYEN, W.K., SIMPSON, R.R. AND SLATER, R.D. (1973), 'Representation of magnetision curves by exponential series', *Proceedings IEE*, Vol. 120, No. 8, August, pp. 902–904.

MAHAMOUD, A.A. AND SCHULTZ, R.D. (1982), 'A method for analysing harmonic distribution in a.c. power systems', *IEEE Transaction on Power Apparatus*, Vol. Pas-101, No. 6, July, pp. 1815–1824.

MAZIERES, C. AND FORQUET, M. (1968), 'Simulation d'une bobine a noyau de fer par representation mathematique du cycle d'hysteresis', *Revue Generale de L'-electricite*, Vol. 77, No. 5, May, pp. 476–481.

MEDINA, A. AND ARRILLAGA, J. (1992), 'Generalised modelling of power transformers in the harmonic domain', *IEEE Transactions on Power Delivery*, Vol. 7, No. 3, July, p. 1458 to 1465.

MEDINA, A., ARRILLAGA, J. AND ACHA, E. (1990), 'Sparsity-oriented hybrid formulation of linear multiports and its applications to harmonic analysis', *IEEE Transactions on Power delivery*, Vol. 5, No. 3, pp. 1453–1458.

MORCHED, A.S., MARTI, L., BRIERLEY, R.H. AND LACKEY, J.G. (1996), 'Analysis of internal winding stresses in ehv generator step-up transformer failures', *IEEE transactions on Power Delivery*, Vol. 11, No. 2, April, pp. 888–895.

MORGAN, T.H., BAIROS, C.A. AND KIMBALL, G.S. (1933), 'The triple-harmonic equivalent circuit in three-phase power transformer banks', *A.I.E.E*, March, pp. 64–71.

OSBORNE, H.S. (1915), 'Discussion of the paper : Harmonics in Transformer Magnetisng Currents by J. F. Peters', *A.I.E.E.*, Vol. XXXIV, September, p. 2175.

PRESS, W.H., TEUKOLSKY, S.A., VETTERLING, W.T. AND FLANNERY, B.P. (1992), *Numerical recipes in Fortran: the art of scientif computing 2e*, Cambridge University Press, second ed.

PRUSTY, S. AND RAO, M.V.S. (1980), 'New method for predetermination of true saturation characteristics of transformers and nonlinear reactors', *Proceedings IEE*, Vol. 127, No. 2, March, pp. 106–110.

RAJAKOVIC, N. AND SEMLYEN, A. (1989), 'Investigation of the inrush phenomenon. a quasi stationary approach in the harmonic domain', *IEEE Trans.*, Vol. PWRD-4, No. 4, October, pp. 2114–2120.

SEMLYEN, A. AND CASTRO, A. (1975a), 'A digital transformer model for switching transient calculations in three-phase systems', *9th PICA Conference*, June, pp. 121–126.

SEMLYEN, A. AND CASTRO, A. (1975b), 'A digital transformer model for switching transient calculations in three-phase systems', *9th Power Industry Applications Conference*, June, pp. 121–126. New Orleans, Louisina.

SEMLYEN, A., ACHA, E. AND ARRILLAGA, J. (1987a), 'Harmonic norton equivalent for the magnetising branch of a transformer', *Proceedings IEE Part C*, Vol. 134, No. 2, March, pp. 162–169.

SEMLYEN, A., EGGLESTON, J.F. AND ARRILLAGA, J. (1987b), 'Admittance matrix model of a synchronous machine for harmonic analysis', *IEEE Trans. on Power Systems*, Vol. PWRS, No. 4, November, pp. 833–840.

SEMLYEN, A., ACHA, E. AND ARRILLAGA, J. (1988), 'Newton-type algorithms for the harmonic phasor analysis of non-linear power circuits in periodical steady-state with special reference to magnetic non-linearities', *IEEE Trans. on Power Delivery*, Vol. 3, No. 3, July, pp. 1090–1090.

SMITH, B. (1995), *A harmonic domain model for the interaction of the HVdc convertor with ac and dc systems*, PhD thesis, University of Canterbury.

STEINMETZ (1895), 'Theory of the general alternating transformer', *American Institute of Electrical Engineers.*, Vol. XII, June, pp. 245–256.

STIGANT, S.A., LACEY, H.M. AND STIGANT, S.A. (1941), *The J P Transformer Book*, Jonson and Phillips Limited, eighth ed.

STOER, J. AND BULIRSCH, R. (1993), *Introduction to Numerical Analysis*, Spring-Verlag, second ed.

SWIFT, G.W. (1969), 'An analytical approach to ferroresonace', *IEEE Transactions on Power Apparatus and Systems*, Vol. PAS-88, No. 1, January, pp. 42–46.

SZABADOS, B. (1979), 'Measurement of harmonic currents generated in a power transformer', *IEEE International Electronics Conference*, Vol. 79, No. 90130, October, p. pp82084.

SZABADOS, B. (1981), 'Harmonic impedance measurements on transformers', *IEEE Transactions on Power Apparatus adn systems*, Vol. PAS-100, No. 12, December, pp. 5020–5026.

TALUKDAR, S.N., DUGAN, J.K.D.R.C. AND SPRINZEN, M.J. (1974), 'On modeling transformer and reactor saturation characteristics for digital and analog studies',

IEEE Transactions on Power Apparatus and Systems, Vol. PAS-94, No. 2, April, pp. 612–621.

TRUTT, F.C., ERDELYI, E.A. AND HOPKINS, R.E. (1968), 'Representation of the magnetization charateristic of dc machines for computer use', *IEEE Transactions on Power Apparatus and Systems*, Vol. PAS-87, No. 3, March, pp. 665–669.

WHITEFIELD, A.H. (1986), 'Transfer function synthesis using frequency response data', *International Journal of Control*, Vol. 43, No. 5, pp. 1413–1426.

WIDGER, G.F.T. (1969), 'Representation of magnetisation curves over extensive range by rational-fraction approximations', *Proceedings of IEE*, Vol. 116, No. 1, January, pp. 156–160.

WOOD, A.R. (1993), *An analysis of non-ideal convertor behaviour in the frequency domain, and a new control proposal*, PhD thesis, University of Canterbury.

XIA, D. AND HEYDT, G.T. (1982), 'A multiphase harmonic load flow solution technique', *IEEE Transactions PAS*, Vol. PAS-101, No. 6, pp. 1257–1265.

XU, W., MARTI, J.R. AND H.W.DOMMEL (1991a), 'Harmonic analysis of systems with static compensator', *IEEE Trans. PWRS paper 90 WM 099-2.*

XU, W., MARTI, J.R. AND H.W.DOMMEL (1991b), 'A multiphase harmonic load-flow solution technique', *IEEE Trans. PWRS paper 90 WM 098-4.*